

Astroparticle Physics

2021/22

1. Historical introduction - basic properties of cosmic rays
2. Hadronic interactions and accelerator data
3. Cascade equations
4. Electromagnetic cascades
5. Extensive air showers
6. Detectors for extensive air showers
7. High-energy cosmic rays and the knee in the energy spectrum of cosmic rays
8. Radio detection of extensive air showers
9. Acceleration, Astrophysical accelerators and beam dumps
10. Extragalactic propagation of cosmic rays
11. Ultra-high-energy energy cosmic rays
12. Astrophysical gamma rays and neutrinos
13. Neutrino astronomy
14. Gamma-ray astronomy

lecture 7

High energy cosmic rays and the knee in the energy spectrum

Gaisser chapter 17

17 Very high energy cosmic rays	341
17.1 The knee of the spectrum	342
17.2 Depth of shower maximum and composition	345
17.3 Ultra-high-energy cosmic rays	348
17.4 Sources of extragalactic cosmic rays	351
17.5 Future experiments	355

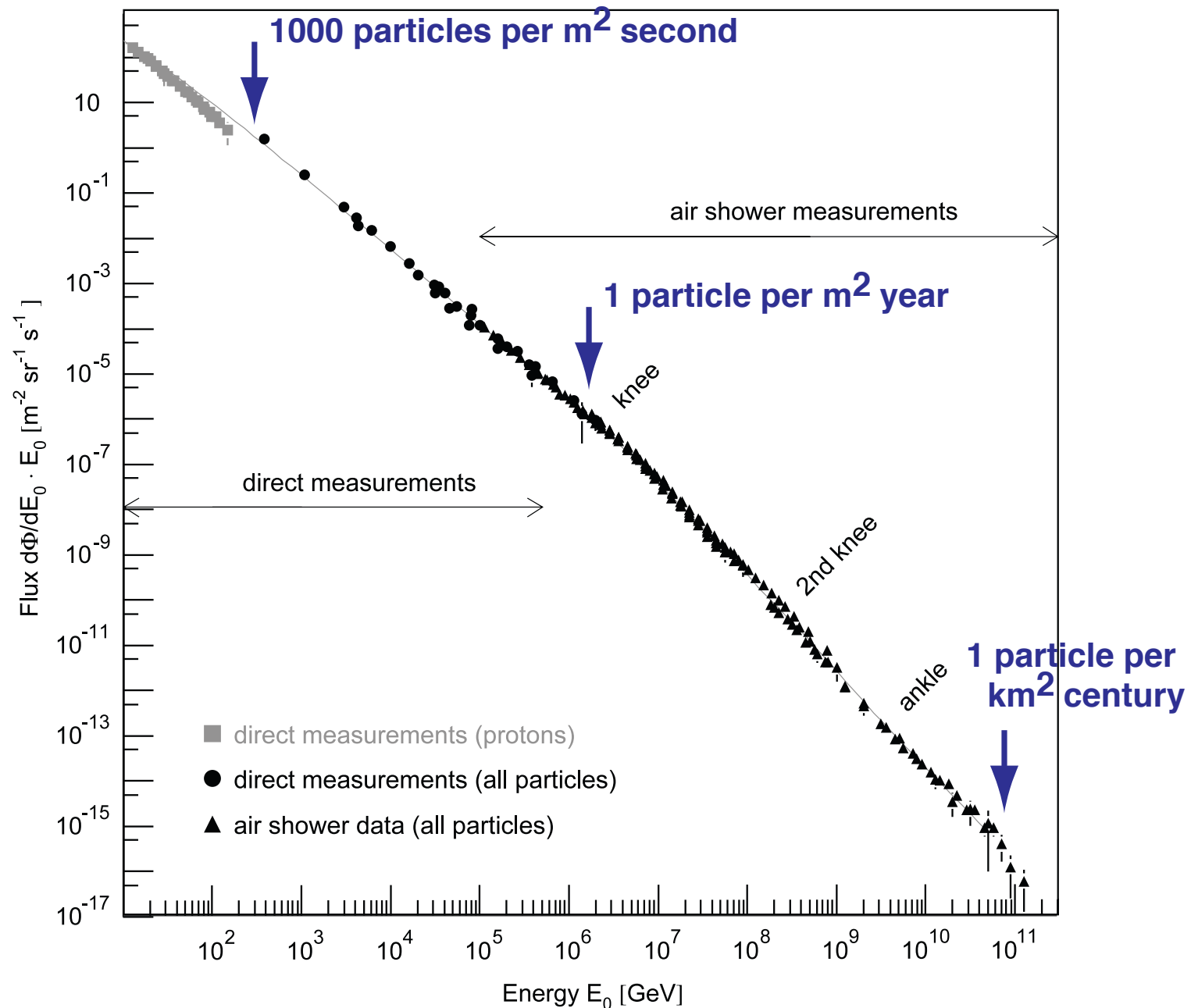


Fig. 1. All-particle energy spectrum of cosmic rays as measured directly with detectors above the atmosphere and with air shower detectors. At low energies, the flux of primary protons is shown.

Energy spectrum of cosmic rays

energy density

$$\rho_E = \frac{4\pi}{c} \int \frac{E}{\beta} \frac{dN}{dE} dE \approx 1 \text{ eV/cm}^3$$

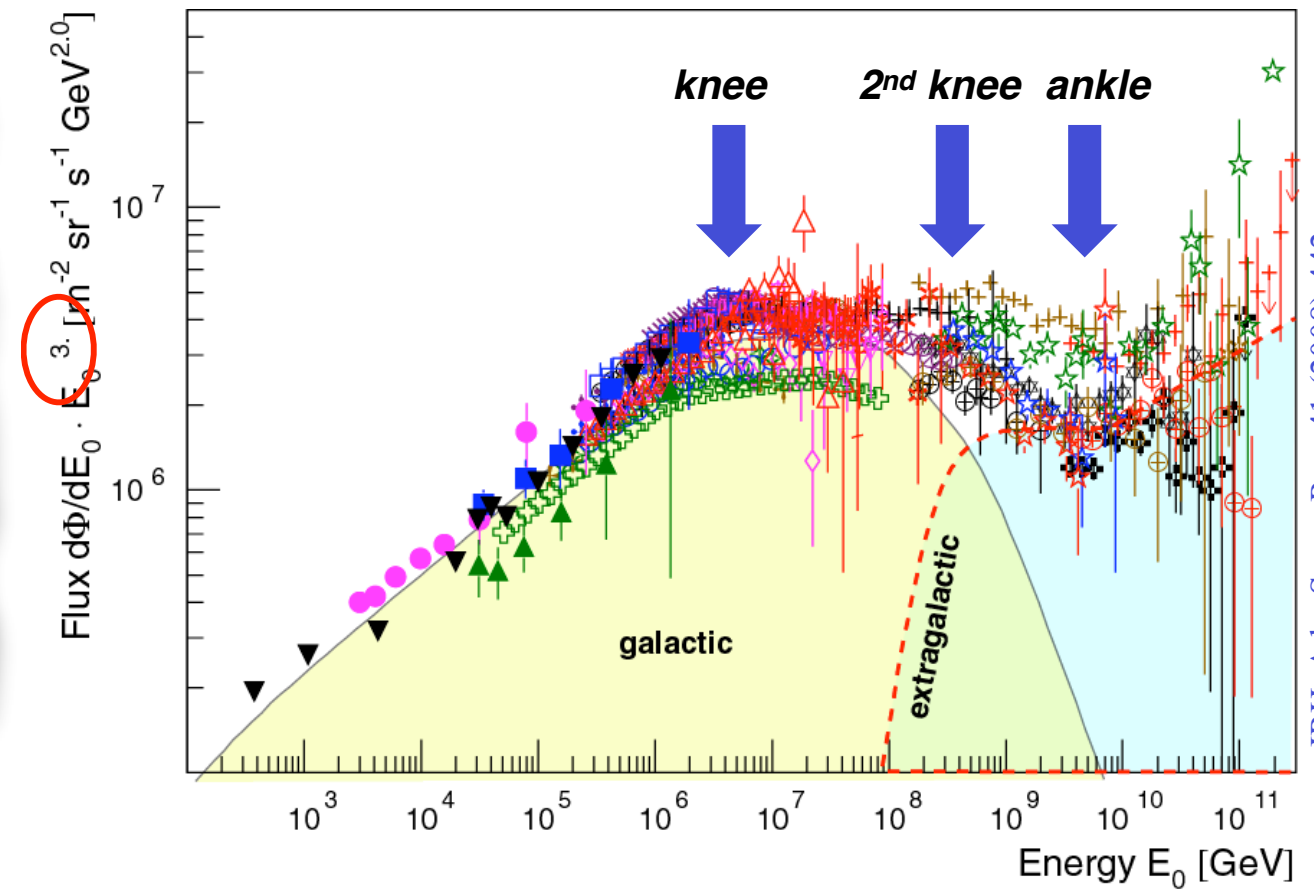
for comparison:

$$\rho_B = \frac{B^2}{2\mu_0} \approx 0.25 \text{ eV/cm}^3$$

$$\rho_{SL} \approx 0.3 \text{ eV/cm}^3$$

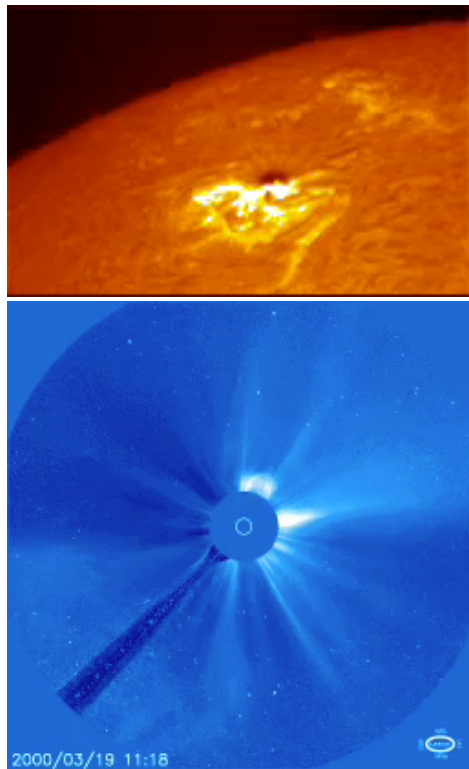
$$\rho_{IR} \approx 0.4 \text{ eV/cm}^3$$

$$\rho_{3K} \approx 0.25 \text{ eV/cm}^3$$

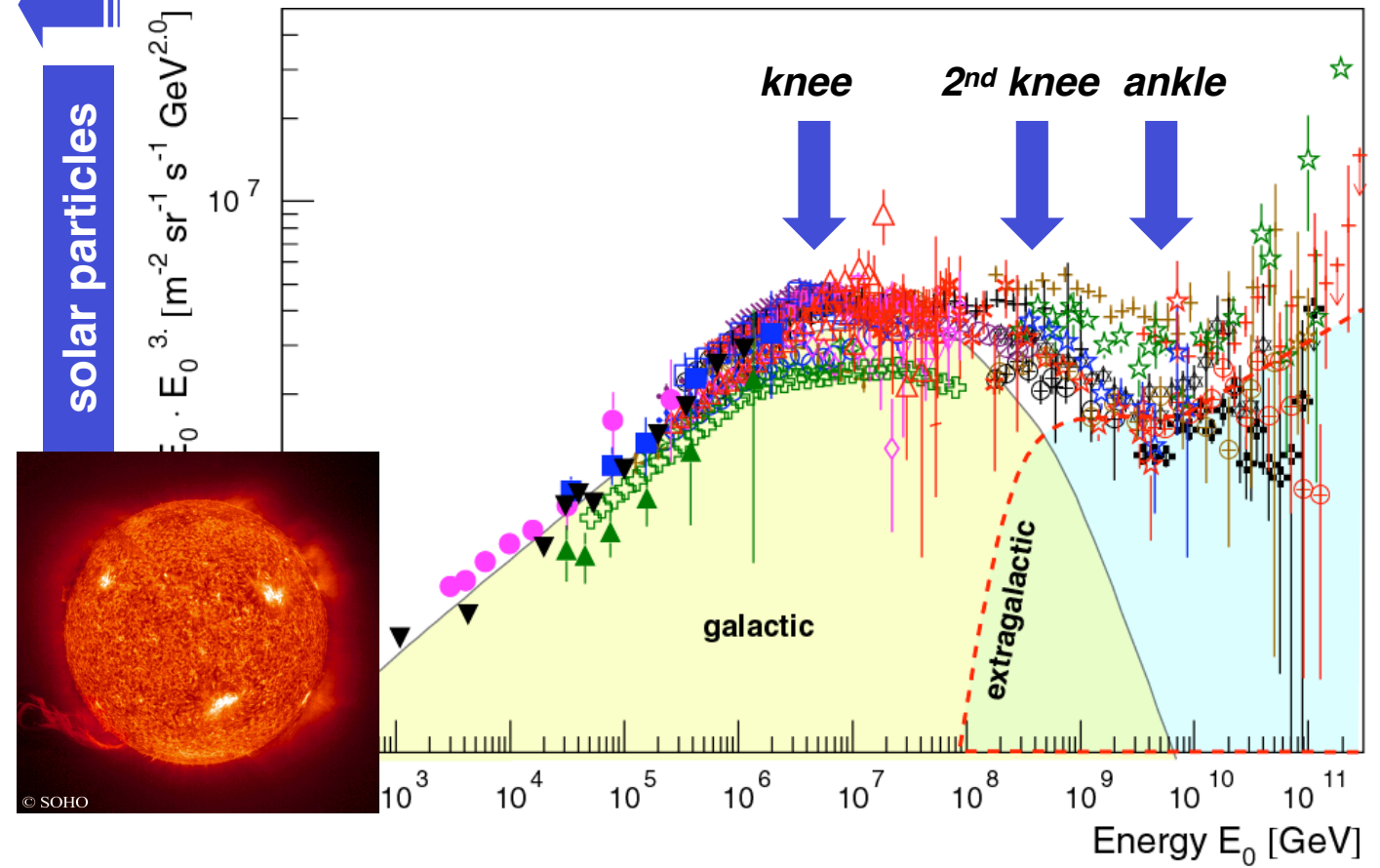


Energy spectrum of cosmic rays

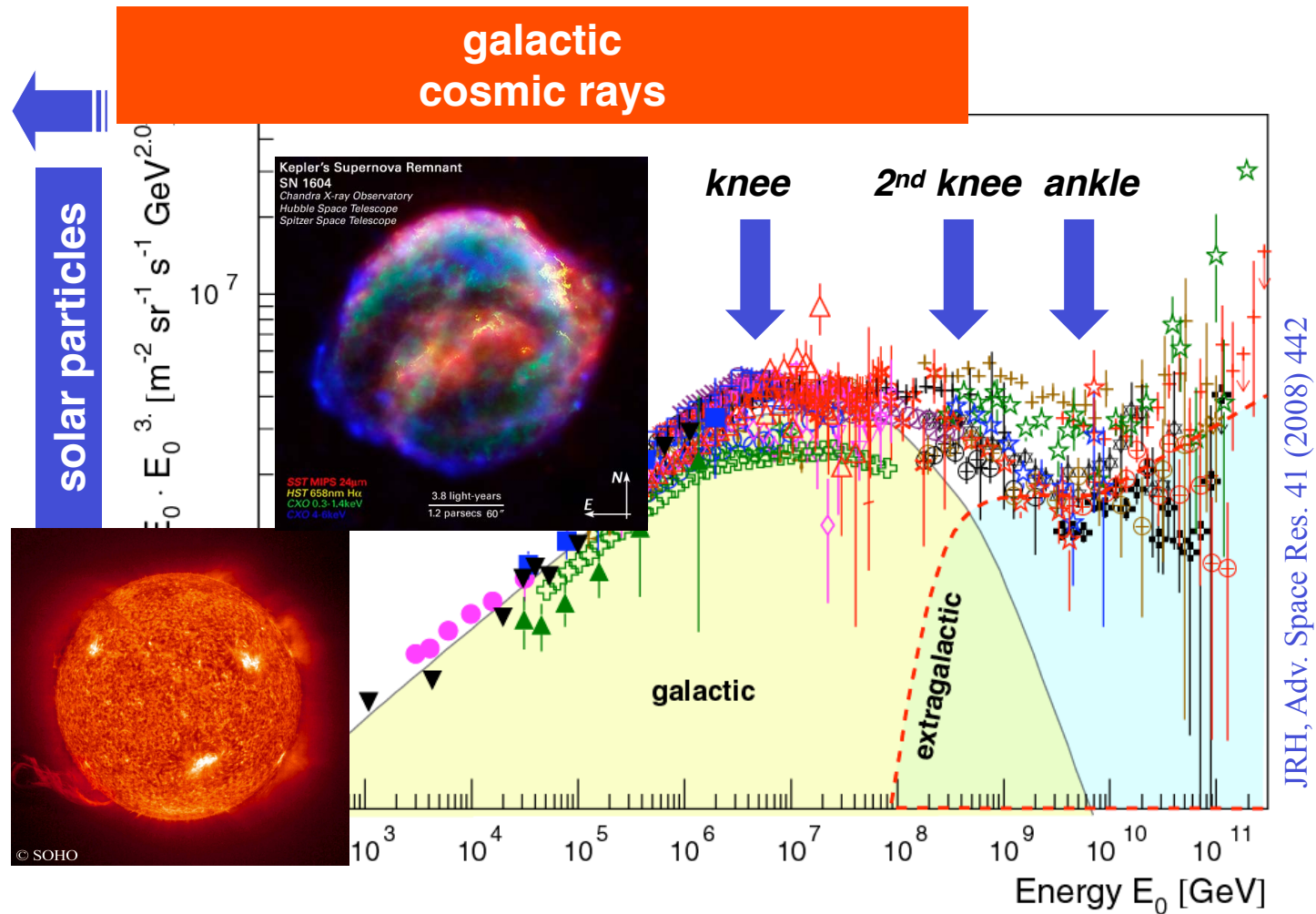
Solar flares



solar particles



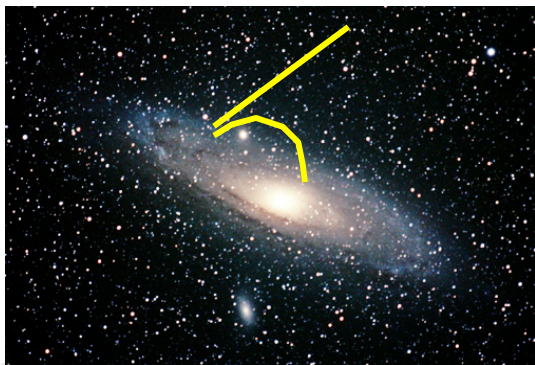
Energy spectrum of cosmic rays



Energy spectrum of cosmic rays

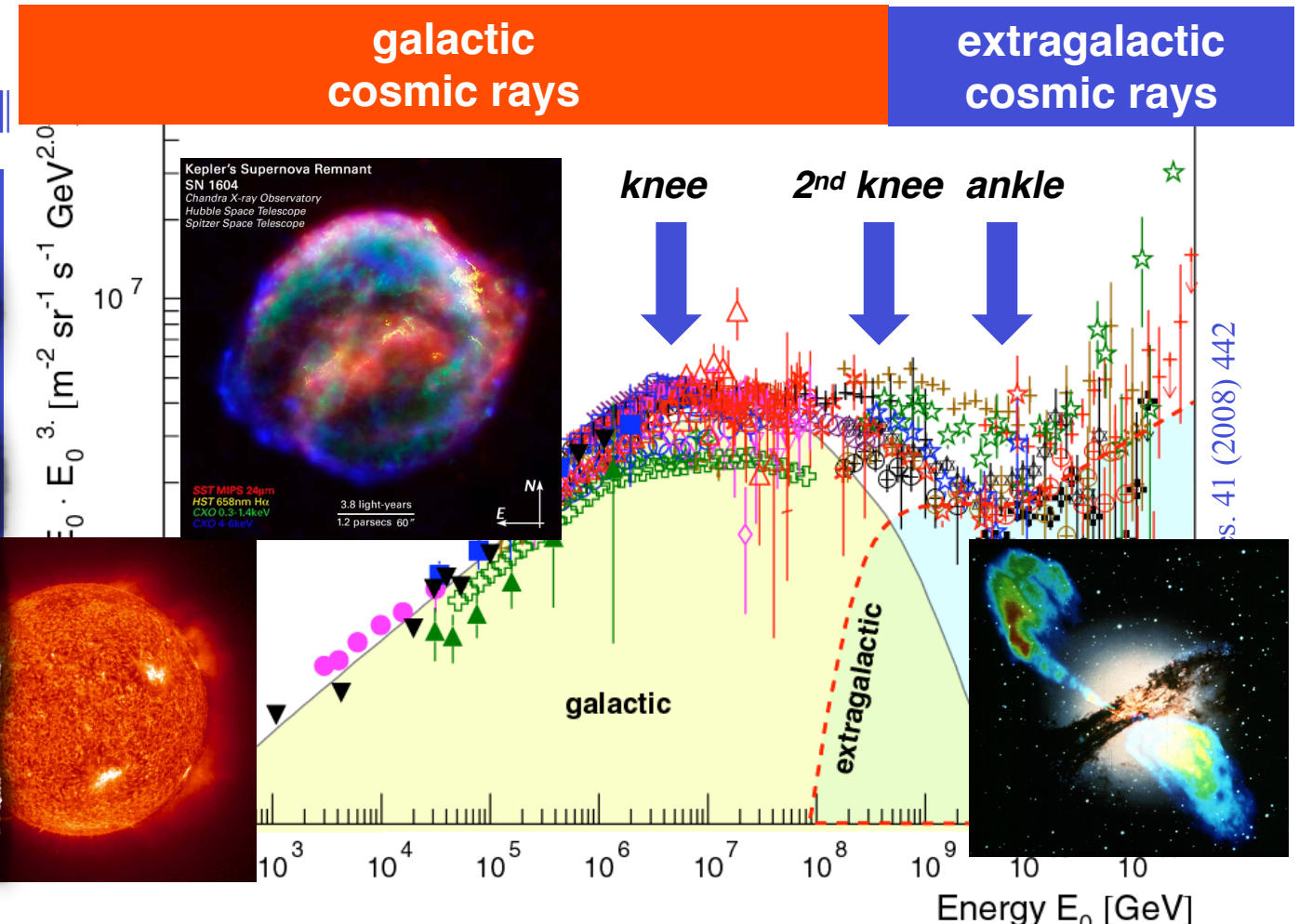
Radius of particle in magnetic field

$$r = \frac{p}{ZeB} \quad r[\text{pc}] = 1.08^* \frac{E [\text{PeV}]}{B [\mu\text{G}]}$$



© SOHO

\leftarrow
 S



$r =$ 0.04 pc 3.6 pc 360 pc 36 kpc

Extensive air showers – Mass

Simple Heitler model of (hadronic) showers

Primary mass:

- Average depth of shower maximum X_{\max}

$$X_{\max}^A \sim \ln \frac{E_0}{A}$$

$$X_{\max}^A = X_{\max}^p - X_0 \ln A$$

$$X_{\max}^{\text{Fe}} = X_{\max}^p - 150 \text{ g/cm}^2$$

- N_e - N_μ ratio

$$\frac{N_e}{N_\mu} \approx 35.1 \left(\frac{E_0}{A \text{ PeV}} \right)^{0.15}$$

or

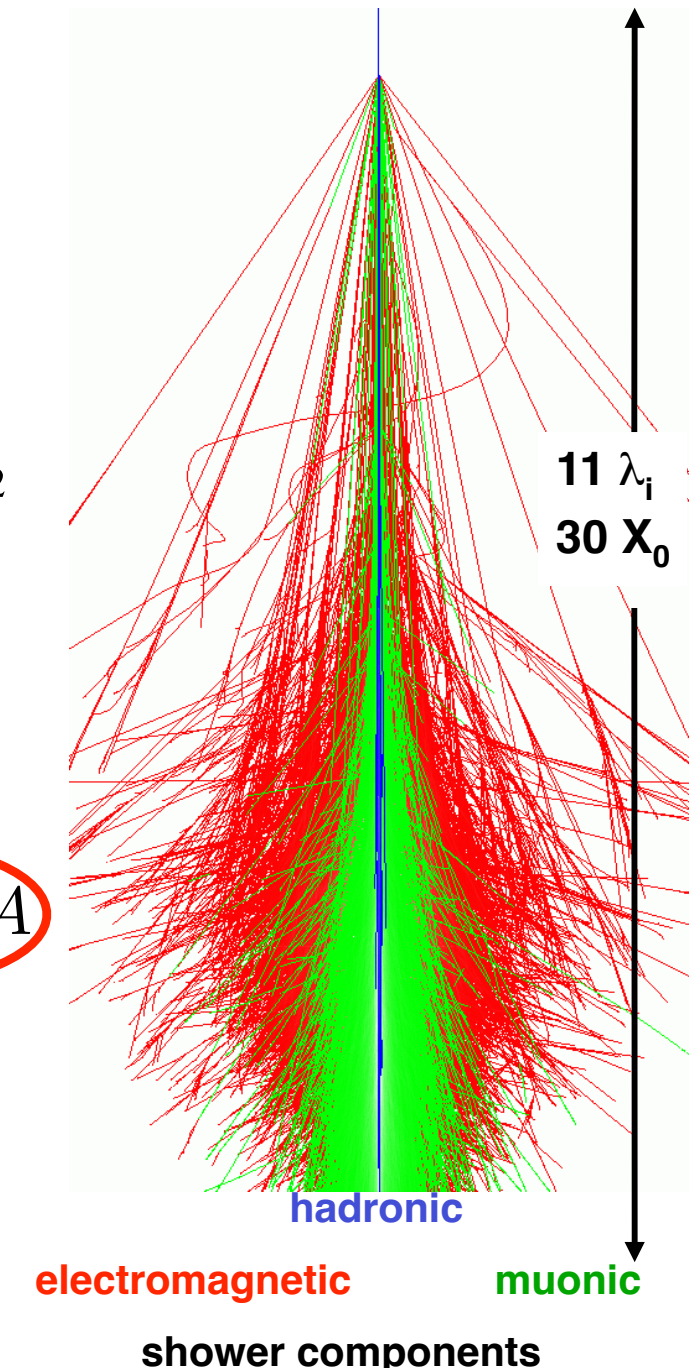
$$\lg \left(\frac{N_e}{N_\mu} \right) = C - 0.065 \ln A$$

$$\Delta \ln A \sim 1$$

$$\rightarrow \Delta X_{\max} \sim 36 \text{ g/cm}^2$$

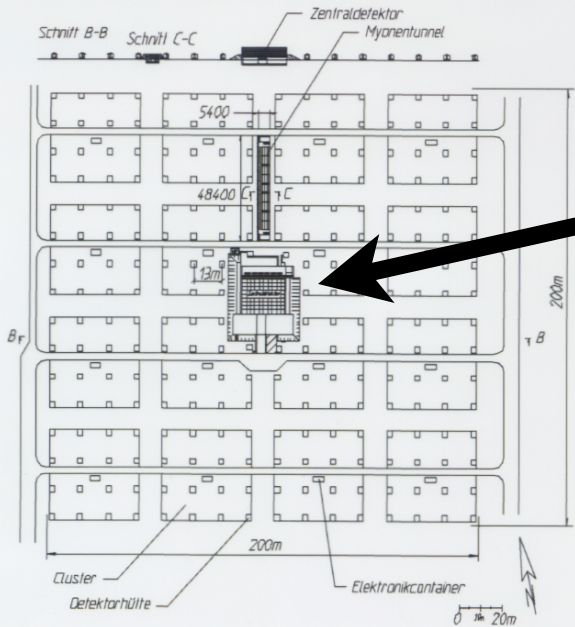
$$\rightarrow \Delta (N_e/N_\mu) \sim 16\%$$

$\Delta \ln A \approx 0.8$
in „best“ experiments



The KASCADE Array

200 m



□ Array

200 m

252 stations with

- e/ γ detectors: 4 cm liquid scintillator ($\approx 3.1 \text{ m}^2$)
- muon detectors: 3 cm plastic scintillator ($\approx 3.2 \text{ m}^2$)

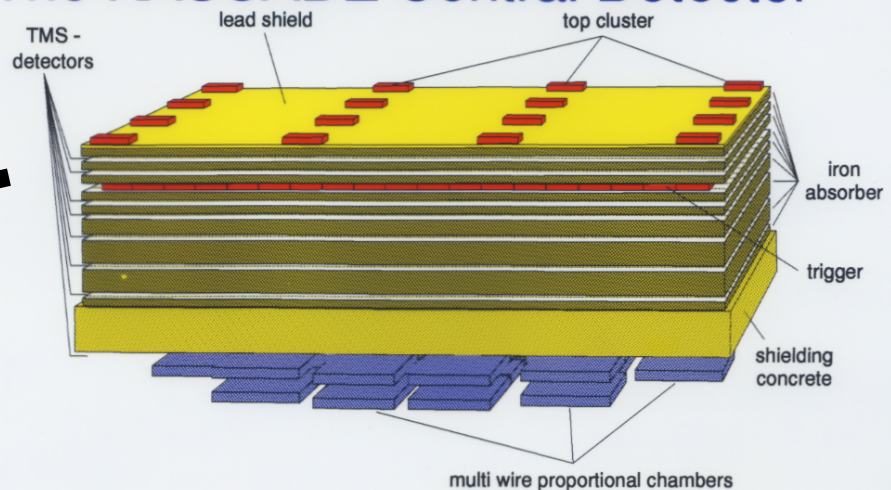
shield 10 cm Pb + 4 cm Fe $\rightarrow 20 X_0$

$\Rightarrow E_\mu > 300 \text{ MeV}$

\rightarrow measurement of particle densities and arrival times

JRH 06/96

The KASCADE Central Detector



4 different detector systems:

- Top array $32 \times 0.45 \text{ m}^2$ scintillation counters (14 m^2)
- Trigger layer $456 \times 0.45 \text{ m}^2$ scintillation counters (206 m^2)
- 32 Multiwire proportional chambers ($2 \times 150 \text{ m}^2$) $E_\mu > 2 \text{ GeV}$
- Iron sampling calorimeter ($16 \times 20 \text{ m}^2$)

8 active layers $\rightarrow 10\,000$ liquid ionisation chambers

40 000 electronic channels

separation of individual hadrons by a fine segmentation

depth $\approx 11 \lambda_i \rightarrow$ hadrons up to 10 TeV 95% contained

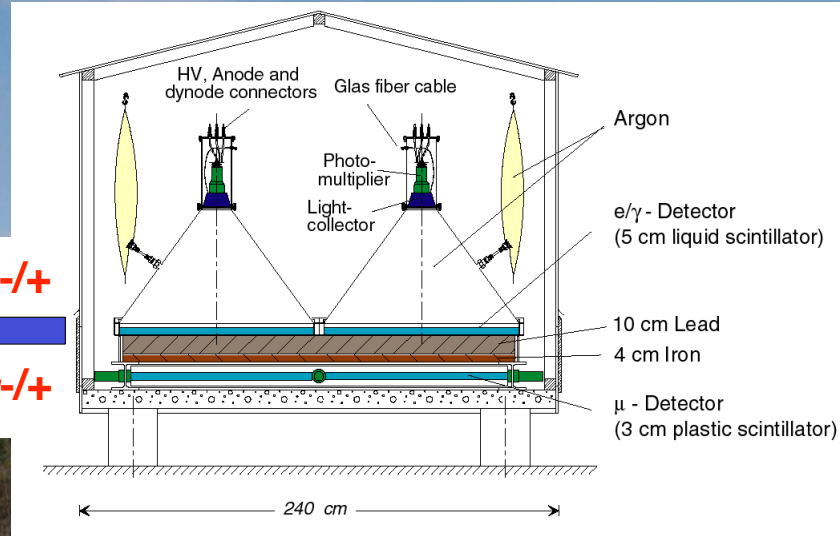
JRH 06/96

KArlsruhe Shower Core and Array DEtector

Simultaneous measurement of
electromagnetic,
muonic,
hadronic
shower components



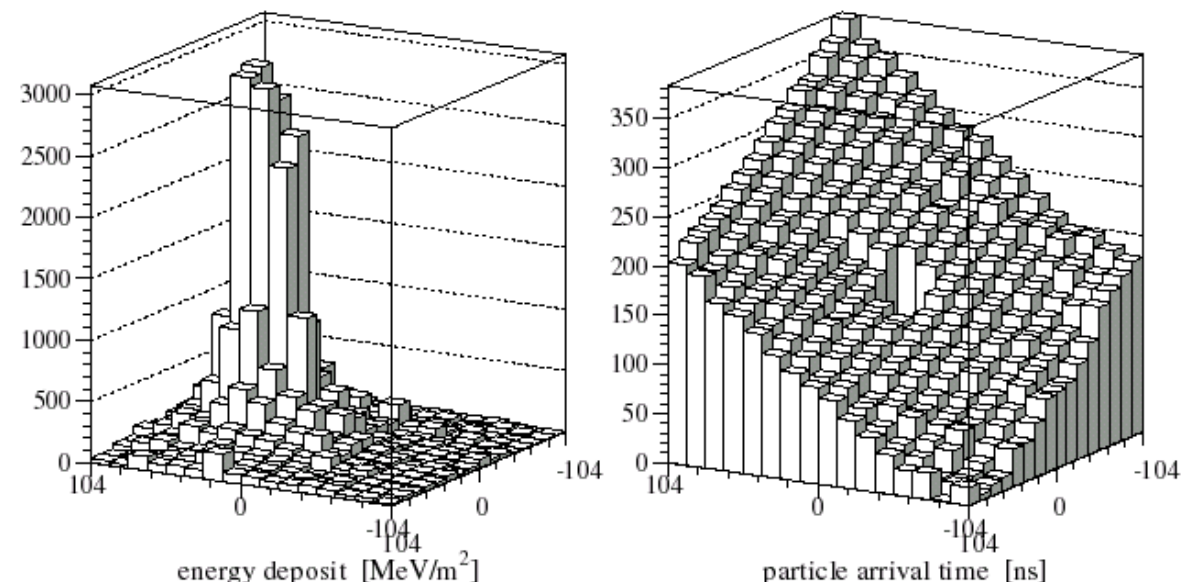
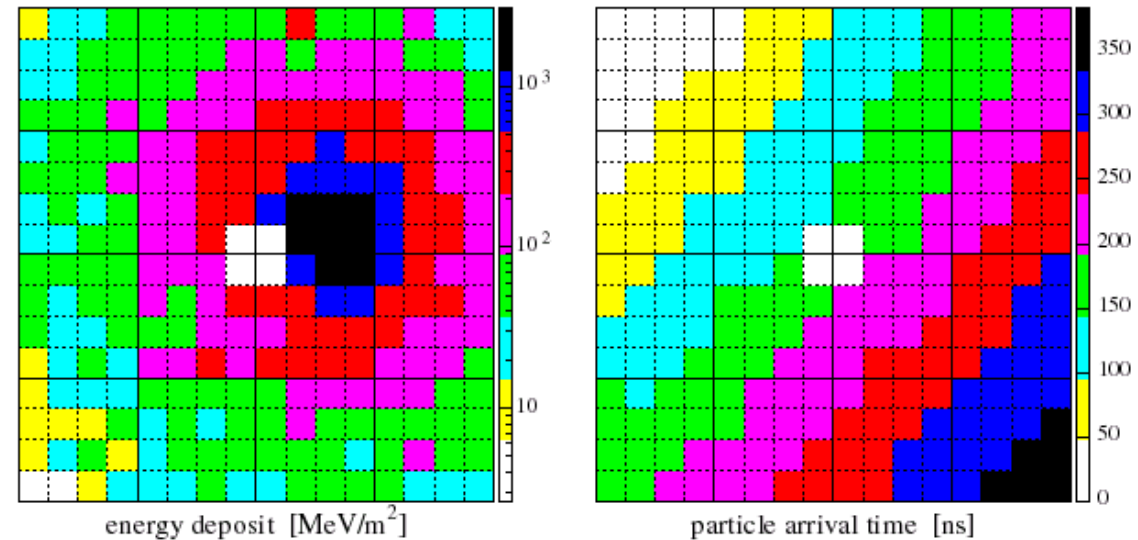
$e^-/+$
 $\mu^-/+$



Event reconstruction in the scintillator array electromagnetic component

e/ γ -Detectors, Run 1, Event 71089, 96-03-05 22:07:48.956078

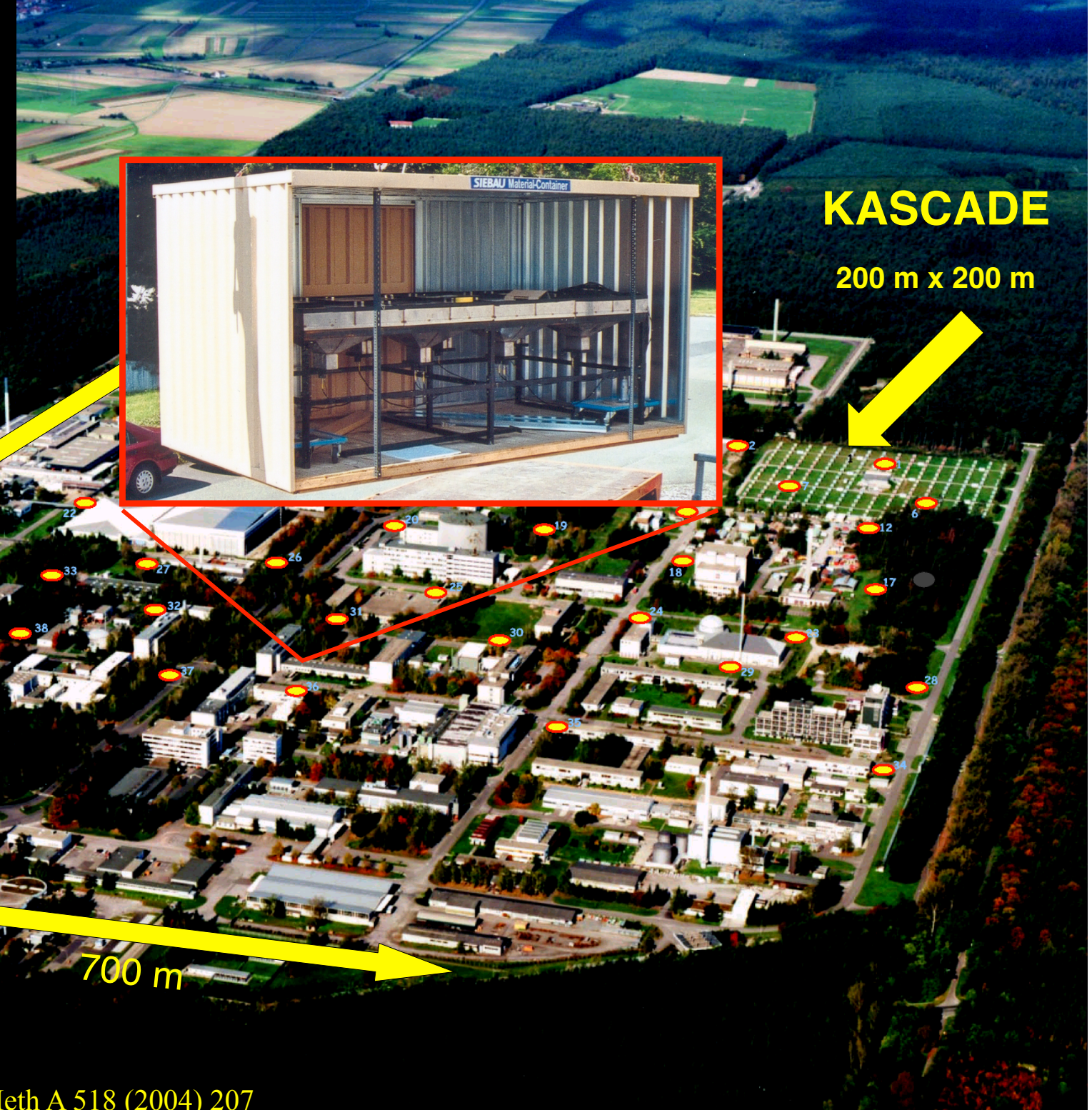
shower core	$\Delta r = 2.5 - 5.5 \text{ m}$
shower direction	$\Delta\alpha = 0.5^\circ - 1.2^\circ$
shower size	$\Delta N_e/N_e = 6 - 12 \%$



KASCADE GRANDE Array

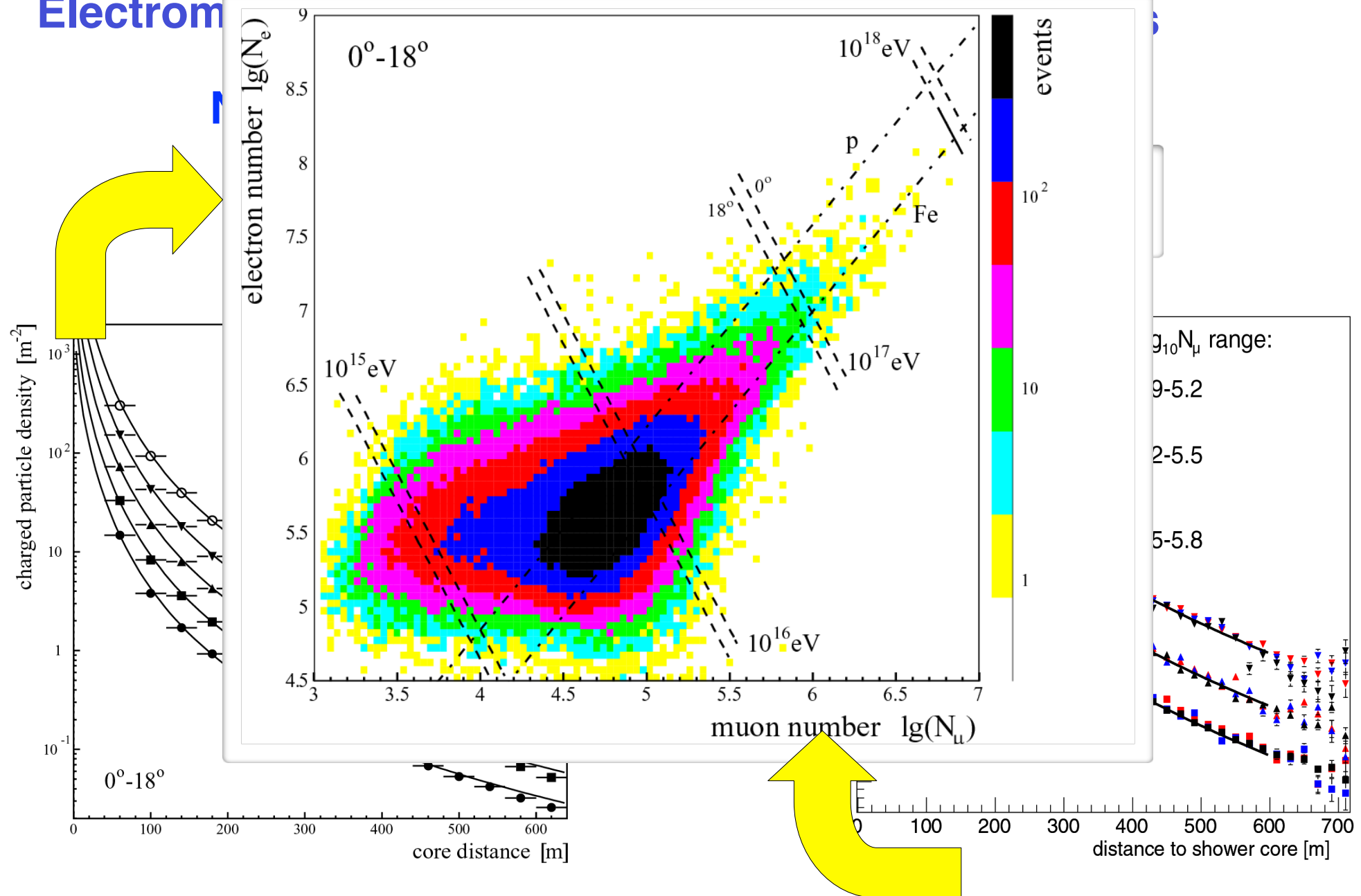
37 detector stations

370 m² e/ γ :
scintillation counter

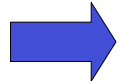
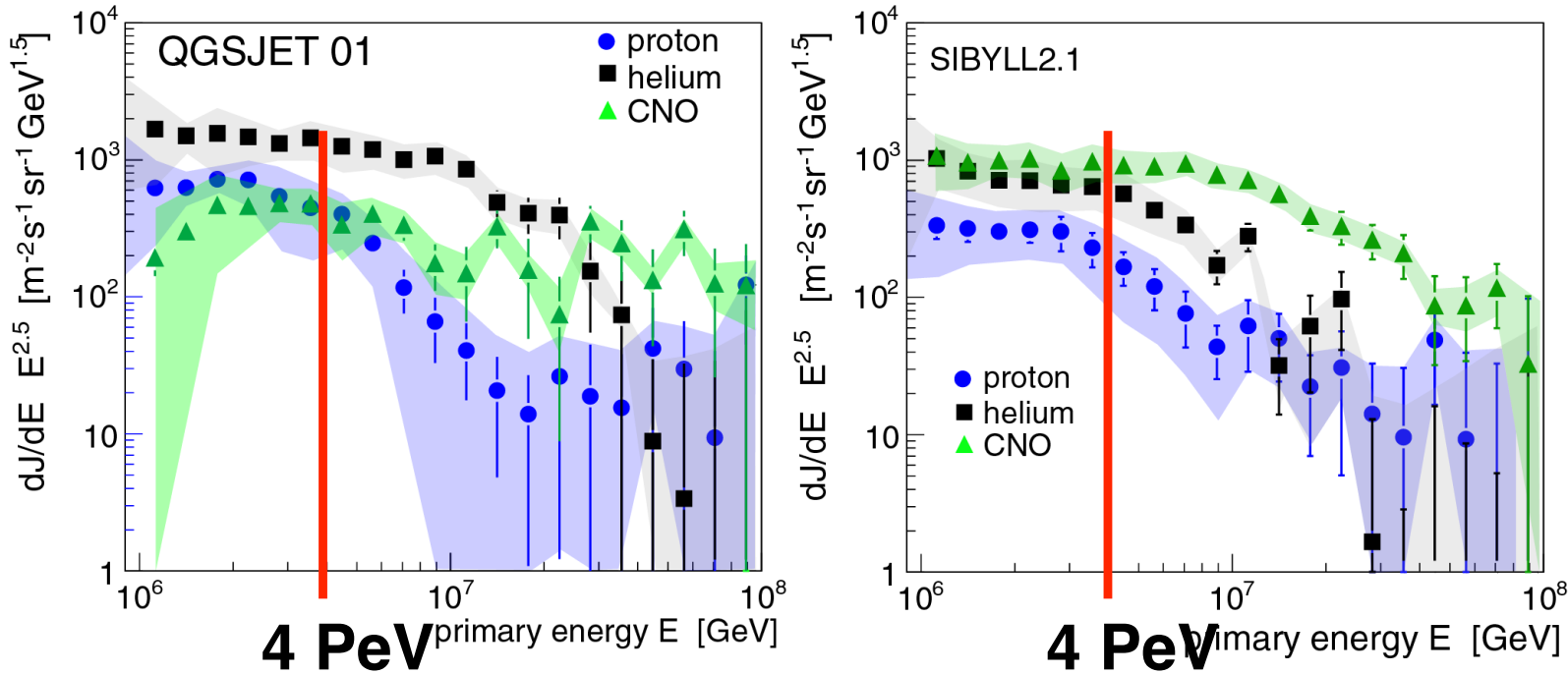


KASCADE-Grande – Lateral distributions

Electromagnetic shower lateral distributions



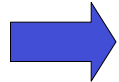
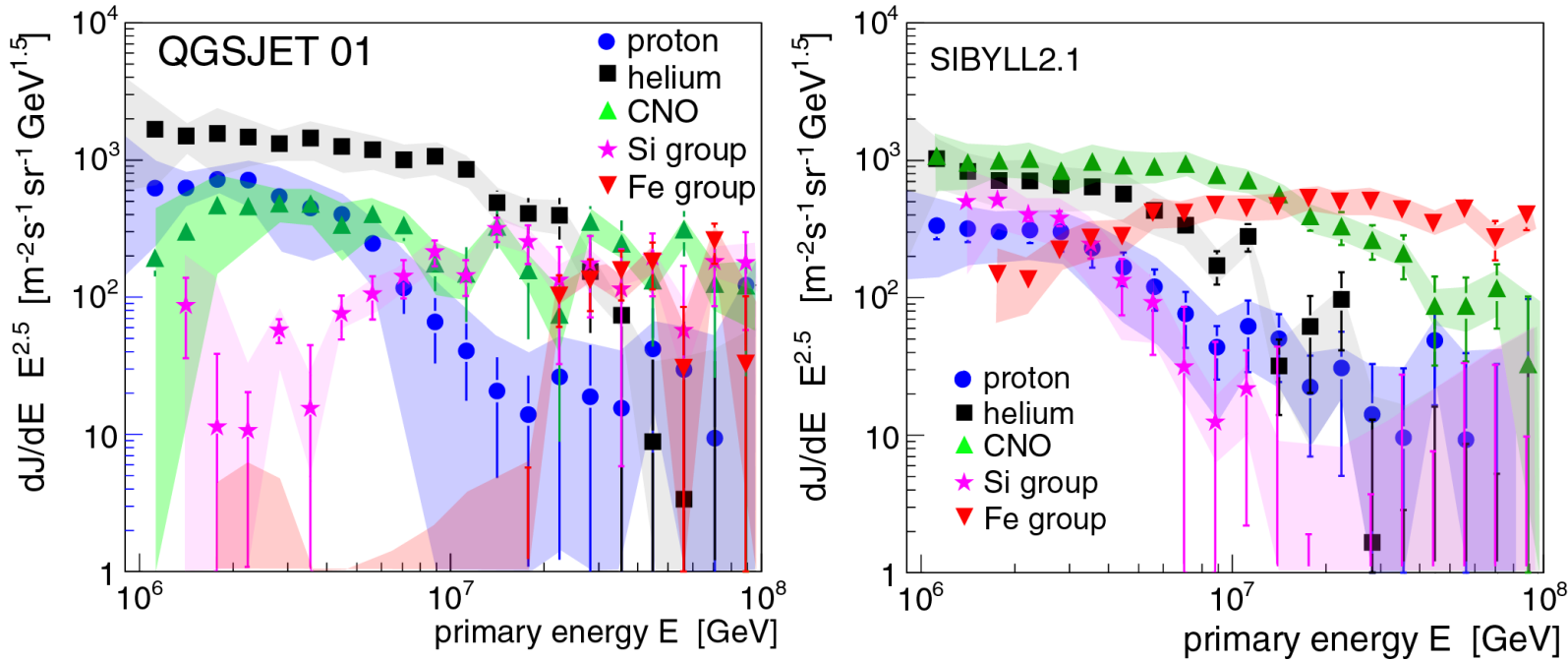
KASCADE: Energy spectra for elemental groups



Knee caused by cut-off for light elements

**Astrophysical interpretation limited
by description of interactions in the
atmosphere**

KASCADE: Energy spectra for elemental groups



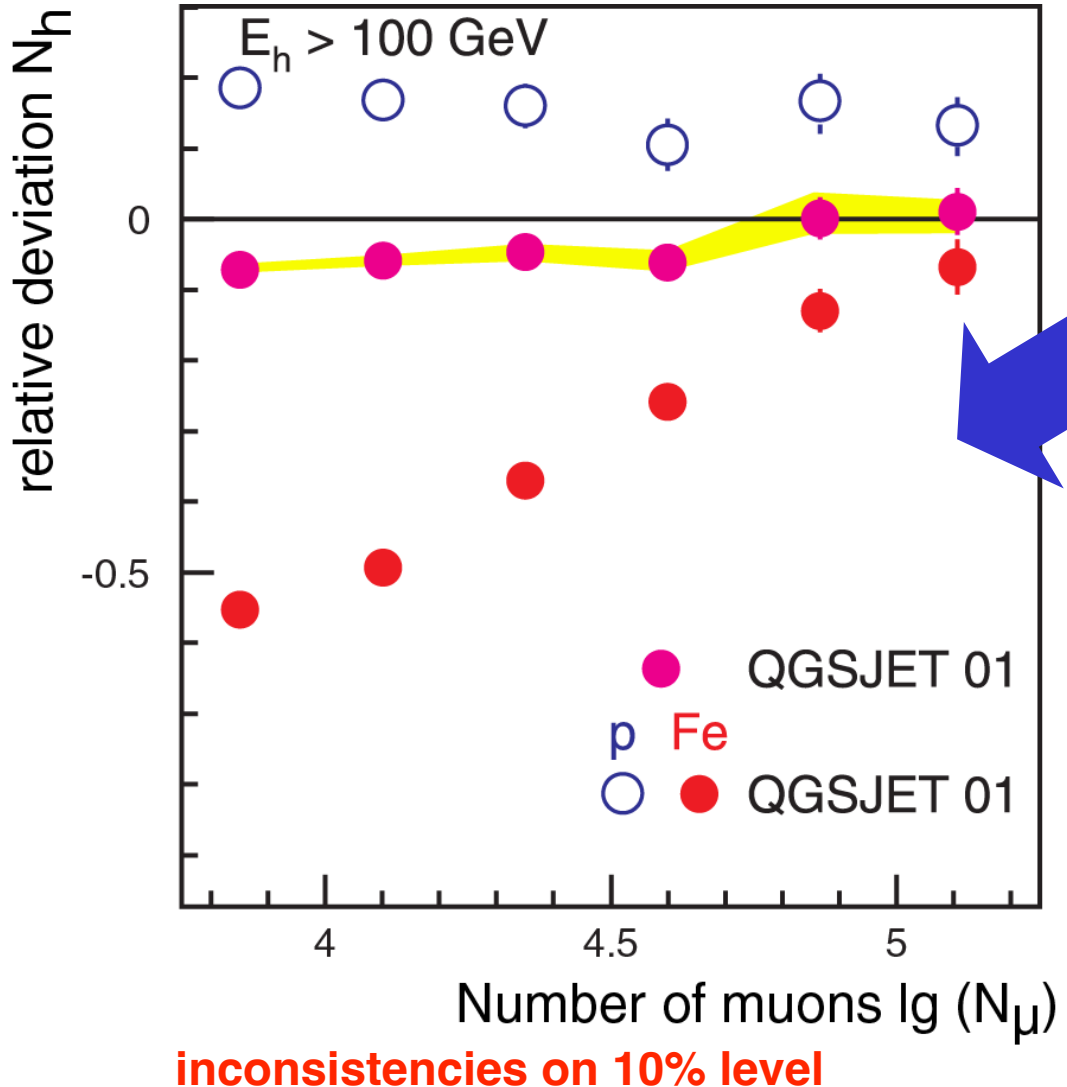
Knee caused by cut-off for light elements

**Astrophysical interpretation limited
by description of interactions in the
atmosphere**

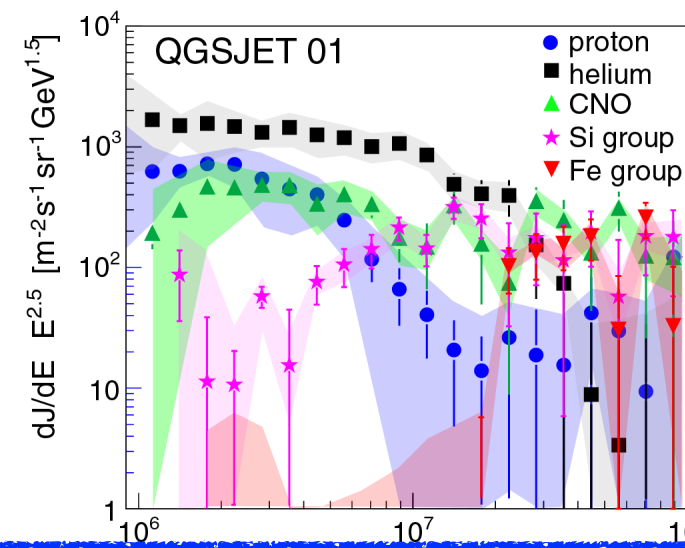
Test of hadronic interaction models

QGSJET 01

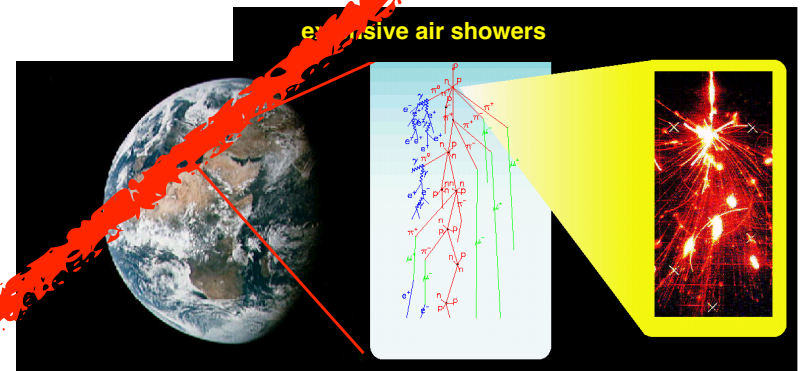
Number of hadrons vs. number of muons



N_e - N_μ analysis



in literature:
ideas that knee is caused by new
interactions in atmosphere
—> energy is carried away by
„invisible channels“



Electron, muon and hadron size spectra of EAS in the "knee" region

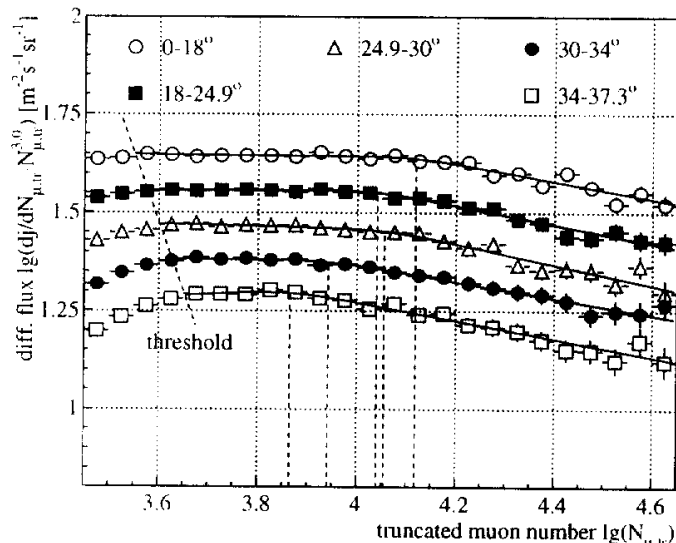
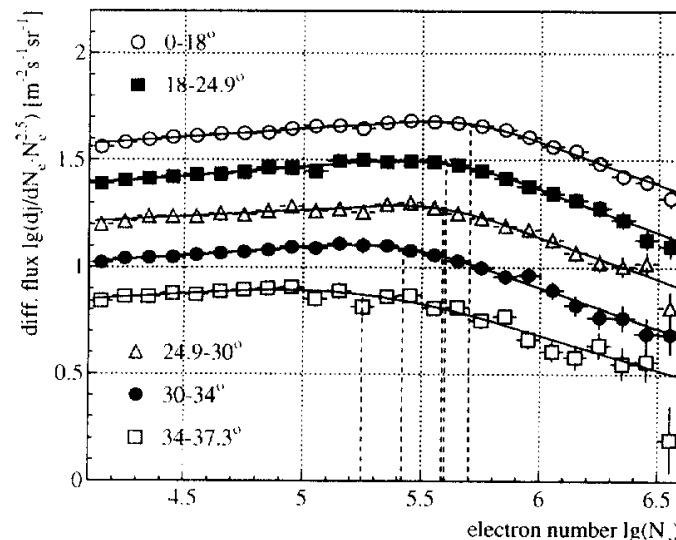
R. Glasstetter^a and J.R. Hörandel^a for the KASCADE Collaboration*

Figure 1. Electromagnetic (top) and muonic (bottom) shower size spectra for different zenith angle bins.

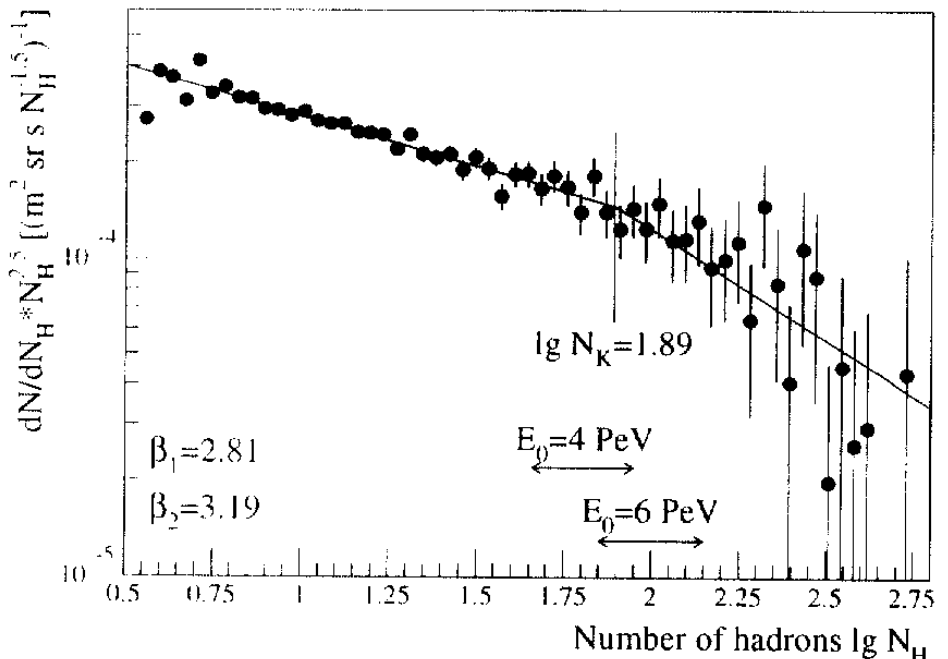


Figure 3. Hadronic shower size spectrum.

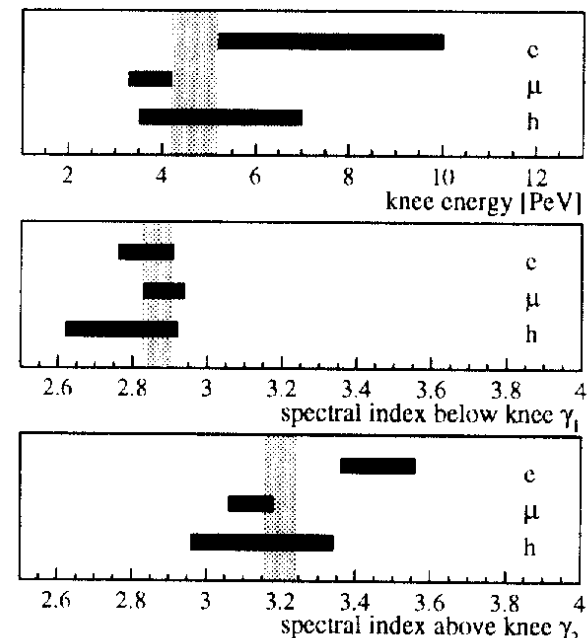
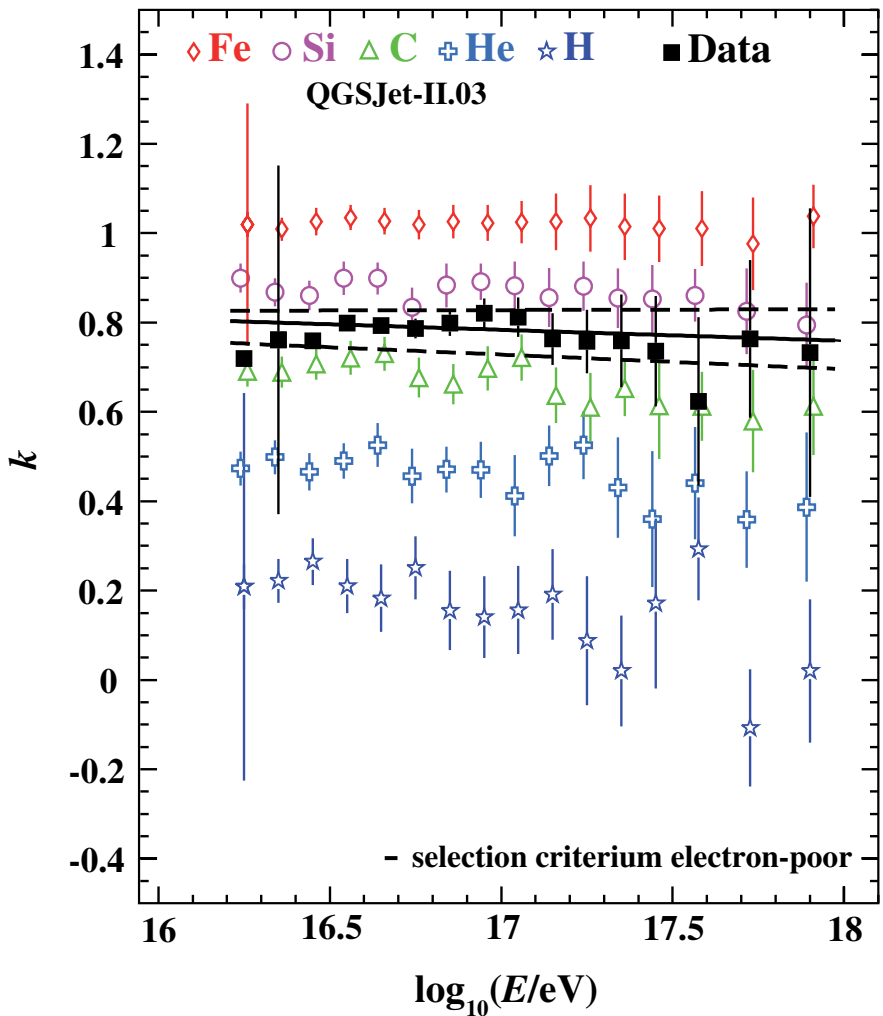


Figure 4. Knee position and spectral indices.

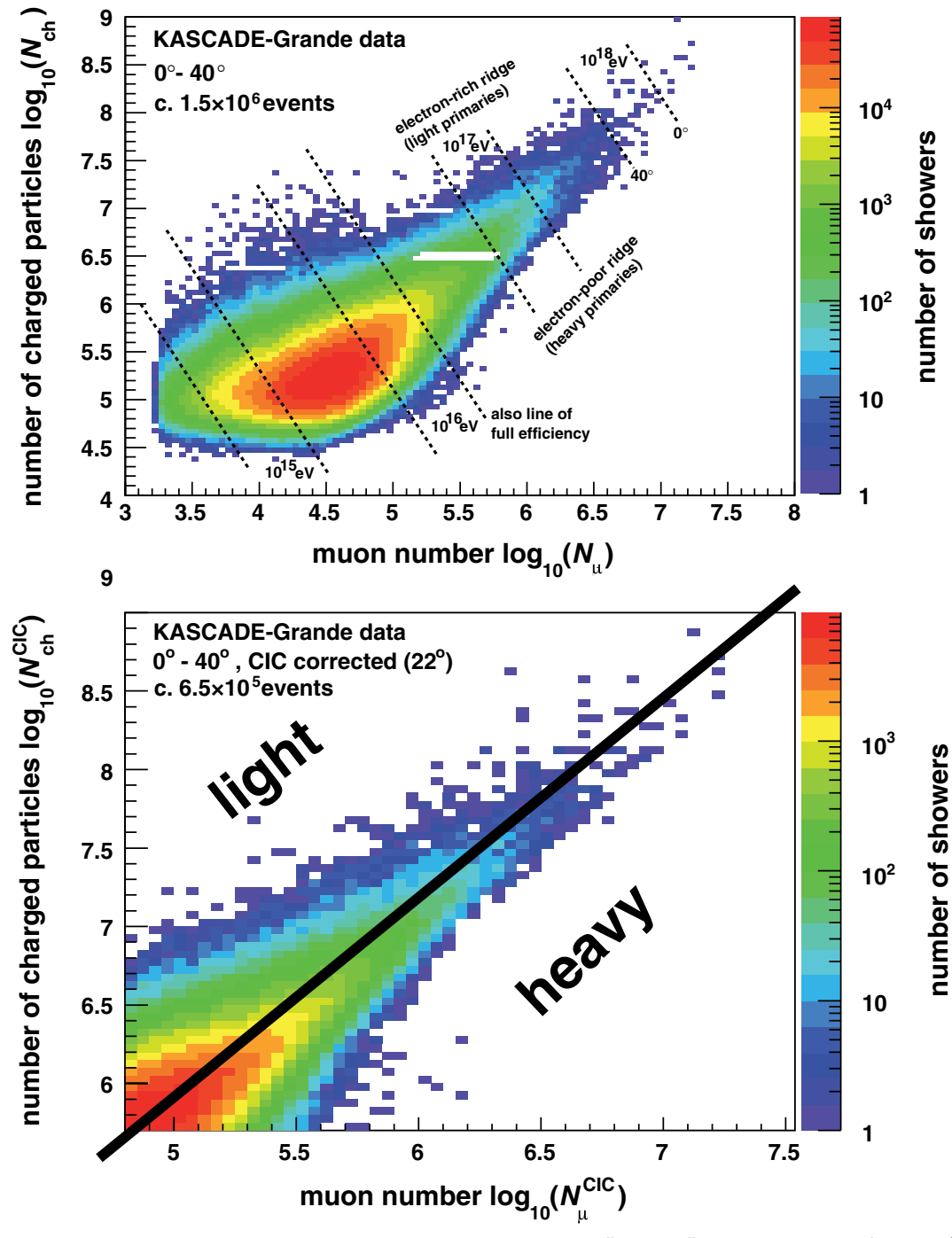
knee observed in all components, electromagnetic, muonic, and hadronic!

KASCADE-Grande

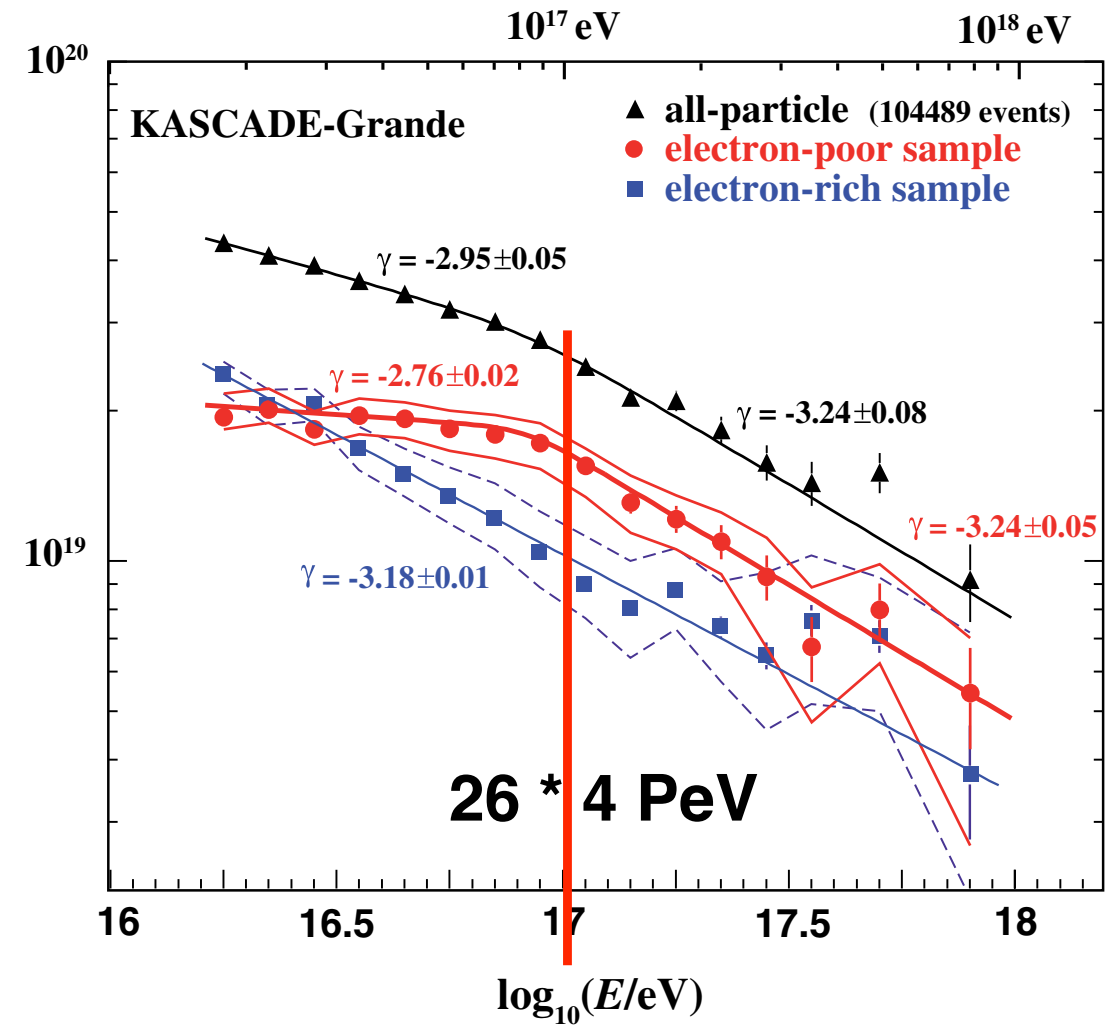
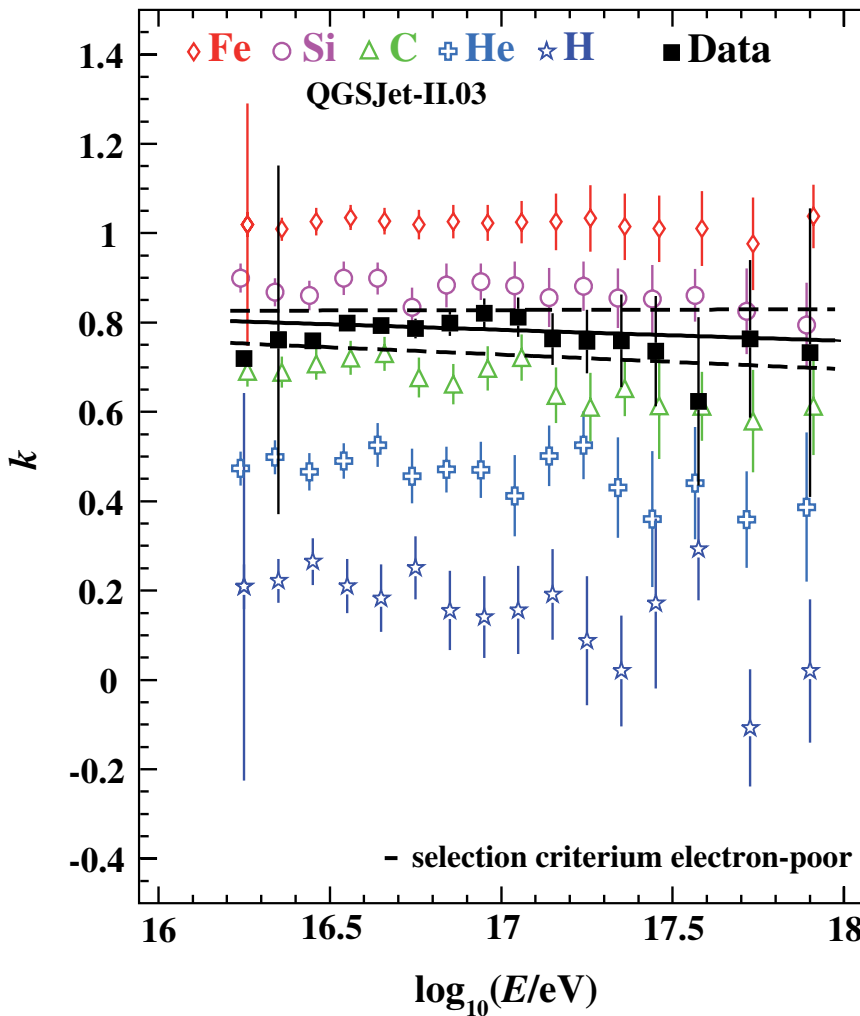


$$k = \frac{\log_{10}(N_{\text{ch}}/N_{\mu}) - \log_{10}(N_{\text{ch}}/N_{\mu})_{\text{H}}}{\log_{10}(N_{\text{ch}}/N_{\mu})_{\text{Fe}} - \log_{10}(N_{\text{ch}}/N_{\mu})_{\text{H}}},$$

W.D. Apel et al., PRL 107 (2011) 171104

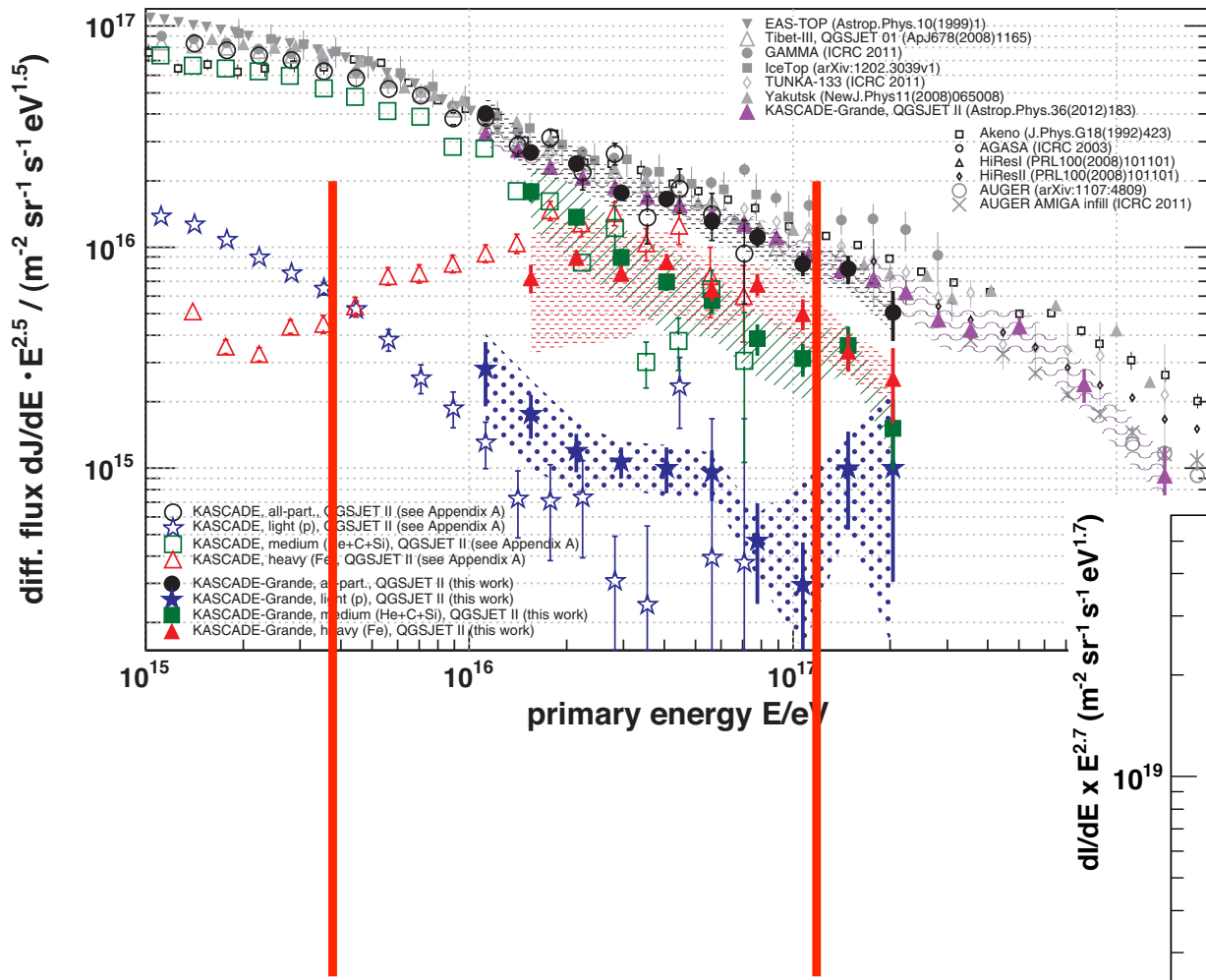


KASCADE-Grande



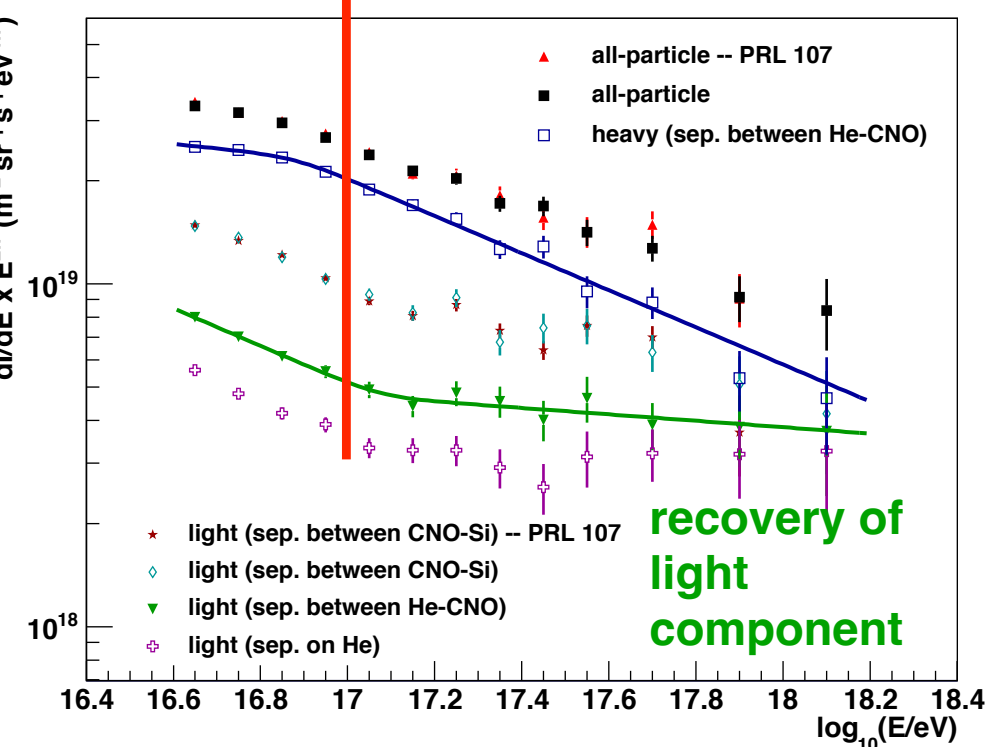
$$k = \frac{\log_{10}(N_{\text{ch}}/N_{\mu}) - \log_{10}(N_{\text{ch}}/N_{\mu})_{\text{H}}}{\log_{10}(N_{\text{ch}}/N_{\mu})_{\text{Fe}} - \log_{10}(N_{\text{ch}}/N_{\mu})_{\text{H}}},$$

KASCADE-Grande



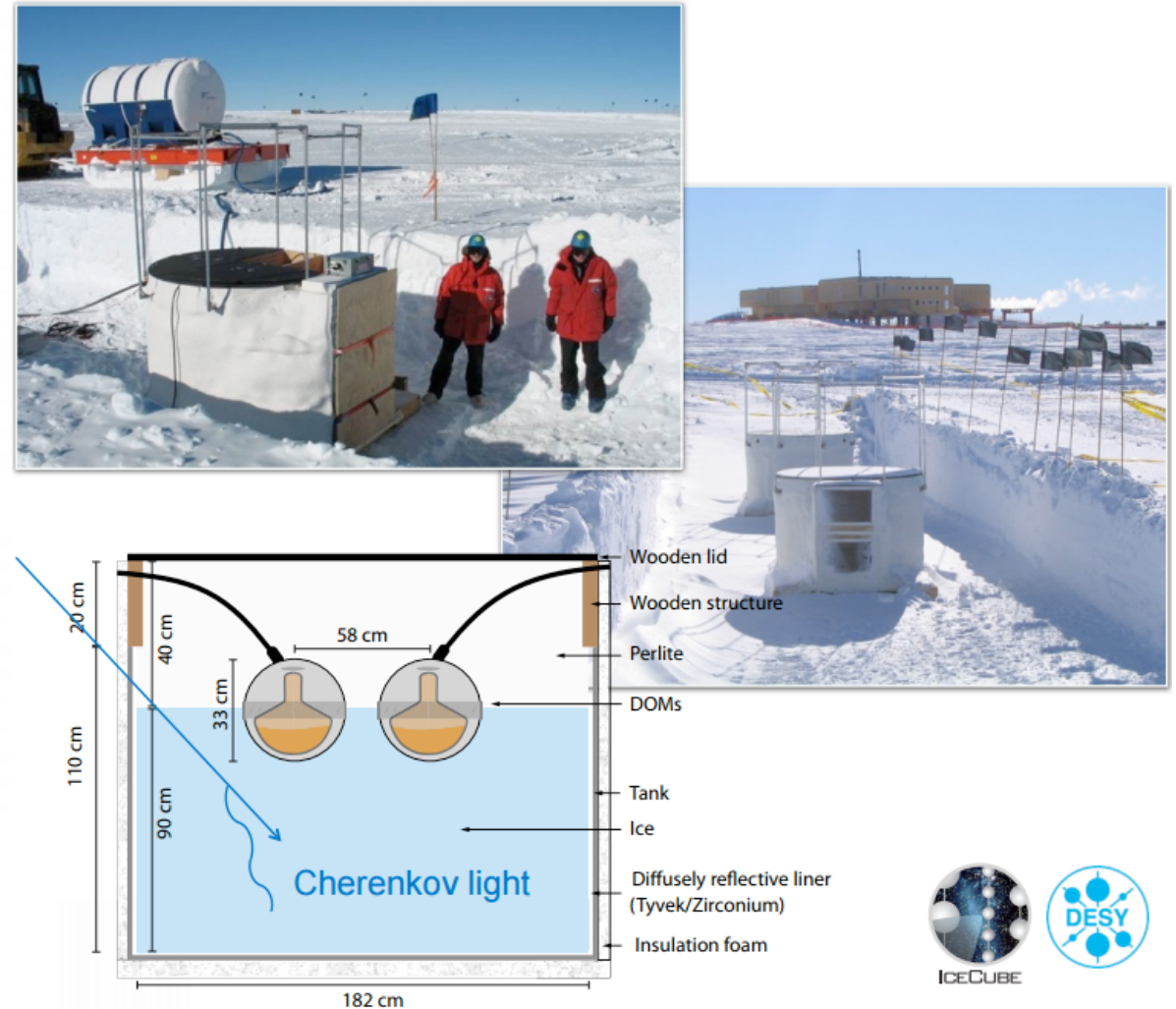
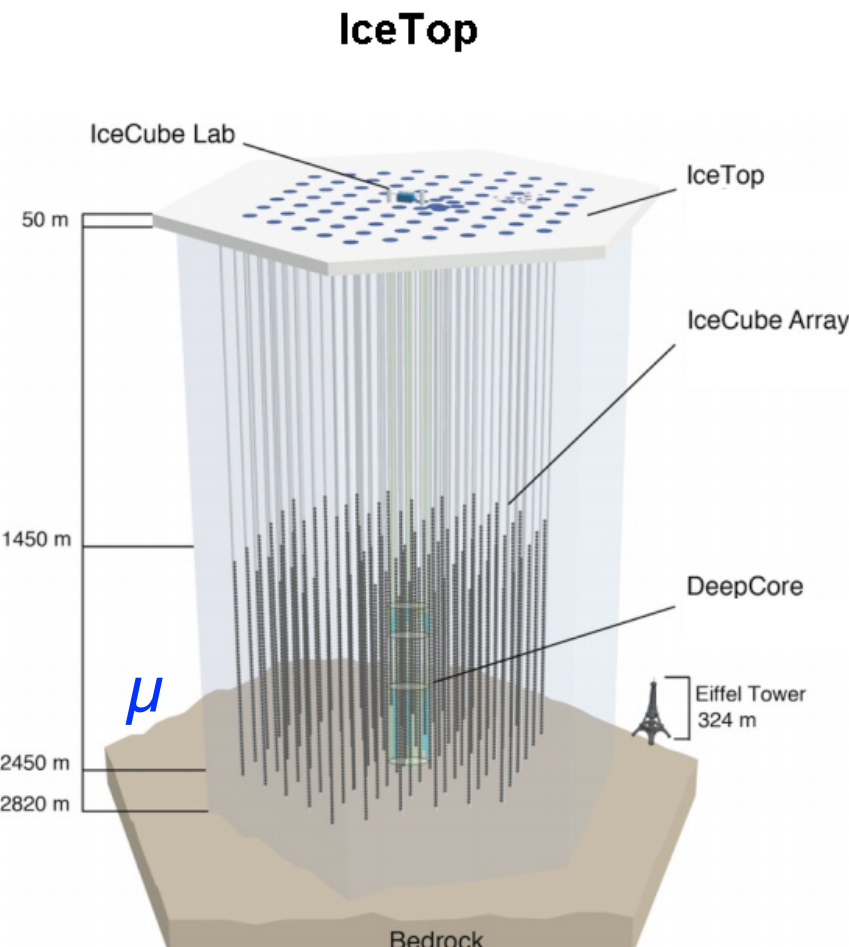
knee 4 PeV

26 * 4 PeV

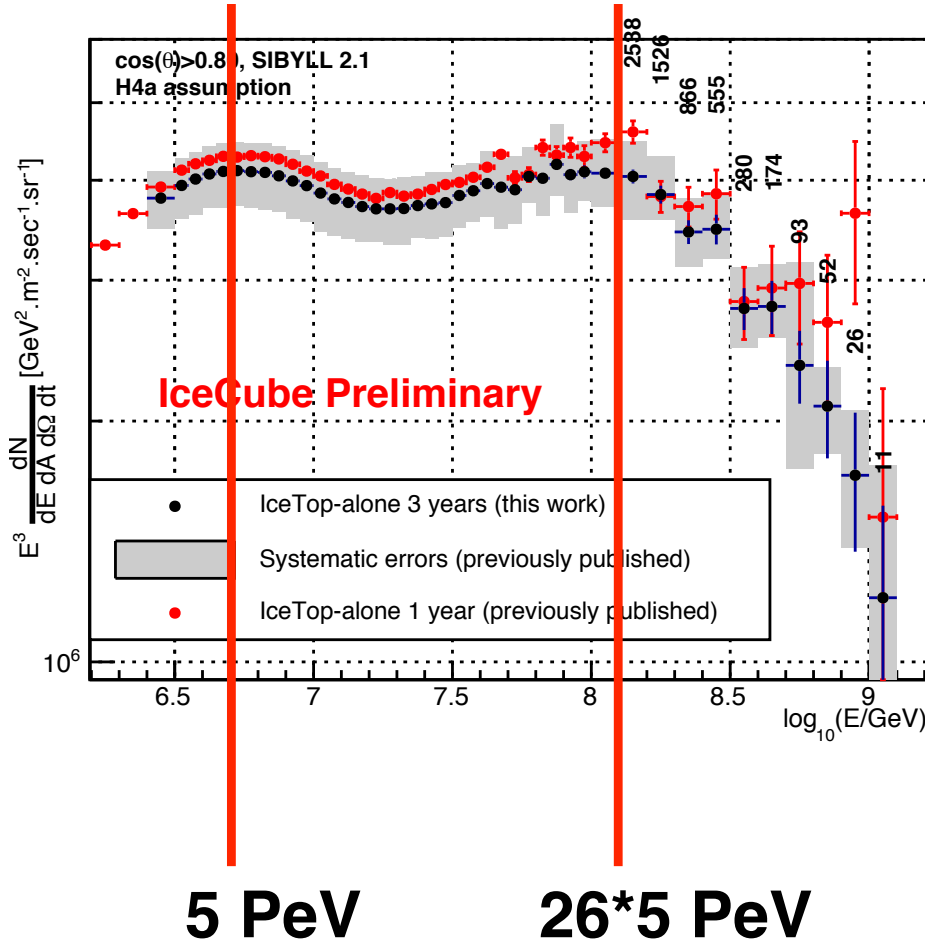


Ice Cube - Ice Top

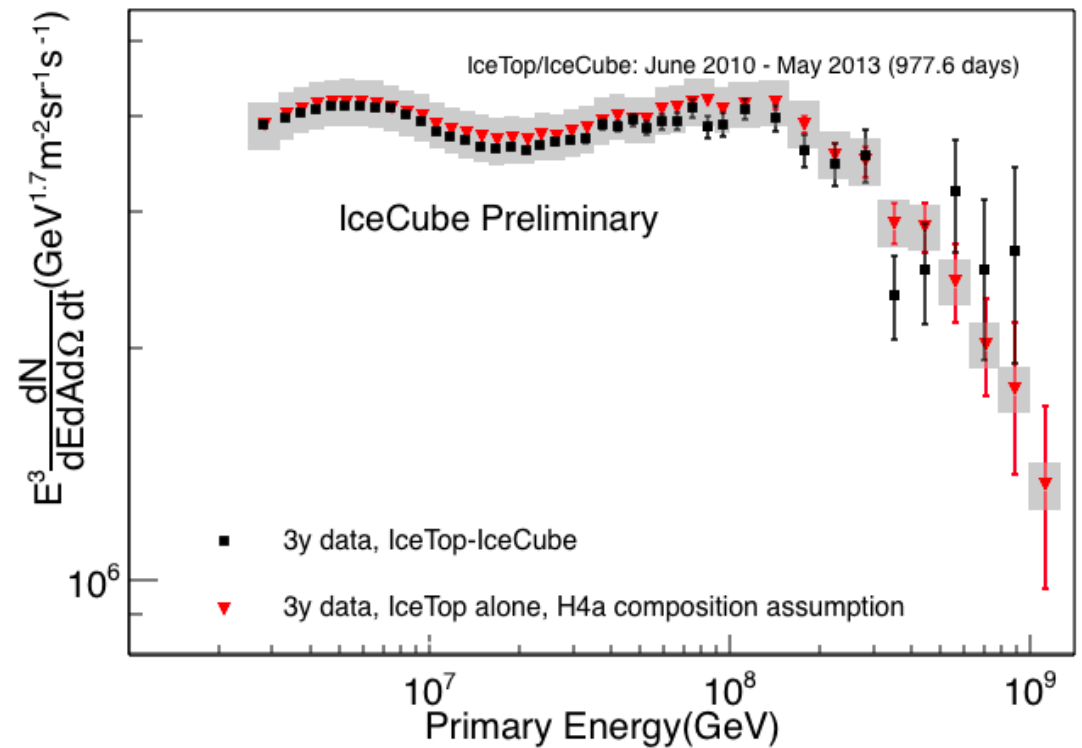
e/m (+ μ)



Ice Cube - Ice Top

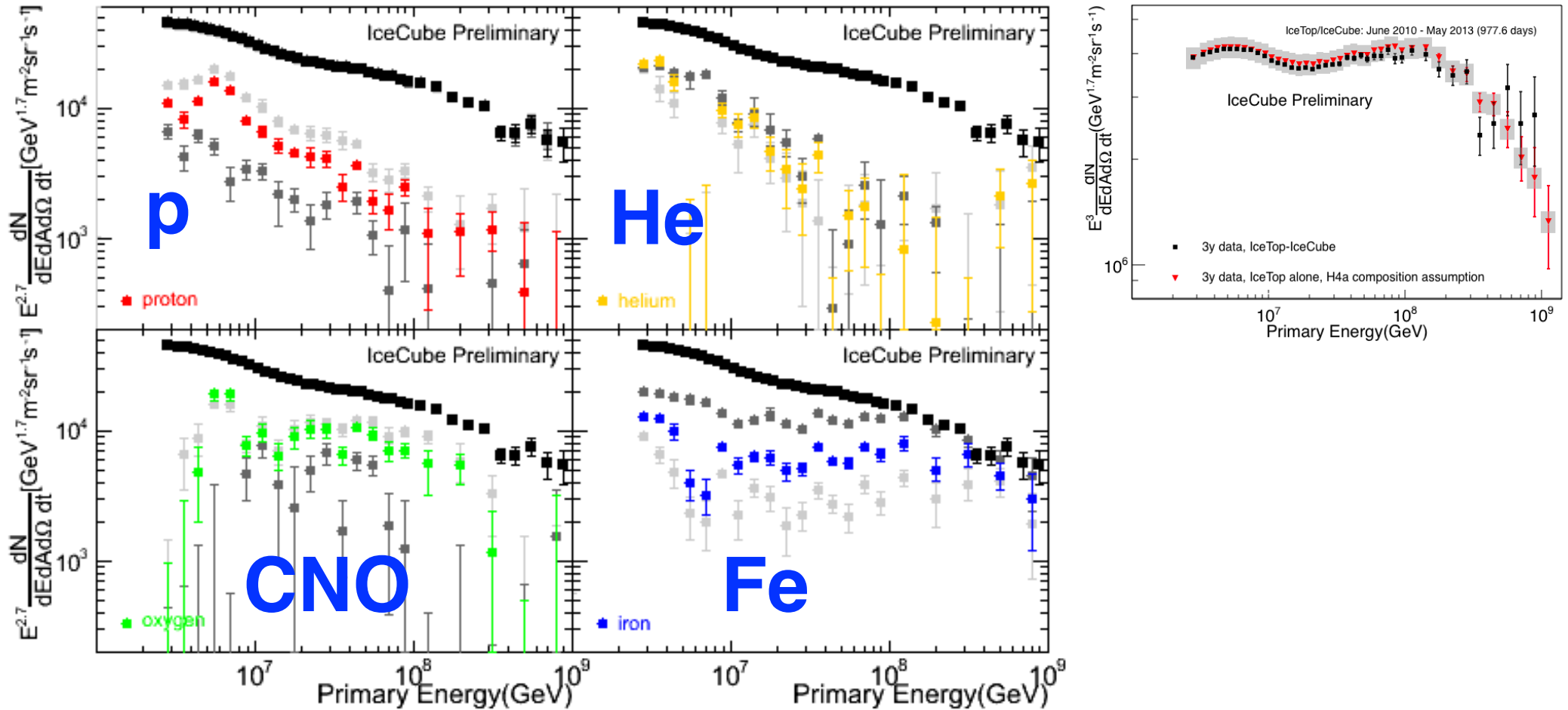


Ice Top only

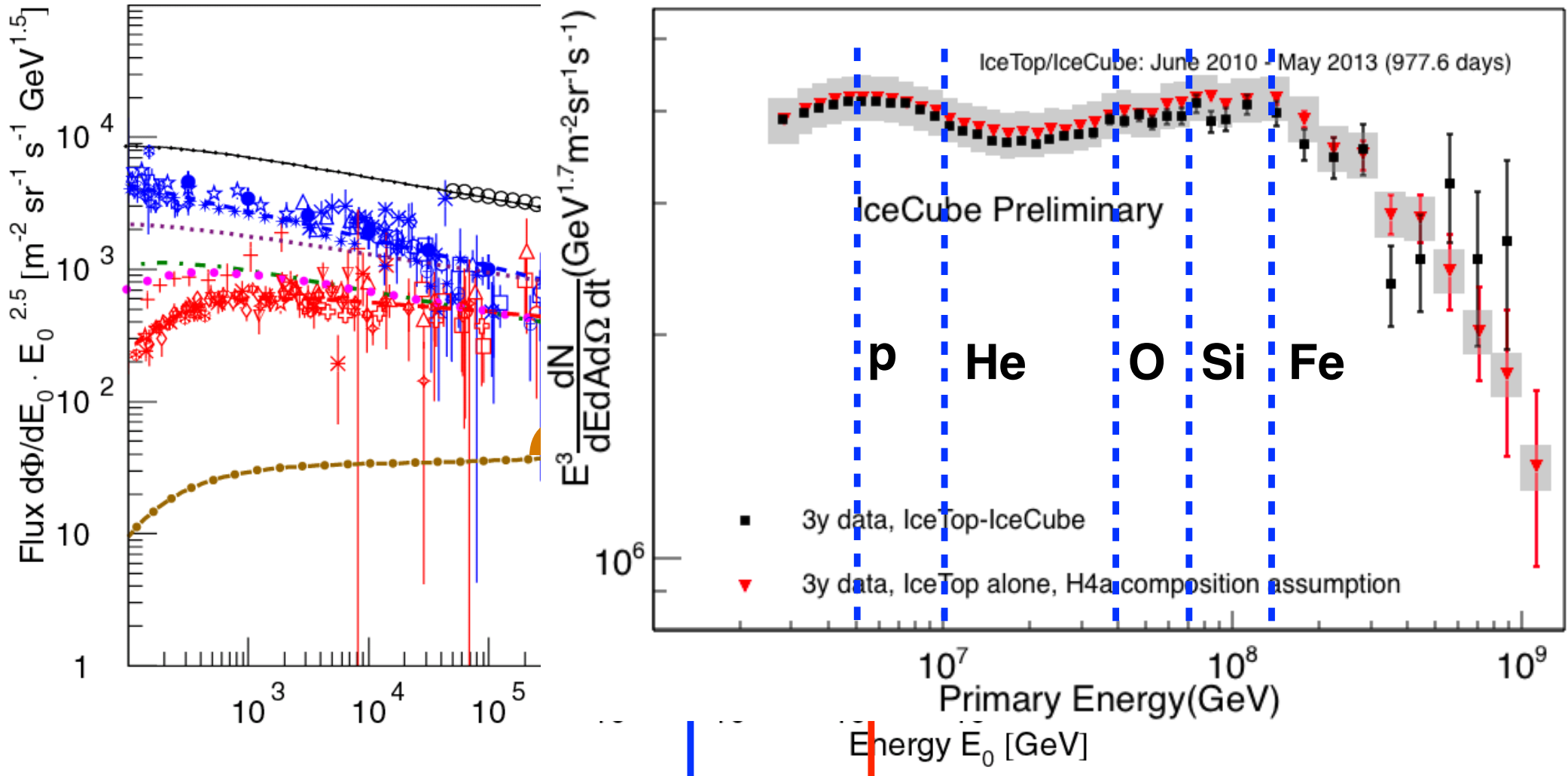


combined

Ice Cube - Ice Top



Cosmic-ray energy spectrum



TALE (TA low-energy extension)

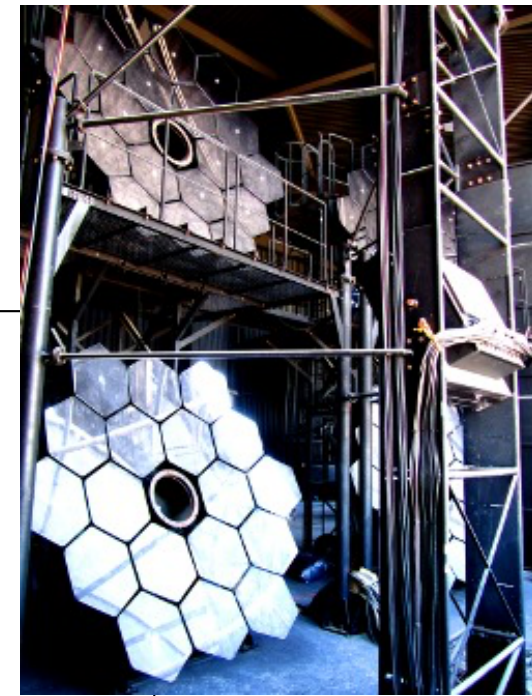
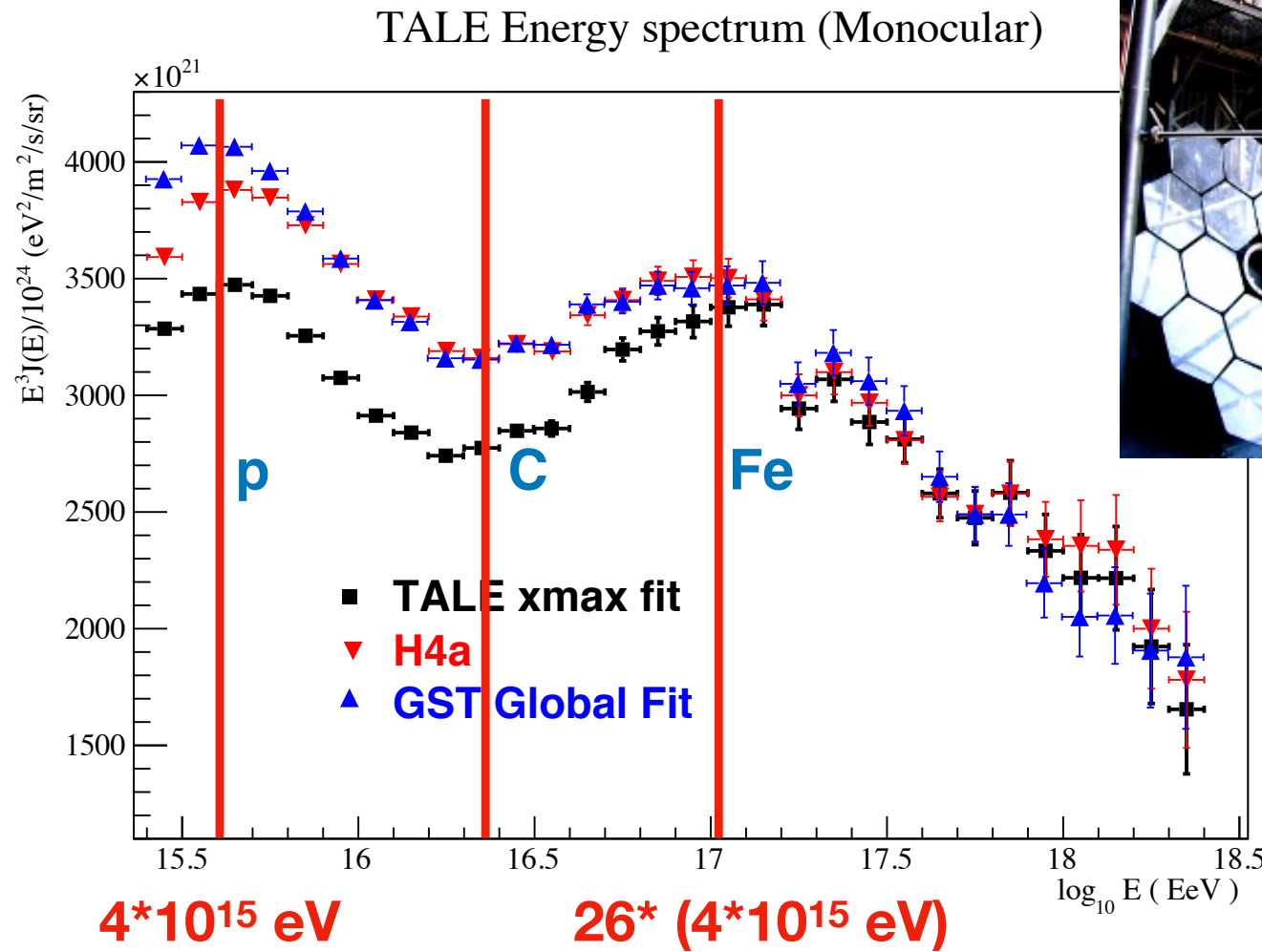
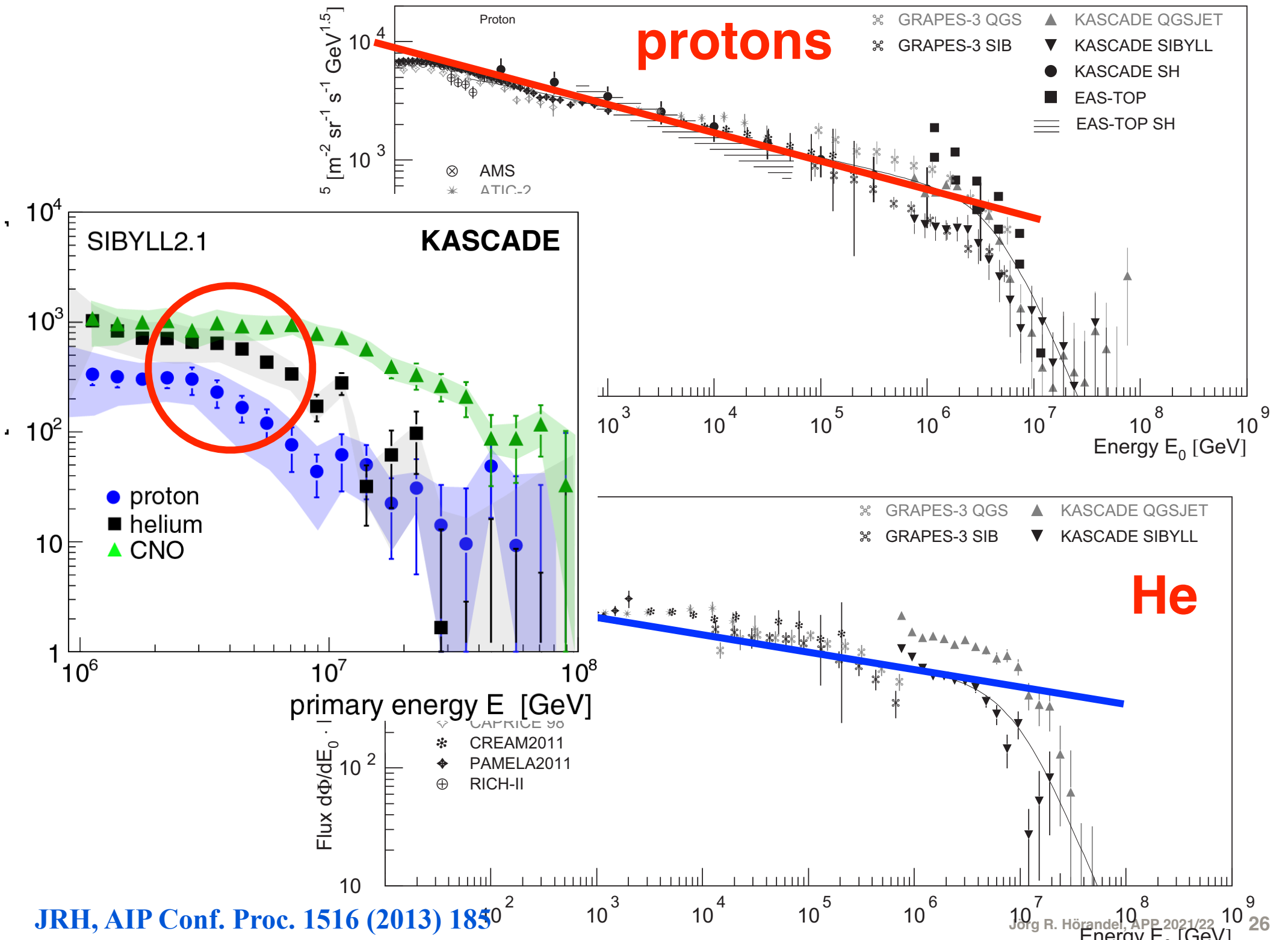
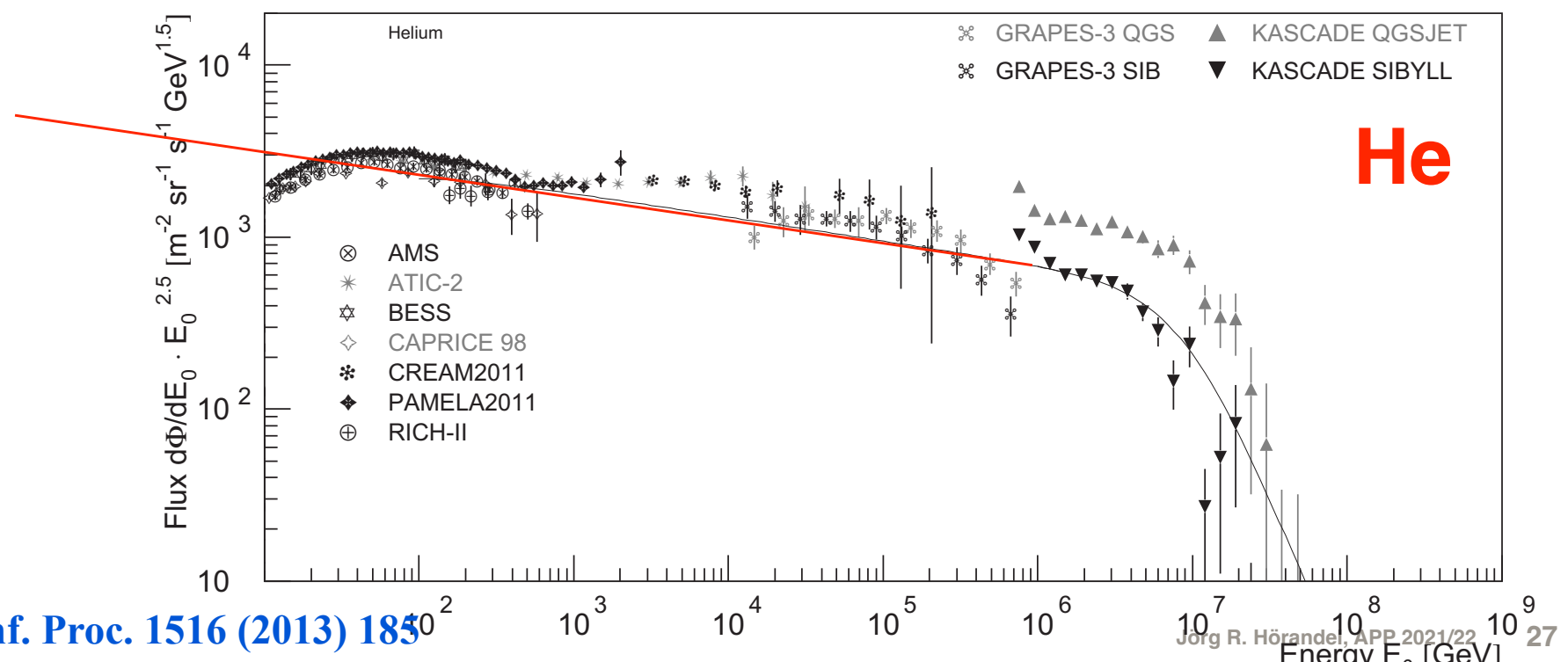
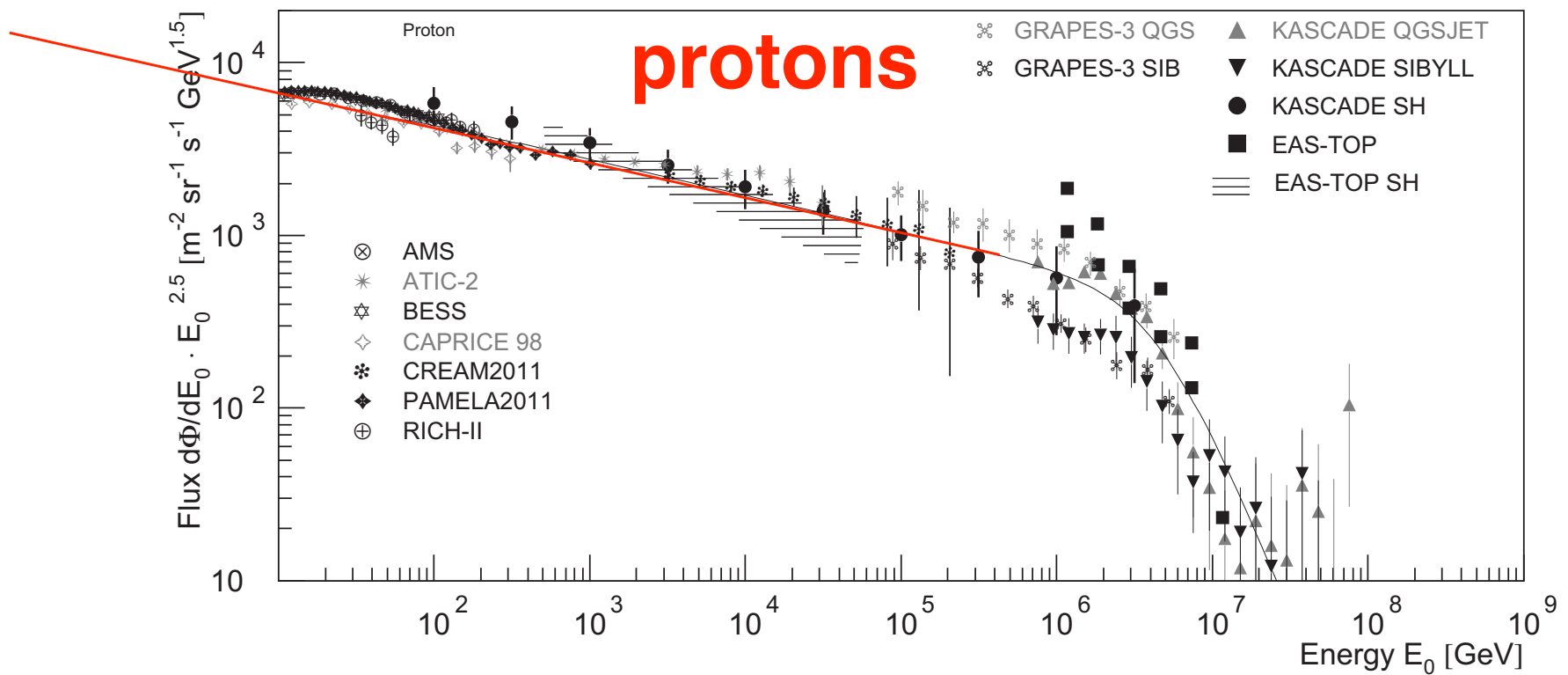


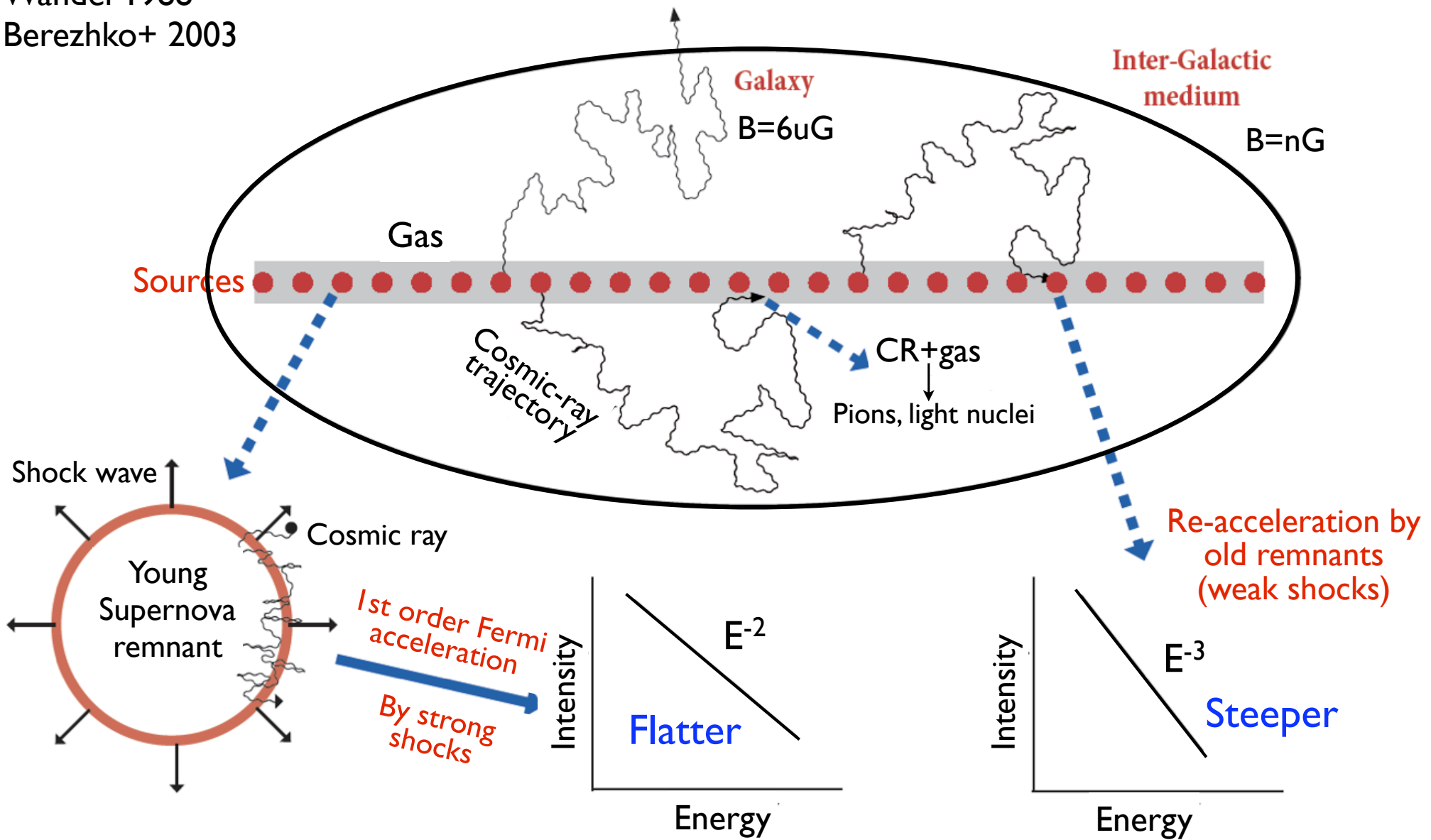
Figure 3: TALE Cosmic rays energy spectrum measured with TALE. The result is based on a QGSJet II-3 hadronic model assumption. A mixed primary composition given by the H4a, and “global fit” models, as well as a TALE derived mix was used in the calculations.





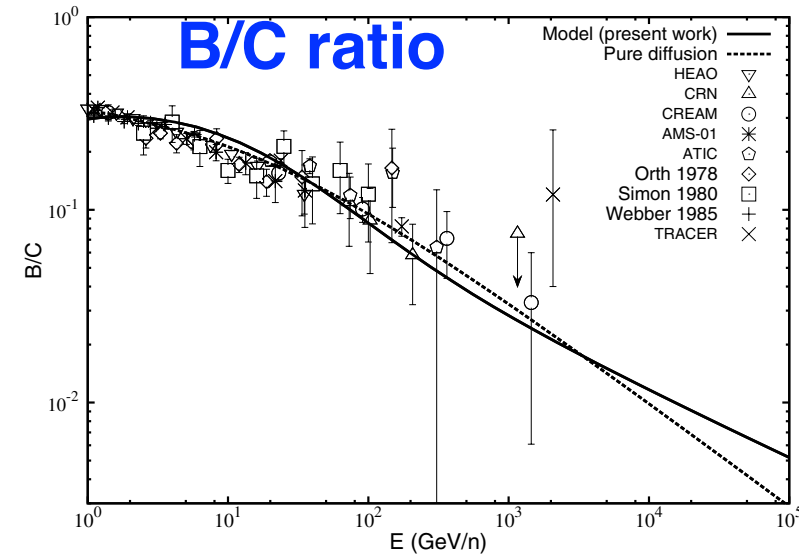
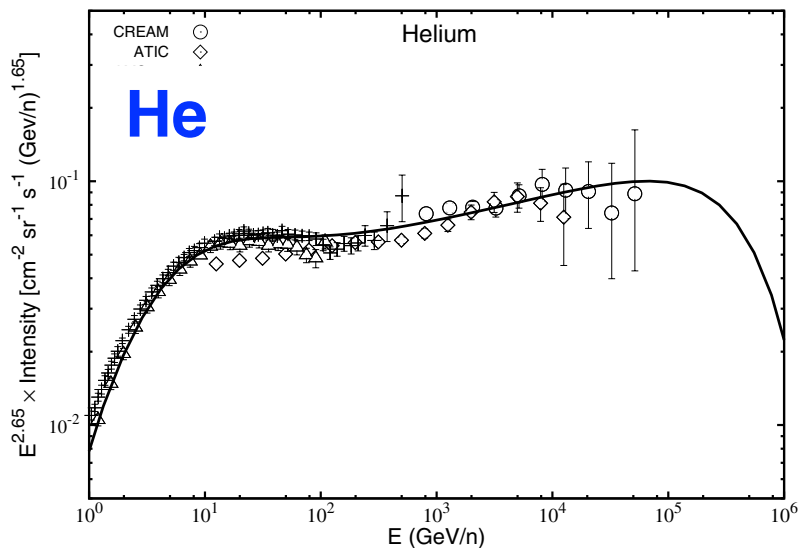
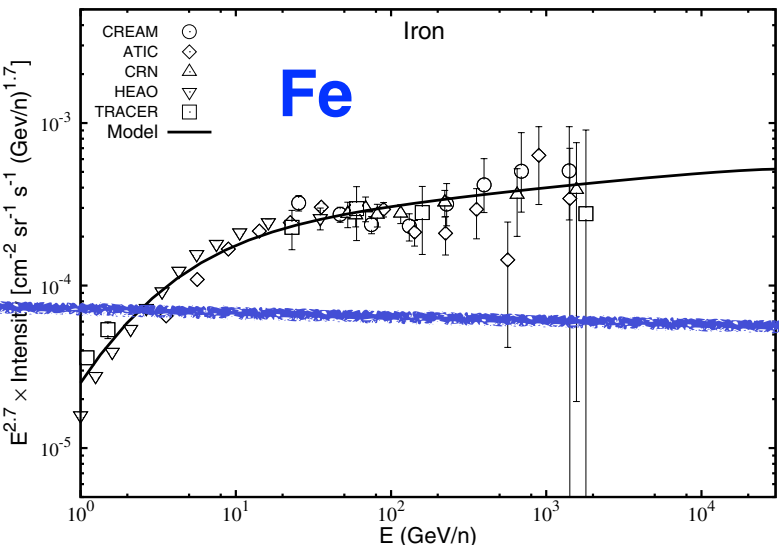
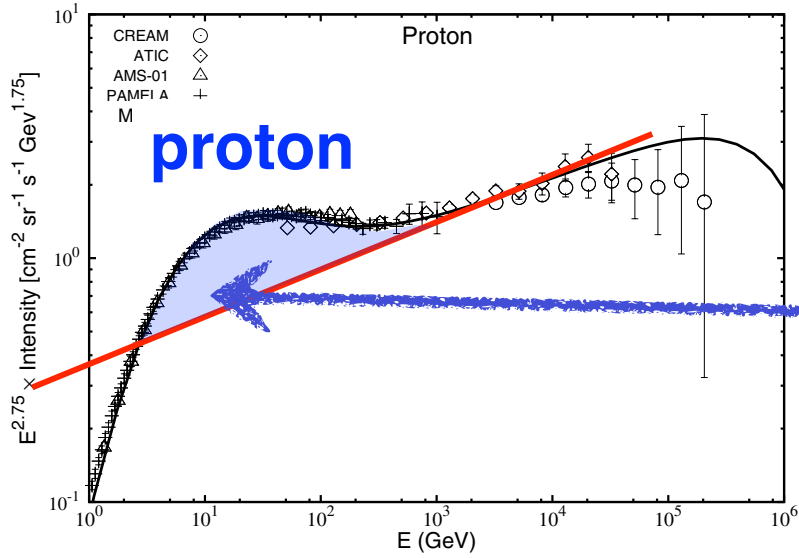
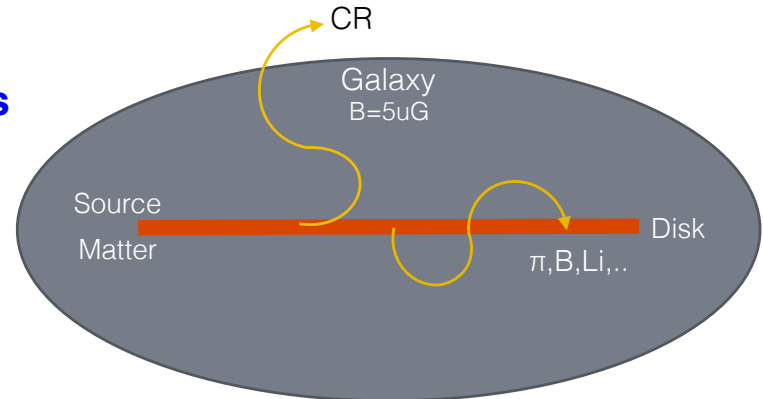
The re-acceleration model

Wandel 1988
Berezhko+ 2003



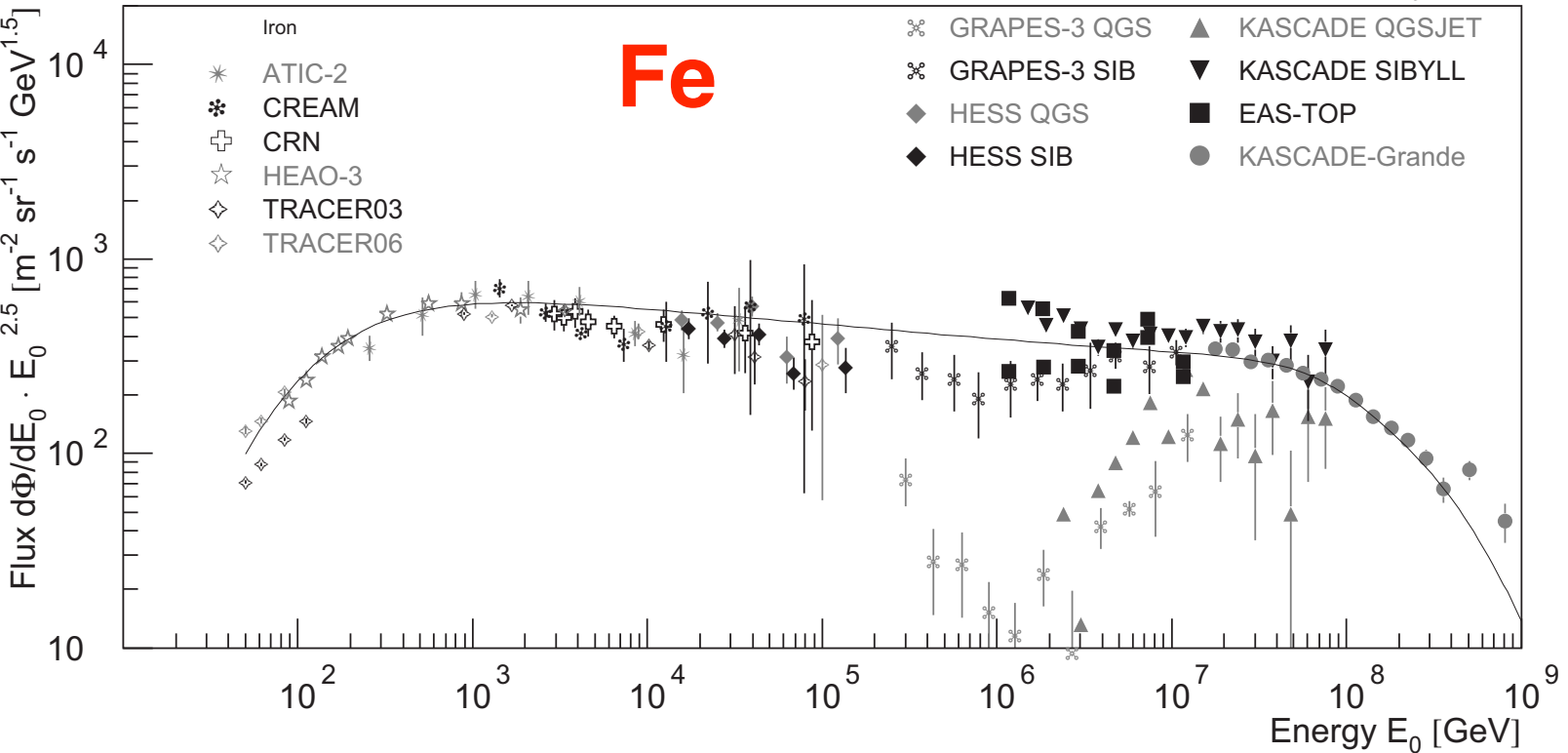
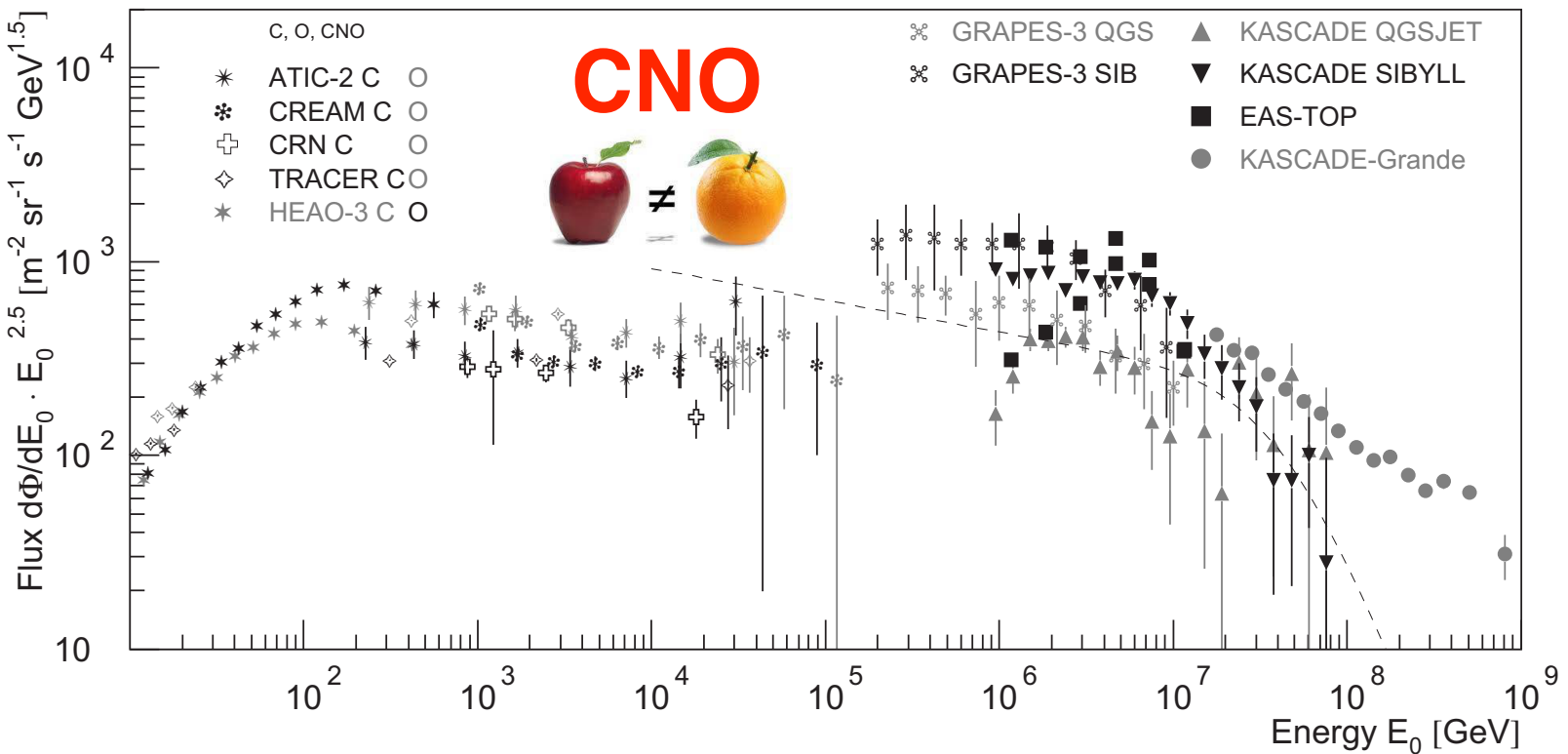
GeV-TeV cosmic-ray spectral anomaly as due to reacceleration by weak shocks in the Galaxy*

Satyendra Thoudam and Jörg R. Hörandel



bump due to
 reacceleration
 by weak
 shocks in the
 Galaxy





Transport equation for cosmic rays in the Galaxy

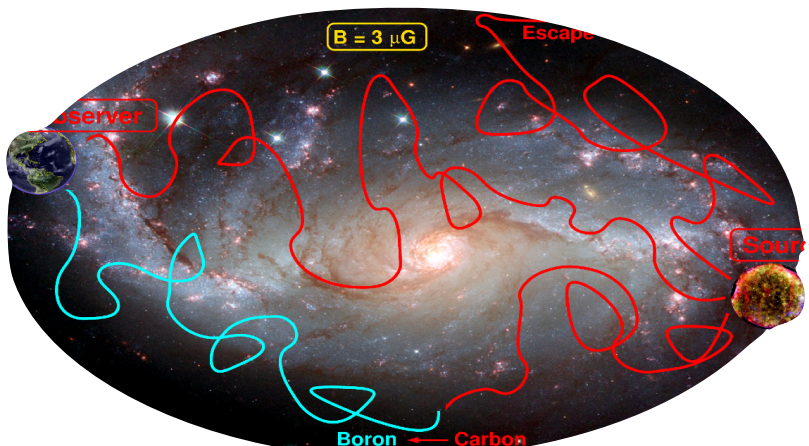
diffusion

energy loss (Bethe Bloch)

loss through interactions
with ISM (spallation)

loss through radioactive decay

$$\frac{\partial N_i}{\partial t} = \nabla(D_i \nabla N_i) - \frac{\partial}{\partial E}(b_i N_i) - n\nu\sigma_i N_i - \frac{N_i}{\gamma\tau_i} + Q_i + \sum_{j>i} n\nu\sigma_{ij} N_j + \sum_{j>i} \frac{N_j}{\gamma_j\tau_{ij}}$$



source term

production through spallation
of heavy nuclei

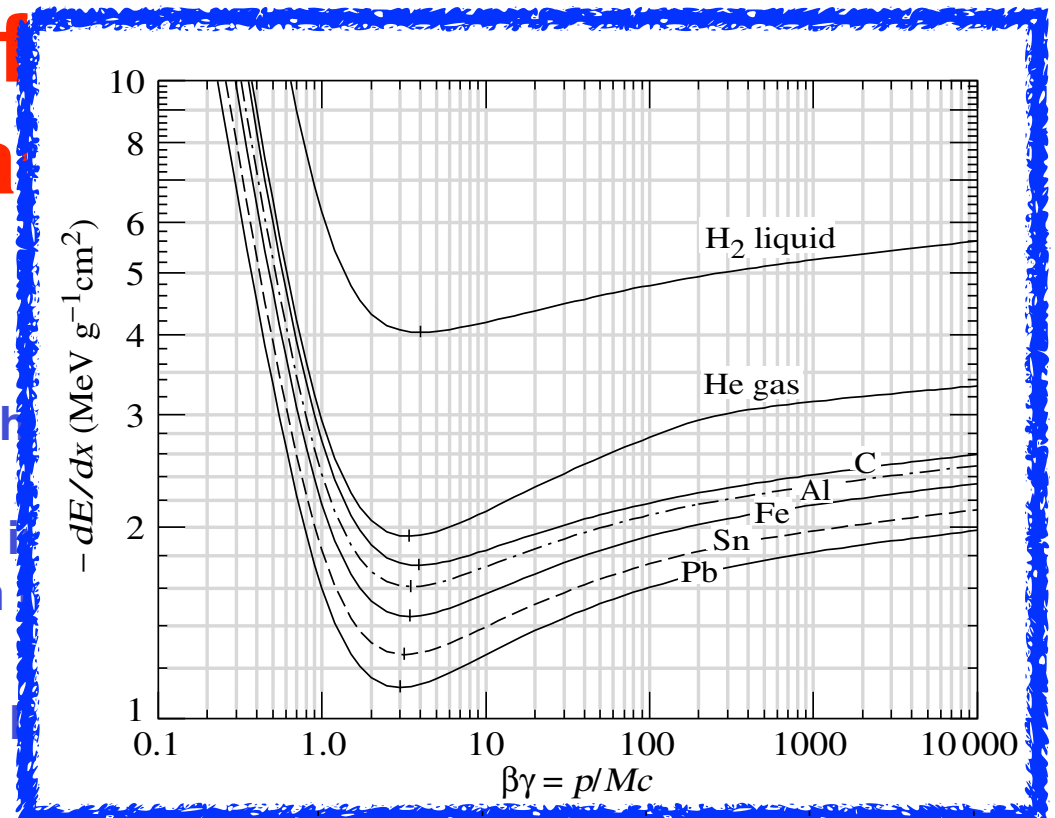
production through decay
of heavy nuclei

Transport equation for GCRs

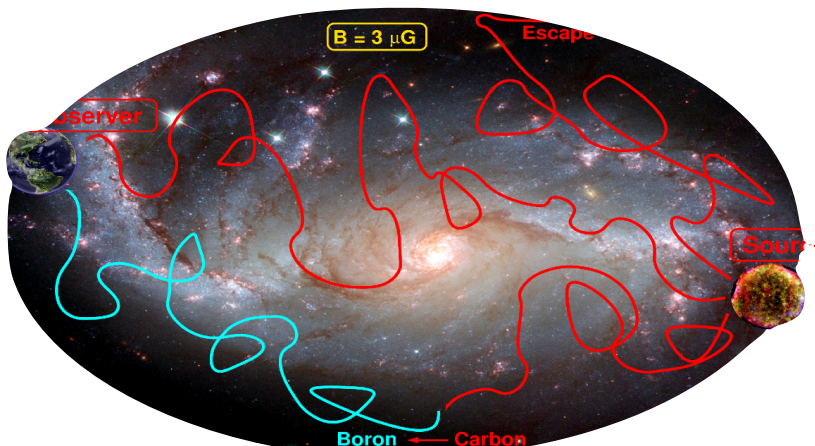
diffusion

energy loss (Bethe Bloch)

loss through interaction with matter



$$\frac{\partial N_i}{\partial t} = \nabla(D_i \nabla N_i) - \cancel{\frac{\partial}{\partial E}(\beta_i N_i)} - n\nu\sigma_i N_i - \frac{N_i}{\gamma\tau_i} + Q_i + \sum_{j>i} n\nu\sigma_{ij} N_j + \sum_{j>i} \frac{N_j}{\gamma_j\tau_{ij}}$$



source term

production through spallation
of heavy nuclei

production through decay
of heavy nuclei

Transport equation for cosmic rays in the Galaxy

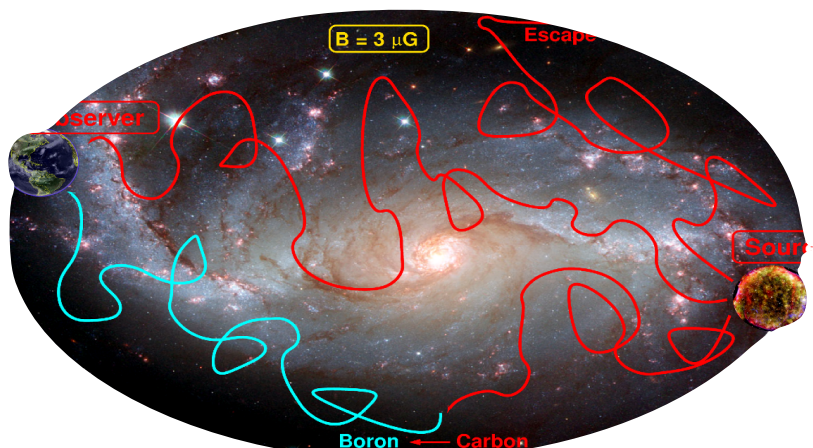
diffusion

energy loss (Bethe Bloch)

loss through interactions
with ISM (spallation)

loss through radioactive decay

$$\frac{\partial N_i}{\partial t} = \nabla(D_i \nabla N_i) - \frac{\partial}{\partial E}(\beta_i N_i) - n\nu\sigma_i N_i - \frac{N_i}{\gamma\tau_i} + Q_i + \sum_{j>i} n\nu\sigma_{ij} N_j + \sum_{j>i} \frac{N_j}{\gamma_j\tau_{ij}}$$

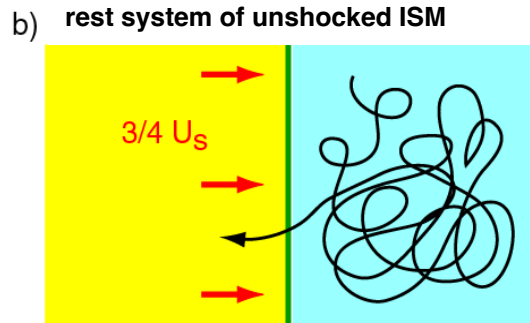
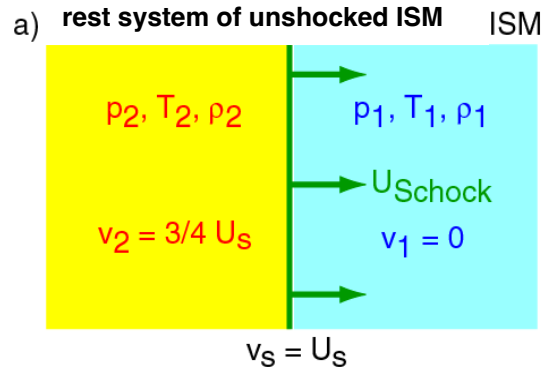


source term

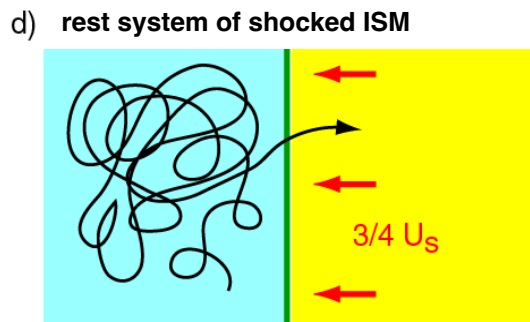
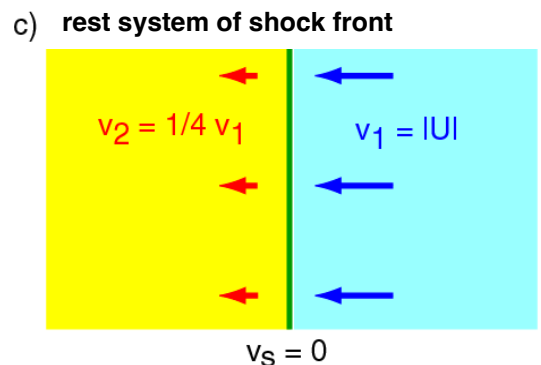
production through spallation
of heavy nuclei

production through decay
of heavy nuclei

1st order Fermi acceleration at strong shock



Bell, Blanford, Ostriker (1978)

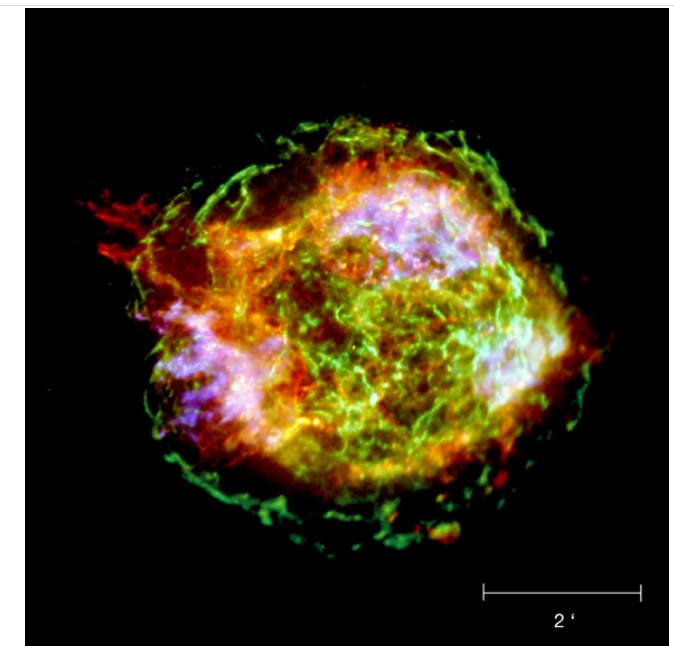


energy gain

$$\frac{\Delta E}{E} \propto \frac{U_s}{c}$$

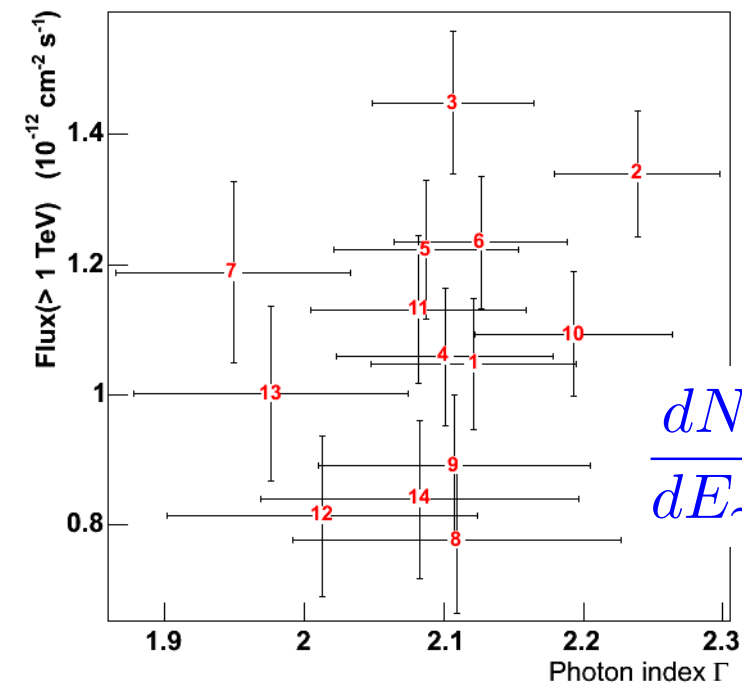
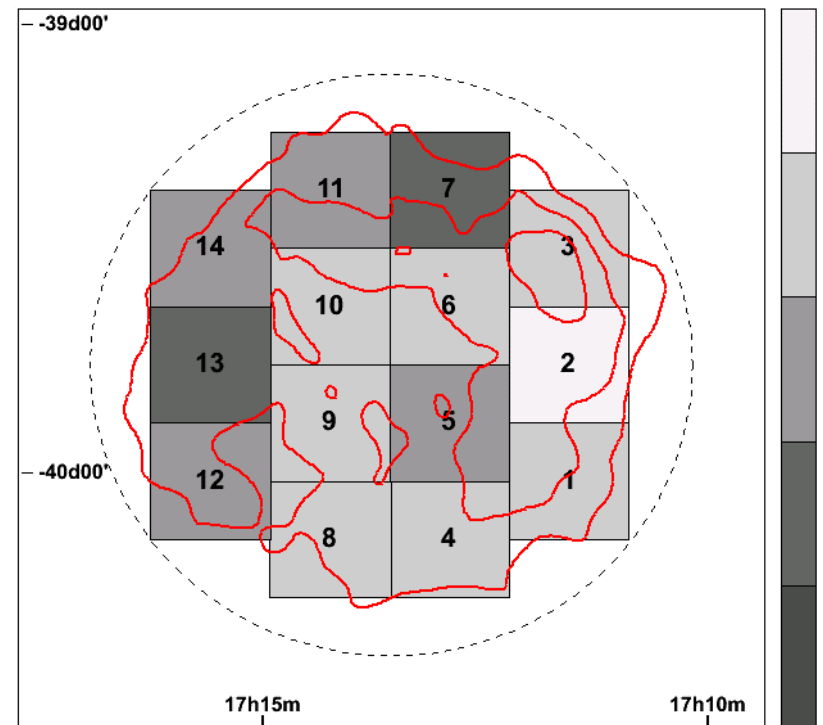
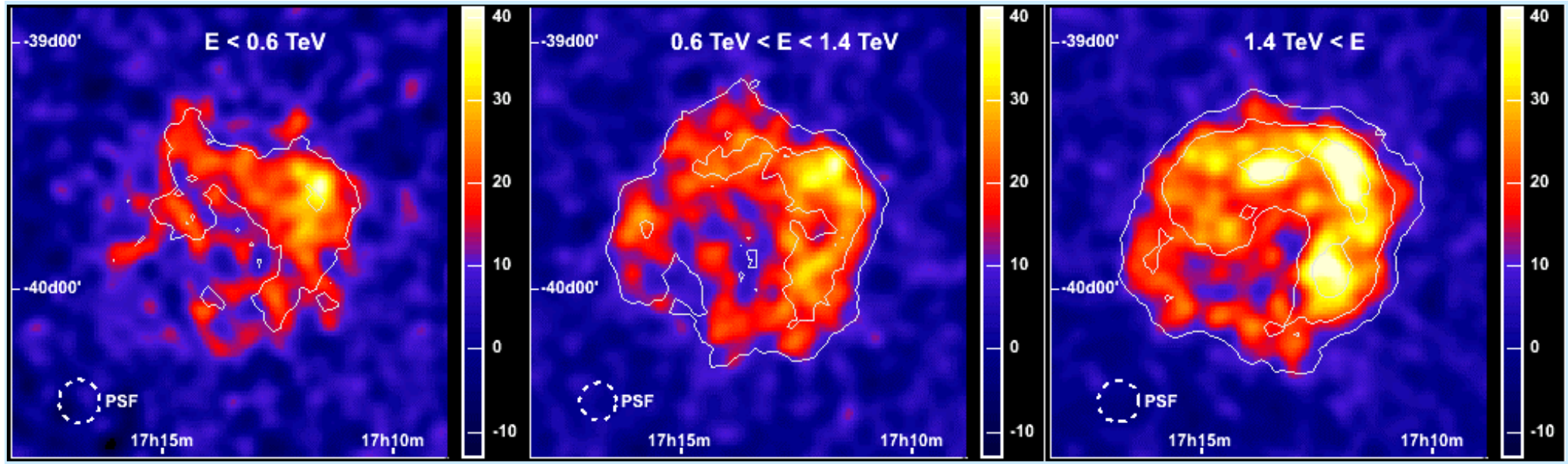
→ $N(E) dE \propto E^{-2} dE$

power law with spectral index
-2.0 ... -2.1



Supernova remnant (SNR) Cassiopeia A

H.E.S.S. supernova remnant RXJ 1713



$$\frac{dN}{dE_\gamma} \propto E_\gamma^{-\Gamma}$$

Acceleration of cosmic rays at SNR

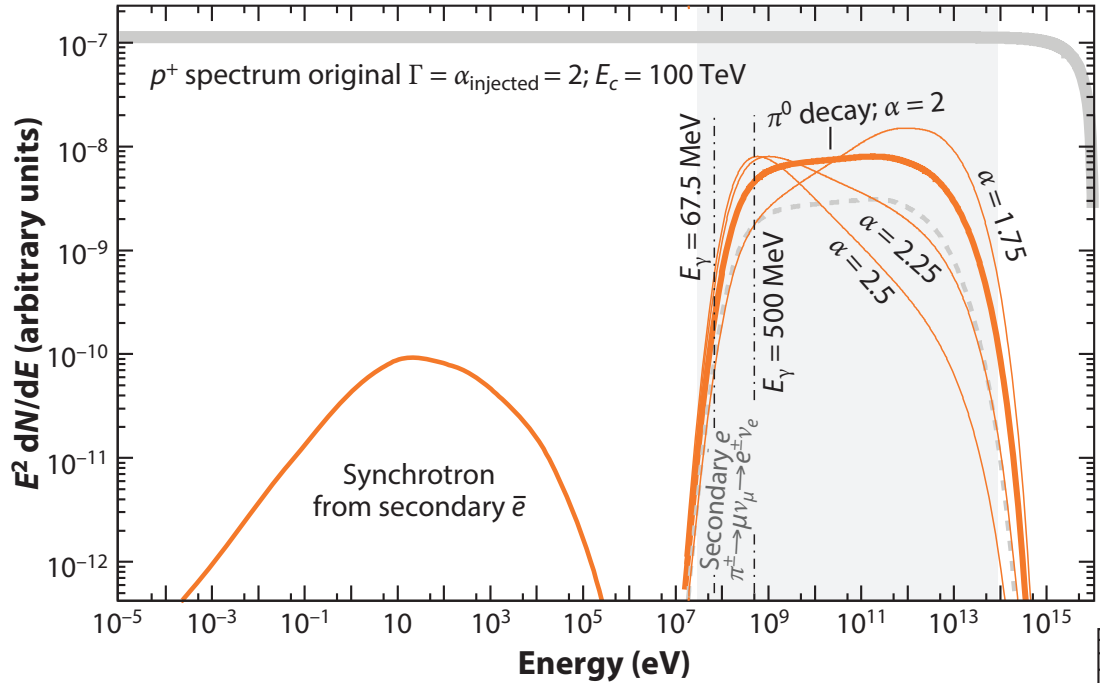


Figure 3

Spectral energy distribution of accelerated protons (power-law index $\alpha_{\text{injected}} = 2.0$ and cutoff at 100 TeV) and γ -rays resulting from inelastic collisions with interstellar material. The dominant emission into photons occurs via the decay $\pi^0 \rightarrow \gamma\gamma$ (solid orange curves). The γ -ray spectrum follows the parent protons' spectrum rather closely in the midenergy range and in the high-energy cutoff region. For all proton indices, the low-energy turnover is a characteristic feature of the pion-decay emission. Also shown is the spectrum of electrons resulting from the inelastic proton–proton interactions via the decay chain $\pi^\pm \rightarrow \mu^\pm + \nu_\mu \rightarrow e^\pm + \nu_e$ (dashed gray curve). For the synchrotron emission from these so-called secondary electrons, a source with age $t_{\text{age}} = 1,000$ years and $B = 30 \mu\text{G}$ have been assumed. The shaded gray region shows the sensitive range of current γ -ray detectors (*Fermi*-LAT, imaging atmospheric Cherenkov detectors).

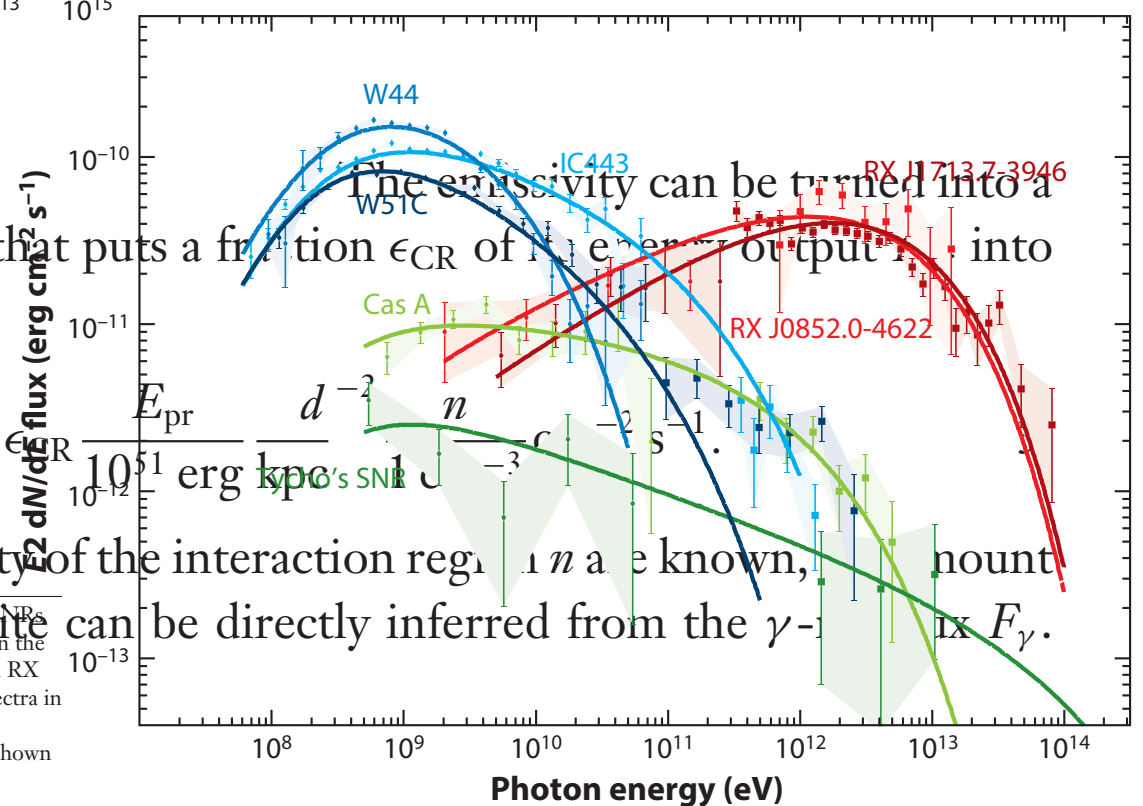
flux at Earth by an astrophysical accelerator that puts a fraction ϵ_{CR} of the energy output E_{CR} into the acceleration of protons:

$$F_\gamma(>100 \text{ MeV}) = 4.4 \times 10^{-7} \epsilon_{\text{CR}} E_{\text{pr}}^{2-\Gamma} \text{ erg cm}^{-2} \text{ s}^{-1}$$

In other words, if the distance d and the density of energy in protons E_{pr} at the interaction site can be directly inferred from the γ -ray flux F_γ .

Figure 6

Typical γ -ray energy spectra for several of the most prominent supernova remnants (SNRs). Young SNRs (<1,000 years) are shown in green. These typically show smaller γ -ray fluxes but rather hard spectra in the GeV and TeV bands. The older (but still referred to as young) shell-type SNRs RX J1713.7-3946 and RX J0852.0-4622 (Vela Junior) of ages $\sim 2,000$ years are shown in shades of red. These show very hard spectra in the GeV band ($\Gamma = 1.5$) and a peak in the TeV band with an exponential cutoff beyond 10 TeV. The middle-aged SNRs ($\sim 20,000$ years) interacting with molecular clouds (W44, W51C, and IC443) are shown in blue. Also shown are hadronic fits to the data (solid lines).



general considerations about accelerators

trajectory of particle in B field

centripetal force = Lorentz force

$$m \frac{v^2}{r} = q \cdot v \cdot B \quad m \cdot v = p \quad \textbf{momentum}$$

$$\frac{p}{r} = Z \cdot e \cdot B$$

$$r_L = \frac{p}{Z \cdot e \cdot B} \quad \textbf{Larmor radius}$$

L dimension of accelerator

$$L > 2 r_L$$

closer look (Hillas 1984):

$$L > \frac{2r_L}{\beta}$$

velocity of scattering centers

$$\beta = \frac{v}{c}$$

$$L > \frac{2 \cdot p}{z \cdot e \cdot B \cdot \beta}$$



$$B \cdot L > \frac{2 \cdot p}{z \cdot e \cdot \beta}$$

Hillas criterion

in astrophysical units

$$r_L = 1.08 \text{ pc} \frac{E_{15}}{Z \cdot B_{\mu G}}$$

$$B_{\mu G} \cdot L_{pc} > \frac{2 \cdot E_{15}}{Z \cdot \beta}$$

**necessary condition
not sufficient**

$$E_{15} < Z \cdot B_{\mu G} \cdot L_{pc} \cdot \frac{\beta}{2}$$

Contribution of (regular) SNR-CR

$$E_c = Z \cdot 4.5 \cdot 10^6 \text{ GeV}$$

$$Q(p) = A Q_0 (Ap)^{-q} \exp\left(-\frac{Ap}{Z p_c}\right),$$

Table 1. Source spectral indices, q , and energy injected per supernova, f , for the different species of cosmic rays used in the calculation of the SNR-CRs spectra shown in Figures 1 and 2.

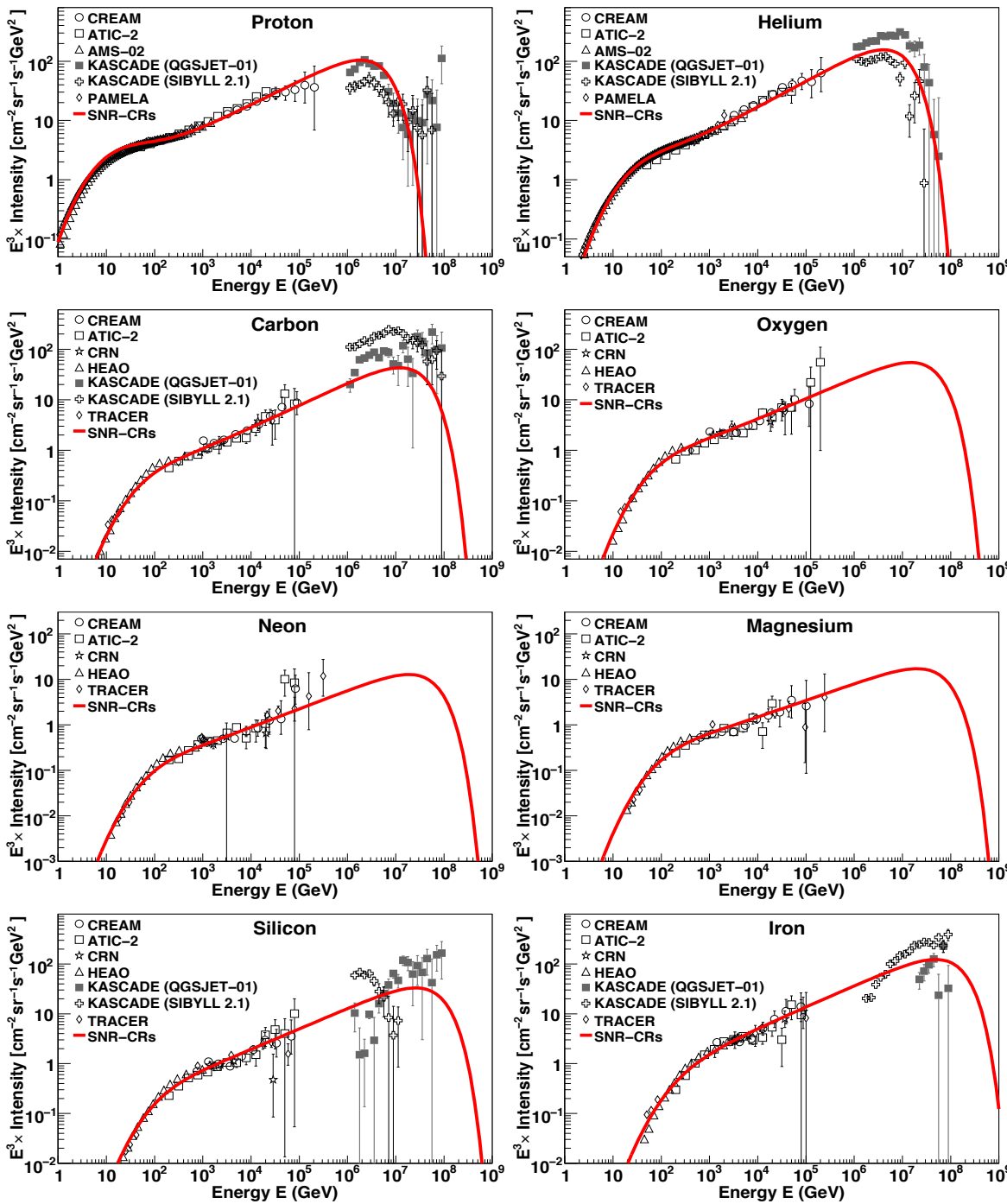
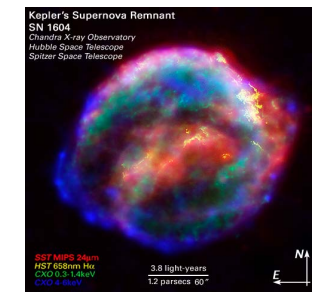


Fig. 1. Energy spectra for different cosmic-ray elements. Solid line: Model prediction for the SNR-CRs. Data: CREAM (Ahn et al. 2009; Yoon et al. 2011), ATIC-2 (Panov et al. 2007), AMS-02 (Aguilar et al. 2015a,b), PAMELA (Adriani et al. 2011), CRN (Müller et al. 1991; Swordy et al. 1990), HEAO (Engelmann et al. 1990), TRACER (Obermeier et al. 2011), and KASCADE (Antoni et al. 2005). Cosmic-ray source parameters (q, f) used in the calculation are given in Table 1. For the other model parameters (D_0, a, η, s), see text for details.



Transport equation for cosmic rays in the Galaxy

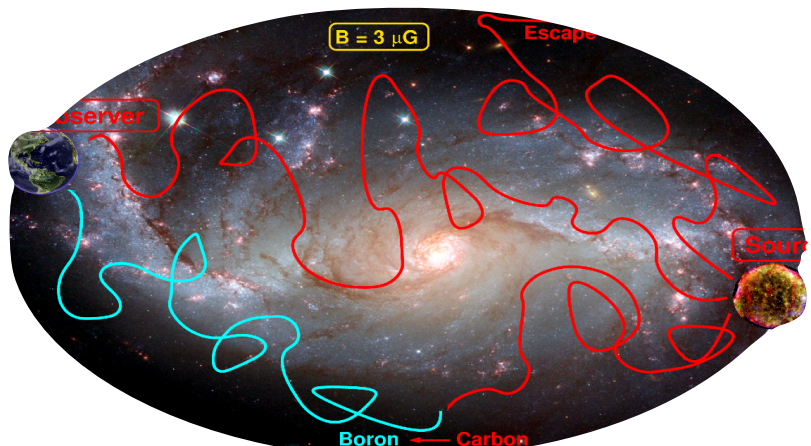
diffusion

energy loss (Bethe Bloch)

loss through interactions
with ISM (spallation)

loss through radioactive decay

$$\frac{\partial N_i}{\partial t} = \nabla(D_i \nabla N_i) - \frac{\partial}{\partial E}(\beta_i N_i) - n\nu\sigma_i N_i - \frac{N_i}{\gamma\tau_i} + Q_i + \sum_{j>i} n\nu\sigma_{ij} N_j + \sum_{j>i} \frac{N_j}{\gamma_j\tau_{ij}}$$



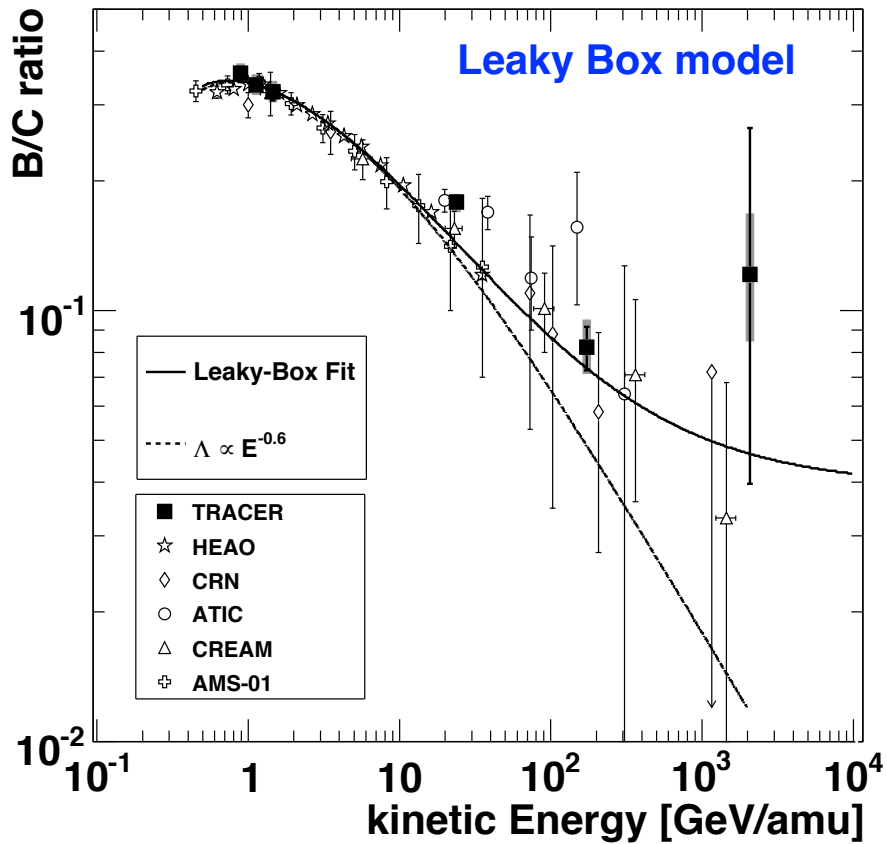
source term

production through spallation
of heavy nuclei

production through decay
of heavy nuclei

Pathlength of cosmic rays in Galaxy

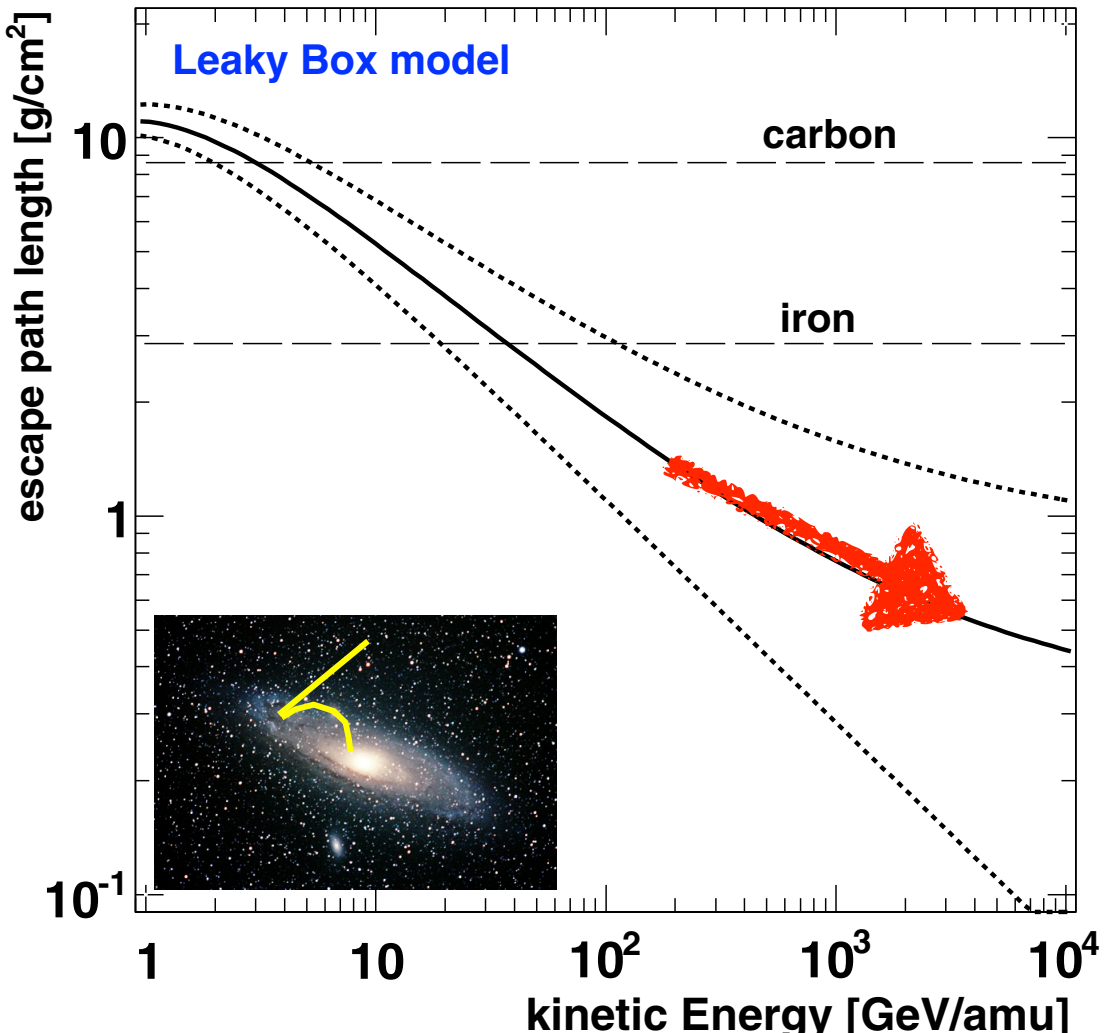
TRACER balloon experiment



Escape Path Length:

$$\Lambda_{esc}(E) = CE^{-\delta} + \Lambda_0$$

- ▶ Propagation index:
 $\delta = 0.64 \pm 0.02$.
- ▶ Residual path length:
 $\Lambda_0 = 0.7 \pm 0.2 \text{ g/cm}^2$.



$$\Lambda(R) = \frac{26.7\beta}{(\beta R)^\delta + (0.714 \cdot \beta R)^{-1.4}} + \Lambda_0 \text{ g/cm}^2,$$

Pathlength vs. interaction length

pathlength in Galaxy

$$\lambda_{esc} = 5 - 10 \text{ g/cm}^2$$

interaction length

nuclear radius

$$r = r_0 A^{1/3} \quad r_0 = 1.3 \cdot 10^{-13} \text{ cm}$$

cross section

$$\sigma_{p-A} = \pi(r_p + r_0 A^{1/3})^2$$

ISM: protons

$$n = 1/\text{cm}^3 \quad \rho = 1.67 \cdot 10^{-24} \text{ g/cm}^3$$

interaction length

$$\lambda_{p-A} = \frac{\rho}{\sigma_{p-A} \cdot n}$$

$$\lambda_{p-p} = 21 \text{ g/cm}^2 \quad > \lambda_{esc}$$

$$\lambda_{p-Fe} = 1.6 \text{ g/cm}^2 \quad < \lambda_{esc}$$

Shape of energy spectrum

$$\frac{dN}{dE} \propto E_0^\gamma$$

at source $\gamma \sim -2.1$

at Earth $\gamma \sim -2.6$ to -2.7

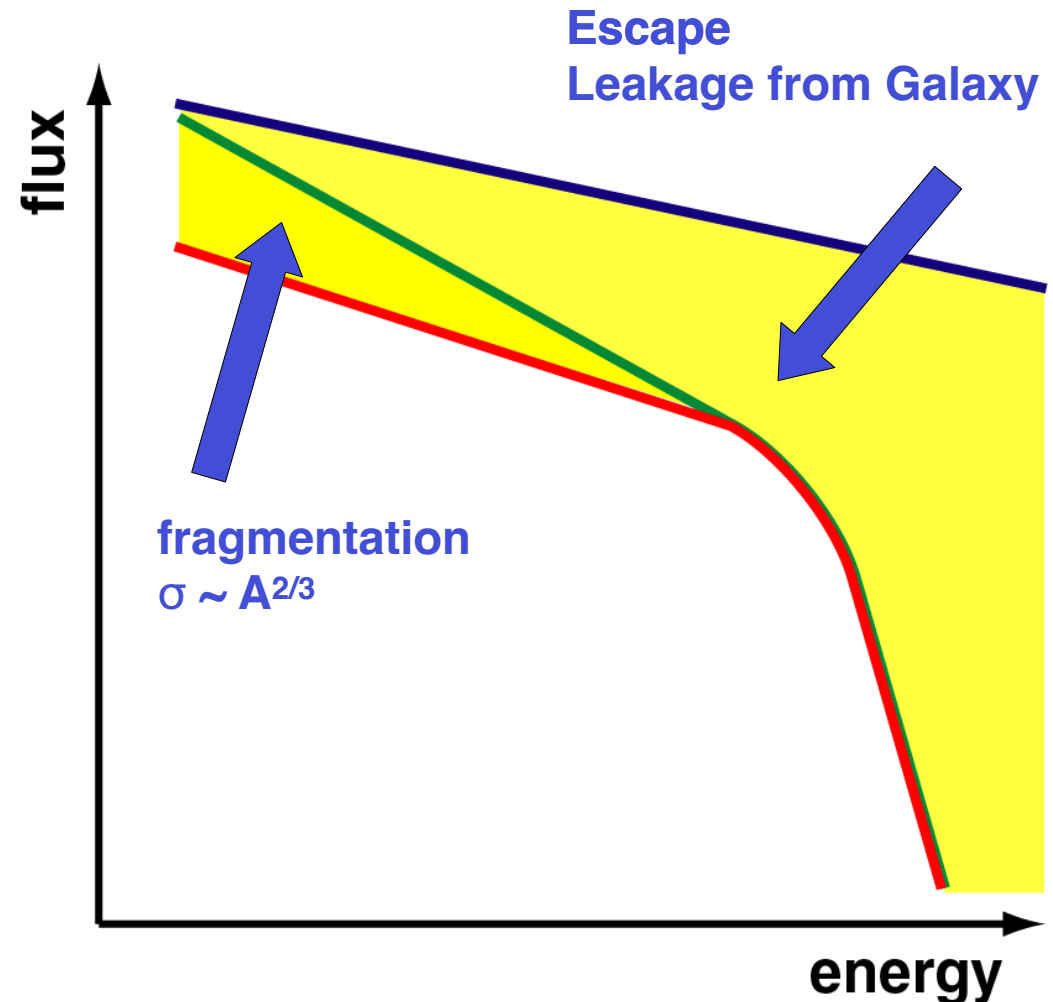
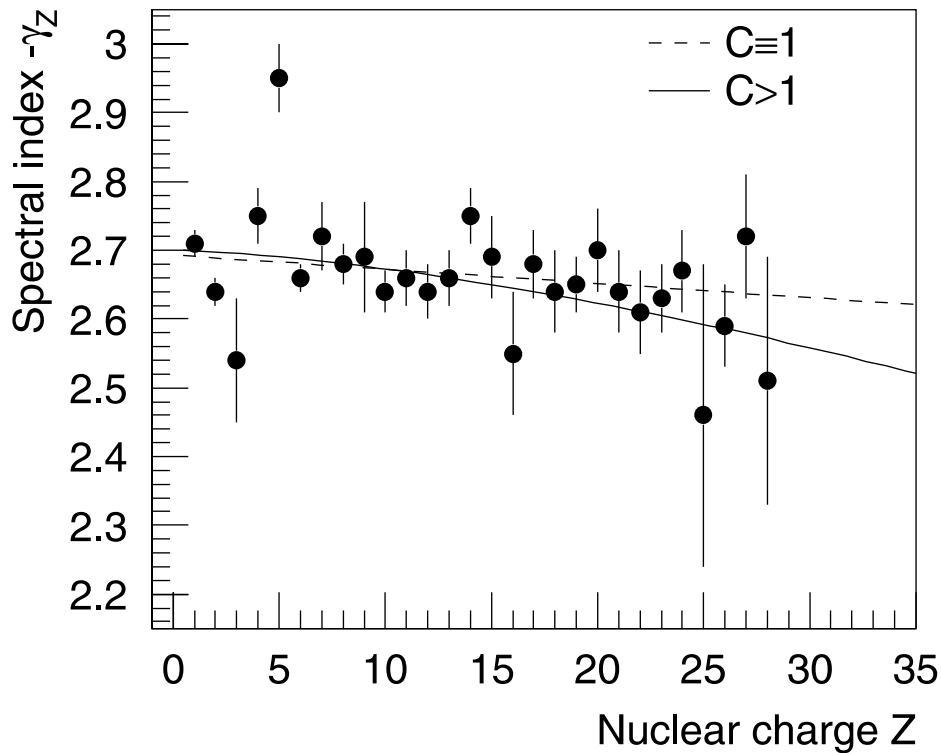
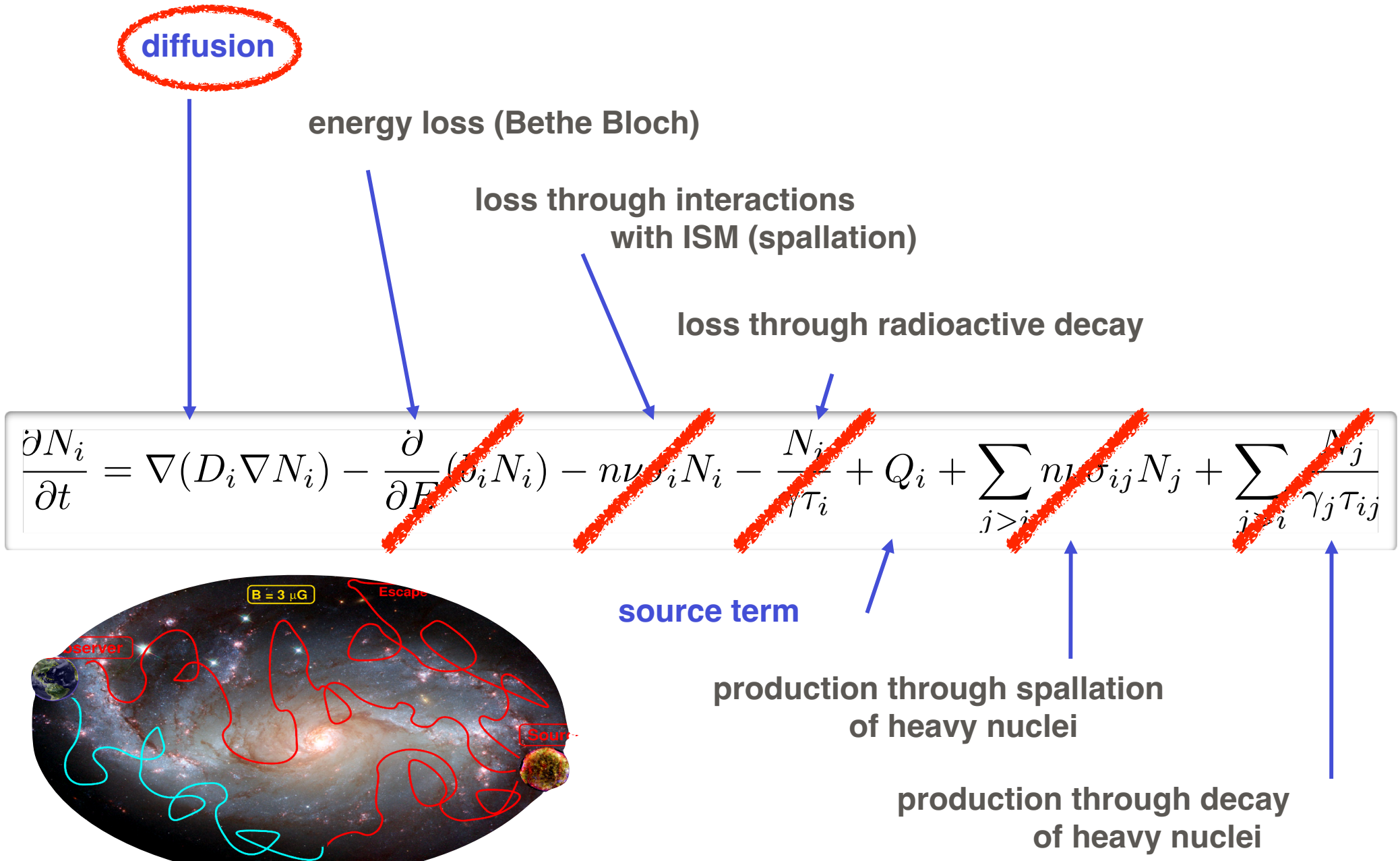


Fig. 5. Spectral index γ_Z versus nuclear charge Z (see Table 1). The solid line represents a three parameter fit according to Eq. (6), the dashed graph a linear fit.

Transport equation for cosmic rays in the Galaxy





ELSEVIER

Available online at www.sciencedirect.com



ScienceDirect

Astroparticle Physics 27 (2007) 119–126

Astroparticle
Physics

www.elsevier.com/locate/astropart

example of knee due to propagation/leakage from Galaxy

Propagation of super-high-energy cosmic rays in the Galaxy

Jörg R. Hörandel ^{a,*}, Nikolai N. Kalmykov ^b, Aleksei V. Timokhin ^c

The steady-state diffusion equation for the cosmic-ray density $N(r)$ is (neglecting nuclear interactions and energy losses)

$$-\nabla_i D_{ij}(r) \nabla_j N(r) = Q(r). \quad (1)$$

$Q(r)$ is the cosmic-ray source term and $D_{ij}(r)$ the diffusion tensor.

Under the assumption of azimuthal symmetry and taking into account the predominance of the toroidal component of the magnetic field, Eq. (1) is presented in cylindrical coordinates as

$$\left[-\frac{1}{r} \frac{\partial}{\partial r} r D_{\perp} \frac{\partial}{\partial r} - \frac{\partial}{\partial z} D_{\perp} \frac{\partial}{\partial z} - \frac{\partial}{\partial z} D_A \frac{\partial}{\partial r} + \frac{1}{r} \frac{\partial}{\partial r} r D_A \frac{\partial}{\partial z} \right] N(r, z) = Q(r, z), \quad (2)$$

where $N(r, z)$ is the cosmic-ray density averaged over the large-scale fluctuations with a characteristic scale $L \sim 100$ pc [3]. $D_{\perp} \propto E^m$ is the diffusion coefficient, where m is much less than one ($m \approx 0.2$), and $D_A \propto E$ the Hall diffusion coefficient. The influence of Hall diffusion becomes predominant at high energies ($>10^{15}$ eV). The sharp

The magnetic field of the Galaxy consists of a large-scale regular and a chaotic, irregular component $\vec{B} = \vec{B}_{\text{reg}} + \vec{B}_{\text{irr}}$. A purely azimuthal magnetic field was assumed for the regular field

$$B_z = 0, \quad B_r = 0, \quad B_{\phi} = 1 \mu\text{G} \exp\left(-\frac{z^2}{z_0^2} - \frac{r^2}{r_0^2}\right),$$

where $z_0 = 5$ kpc and $r_0 = 10$ kpc are constants [3].

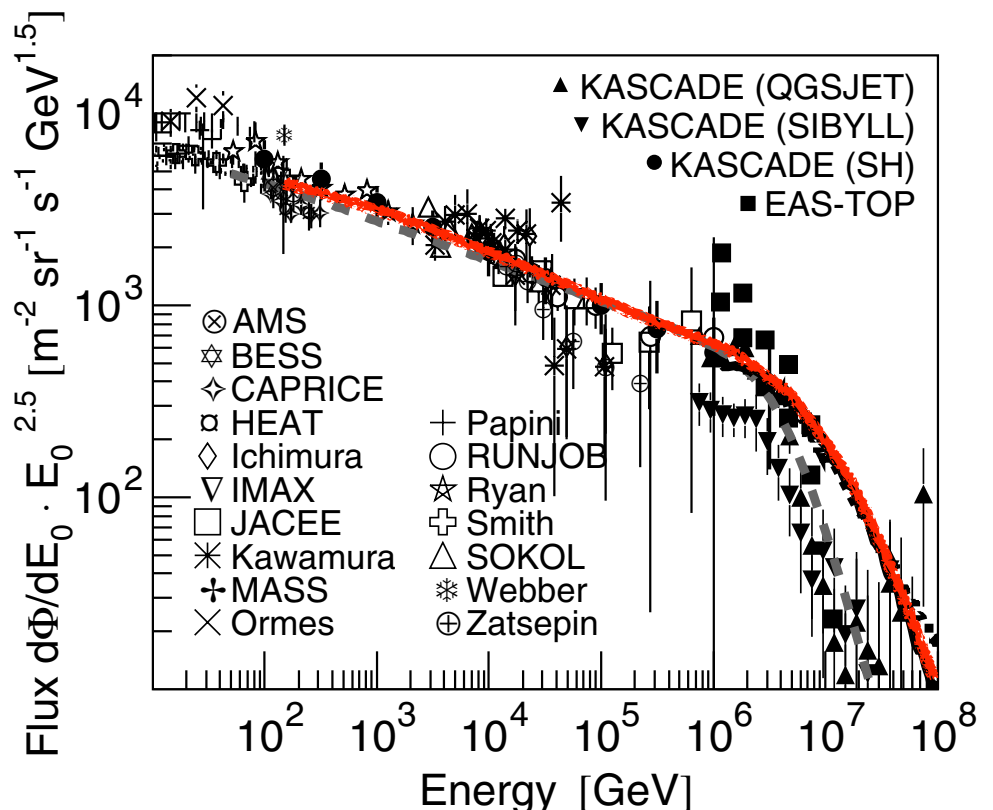


Fig. 7. Proton flux as obtained from various measurements, for references see [28], compared to the spectra shown in Fig. 6 (black lines) and the polygonato model [26] (grey, dashed line).

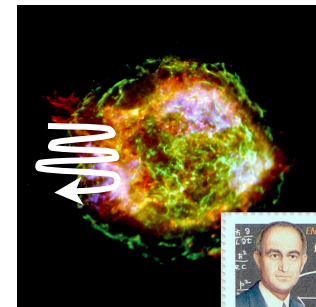
Origin of the knee?

JRH, Astropart. Phys. 21 (2004) 241
(updated)

Acceleration (SNR)

- .. in SNR
- .. in SNR + radio galaxies
- .. in oblique shocks
- .. in variety of SNR
- Single source model
- Reacceleration in galactic wind

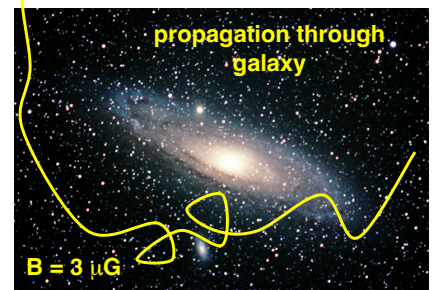
- Berezhko & Ksenofontov
Stanev ..
Kobayakawa ..
Sveshnikova
Erlykin & Wolfendale
Völk & Zirakashvili



Leakage from Galaxy

- Minimum pathlength model
- Anomalous diffusion model
- Hall diffusion model
- Diffusion in turbulent magnetic fields
- Diffusion and drift

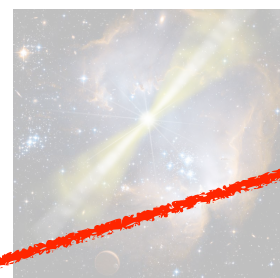
- Swordy
Lagutin ..
Ptuskin .., Kalmykov ..
Ogio & Kakimoto
Roulet ..



γ-ray bursts

- Cannonball model
- Acceleration in GRB + diffusion
- Acceleration in GRB $E_{\text{max}} \sim A$

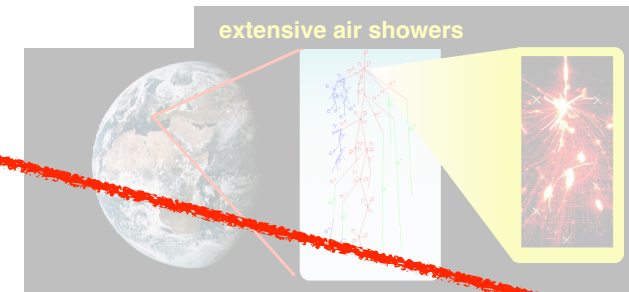
- Plaga
Wick ..
Dar ..



Interaction with background particles

- Diffusion model + photo-disintegration Tkaczyk
- Interaction with neutrinos in galactic halo
- Photo-disintegration (optical and UV photons)

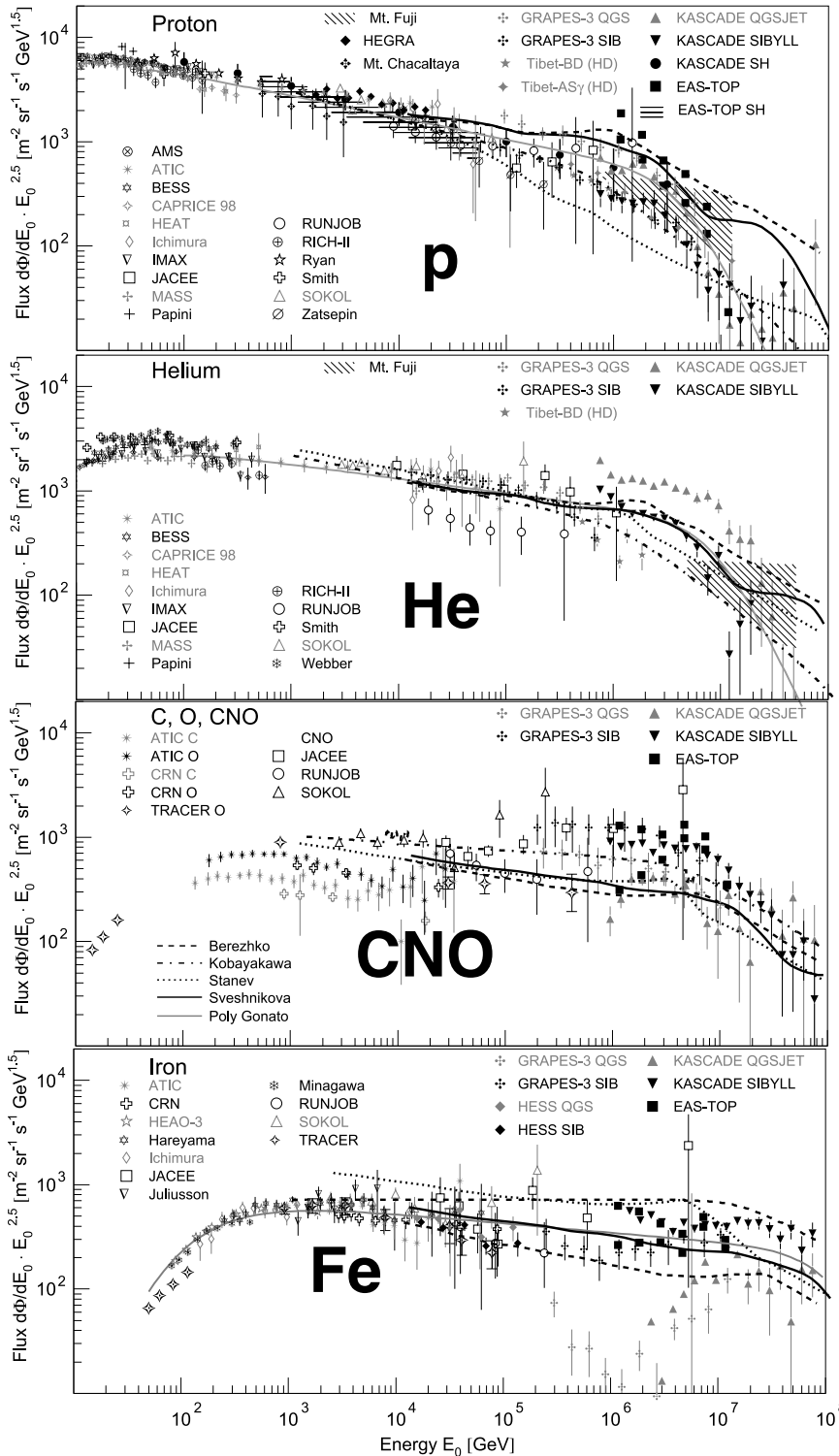
- Dova ..
Candia ..



Particle physics in atmosphere

- Gravitons, SUSY

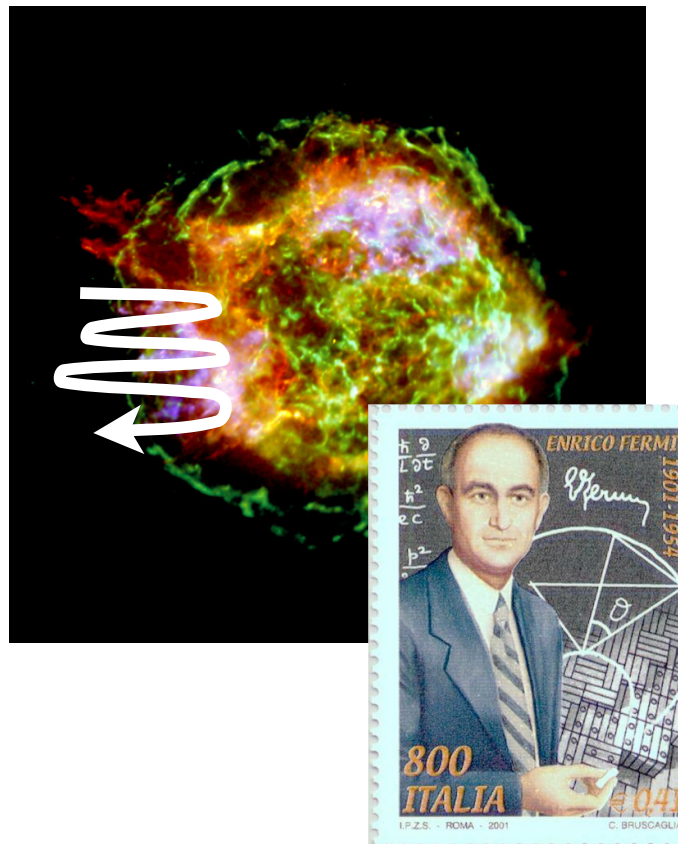
- Kazanas & Nicolaïdis

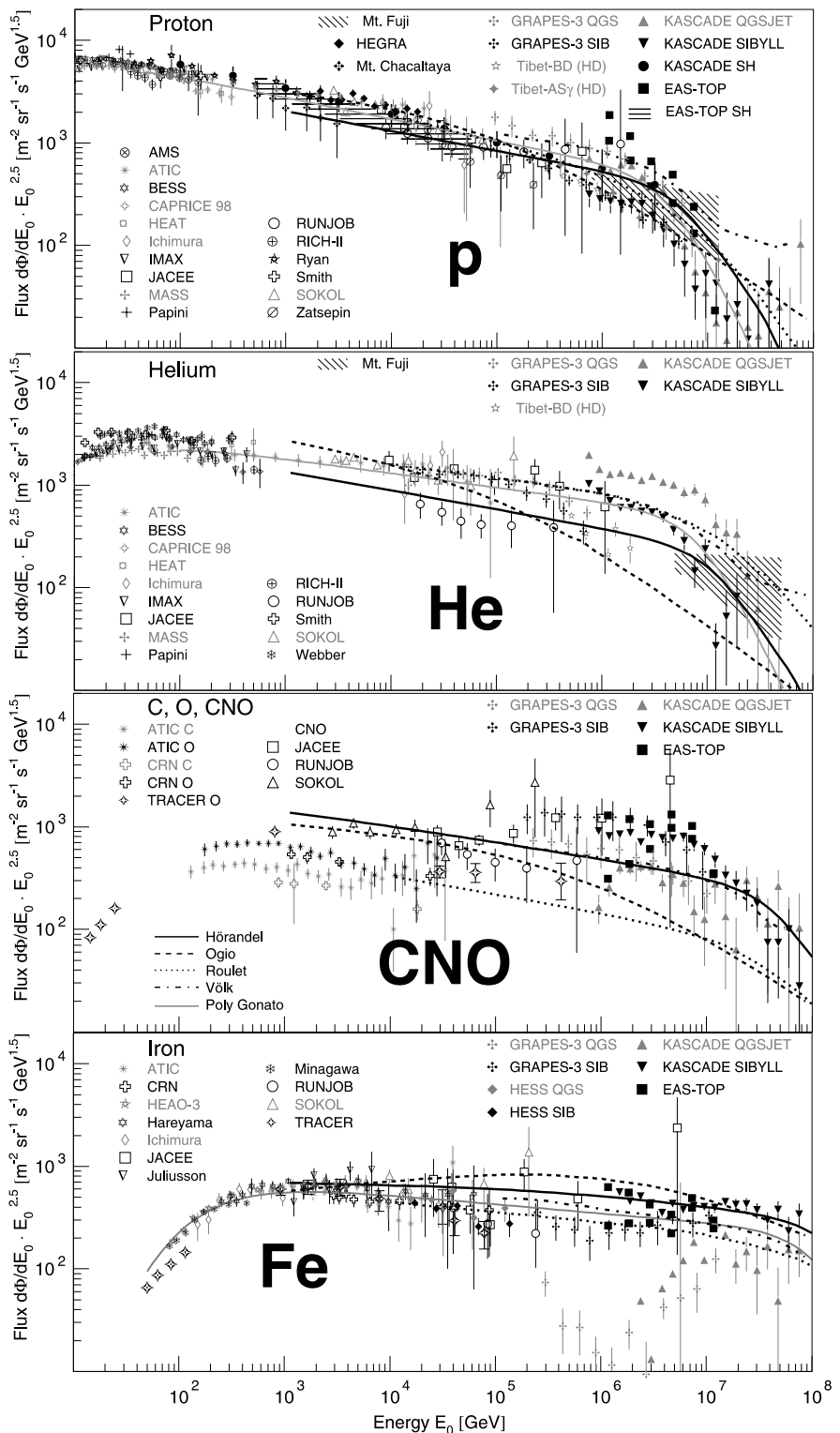


maximum energy

$$E_{max} \propto B \cdot Z$$

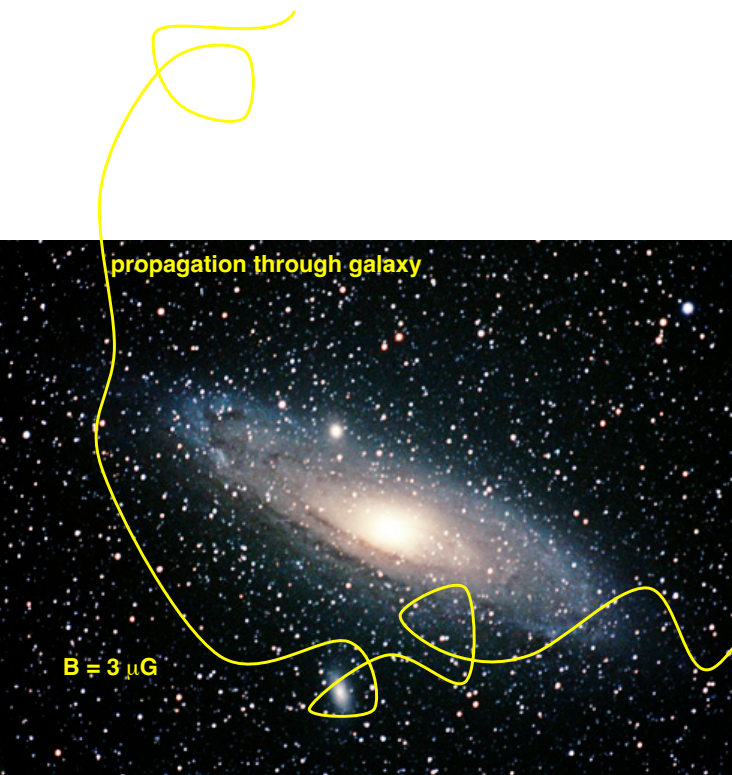
$$E_{max} \approx Z \cdot 100 \text{ TeV} \dots Z \cdot 5 \text{ PeV}$$





leakage from Galaxy

$$E_k \propto Z$$



Transition to extragalactic CR component

J. Blümner et al. / Progress in Particle and Nuclear Physics 63 (2009) 293–338

327

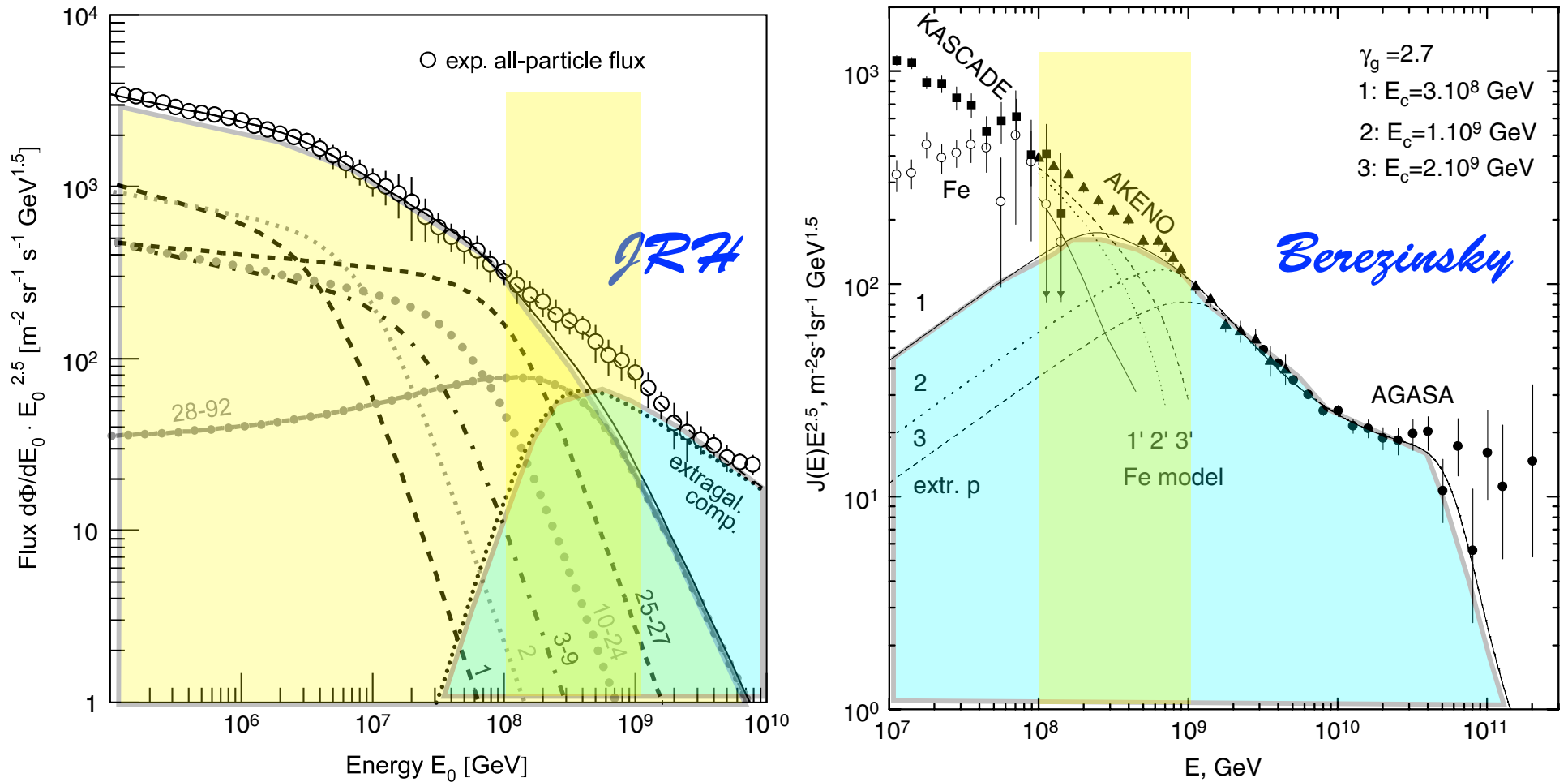
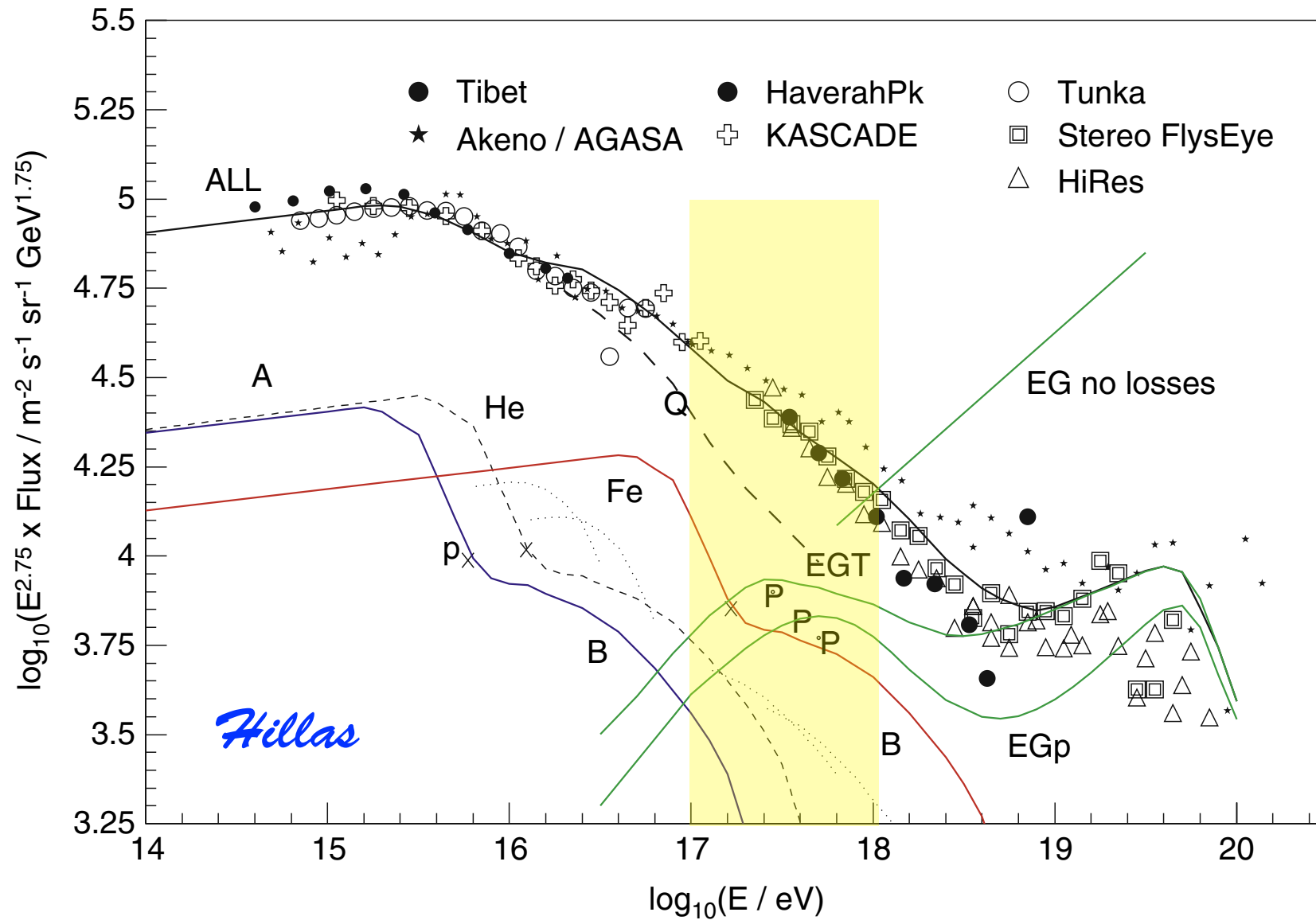


Fig. 26. *Left panel:* Cosmic-ray energy spectra according to the poly-gonato model [2]. The spectra for groups of elements are labeled by their respective nuclear charge numbers. The sum of all elements yields the galactic all-particle spectrum (—) which is compared to the average measured flux. In addition, a hypothetical extragalactic component is shown to account for the observed all-particle flux (---). *Right panel:* Transition from galactic to extragalactic cosmic rays according to Berezinsky et al. [451]. Calculated spectra of extragalactic protons (curves 1, 2, 3) and of galactic iron nuclei (curves 1', 2', 3') are compared with the all-particle spectrum from the Akeno and AGASA experiments. KASCADE data are shown as filled squares for the all-particle flux and as open circles for the flux of iron nuclei.

Transition to extragalactic CR component



„classical“ supernovae + additional component

Contribution of (regular) SNR-CR to all-particle spectrum

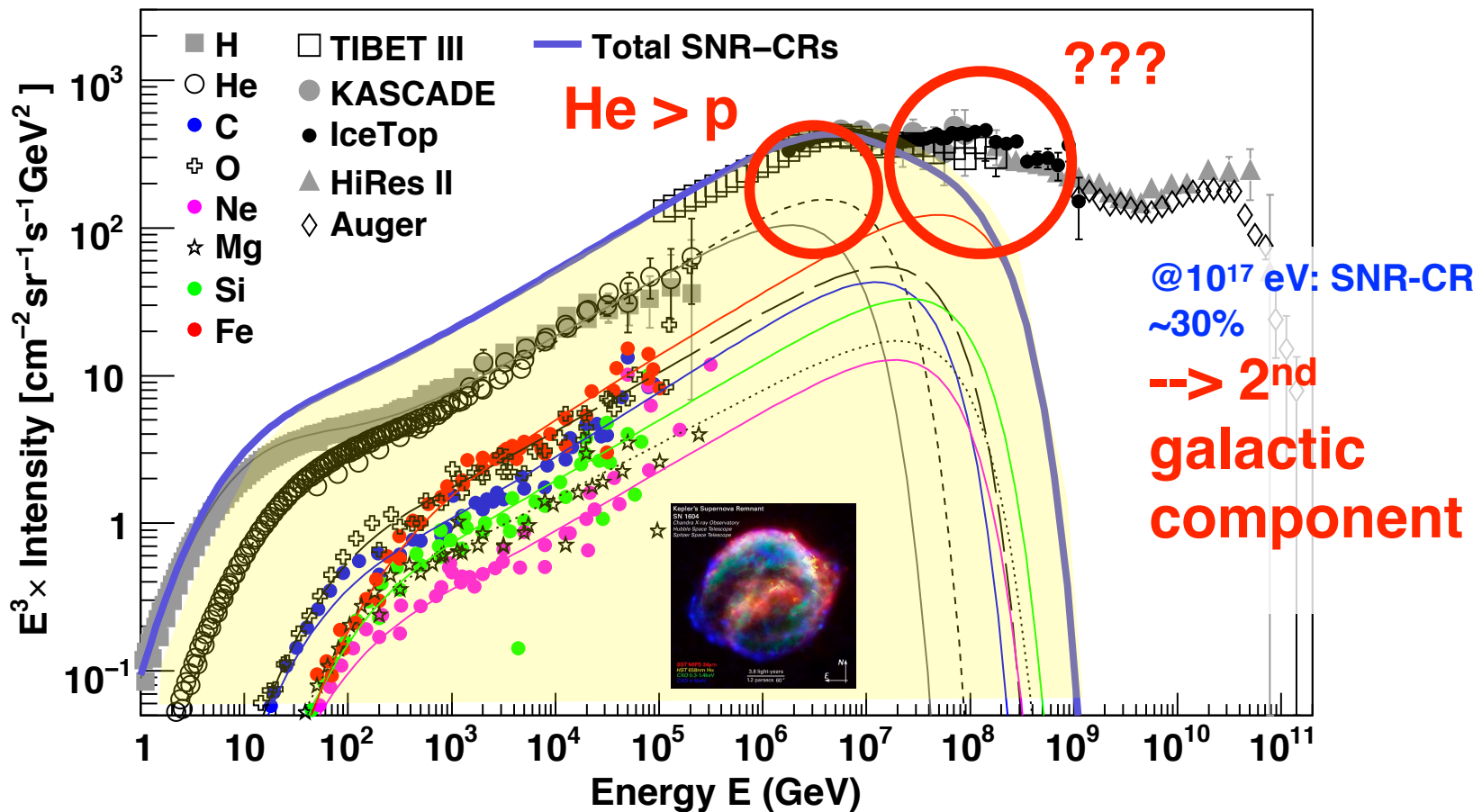
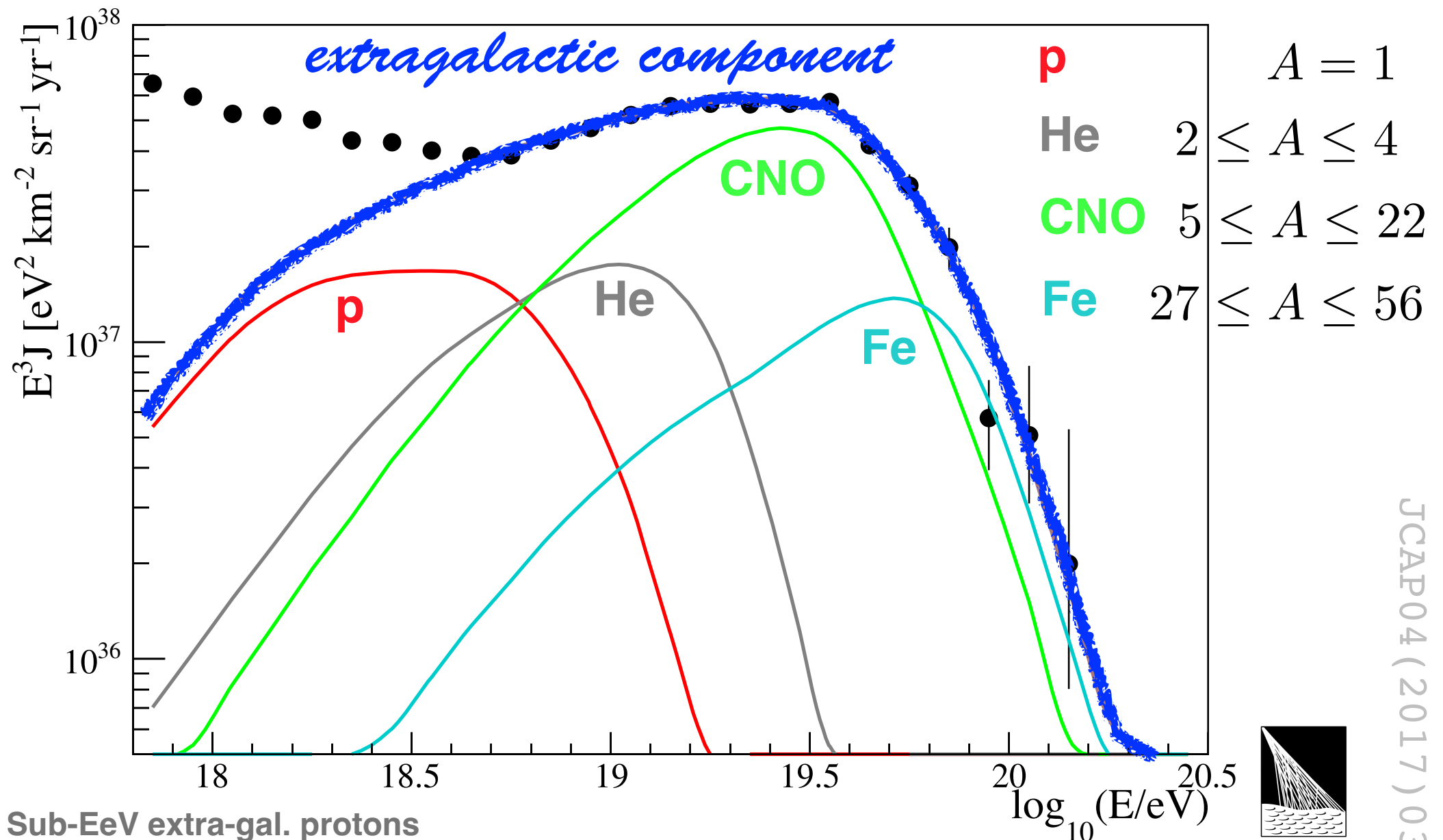


Fig. 2. Contribution of SNR-CRs to the all-particle cosmic-ray spectrum. The thin lines represent spectra for the individual elements, and the thick-solid line represents the total contribution. The calculation assumes an exponential cut-off energy for protons at $E_c = 4.5 \times 10^6$ GeV. Other model parameters, and the low-energy data are the same as in Figure 1. Error bars are shown only for the proton and helium data. High-energy data: KASCADE (Antoni et al. 2005), IceTop (Aartsen et al. 2013), Tibet III (Amenomori et al. 2008), the Pierre Auger Observatory (Schulz et al. 2013), and HiRes II (Abbasi et al. 2009).

~8% of mechanical power of SN --> CRs

Combined fit of spectrum and composition data as measured by the Pierre Auger Observatory



Sub-EeV extra-gal. protons
from interactions of heavier
nuclei

see lecture on UHECR later



all-particle spectra including 2nd galactic component

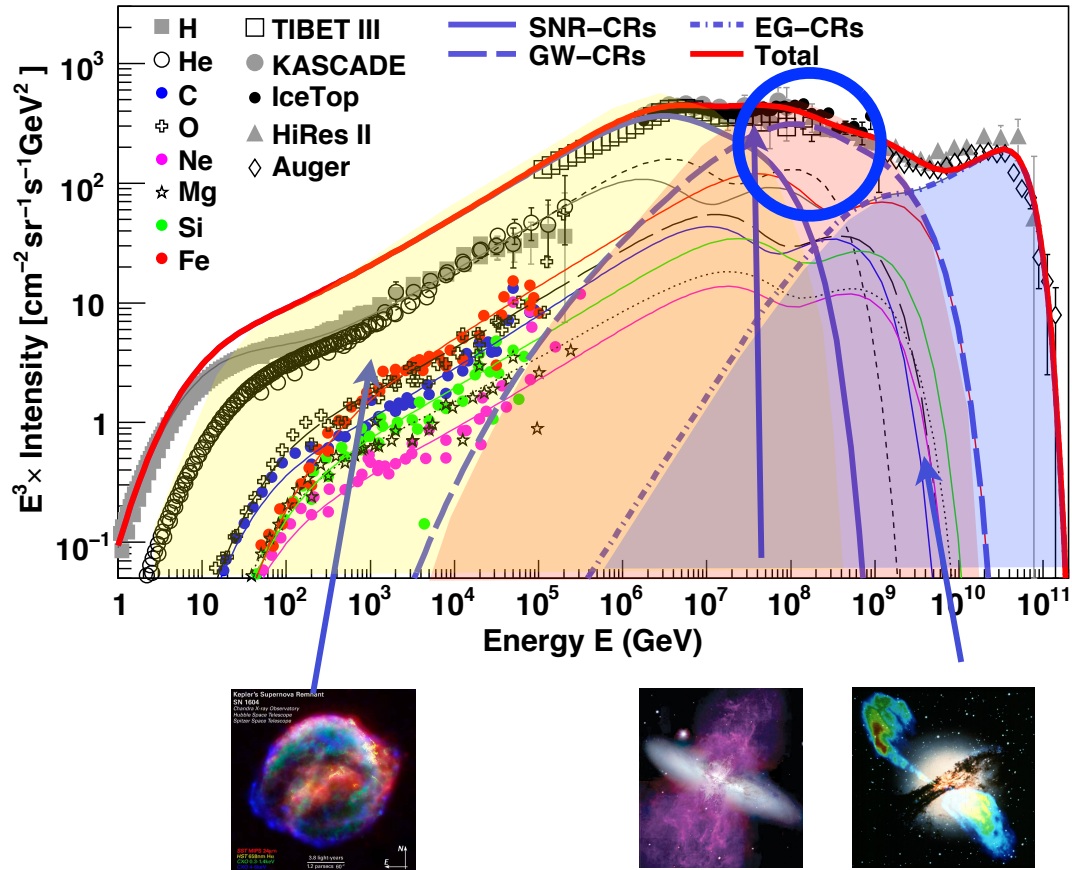
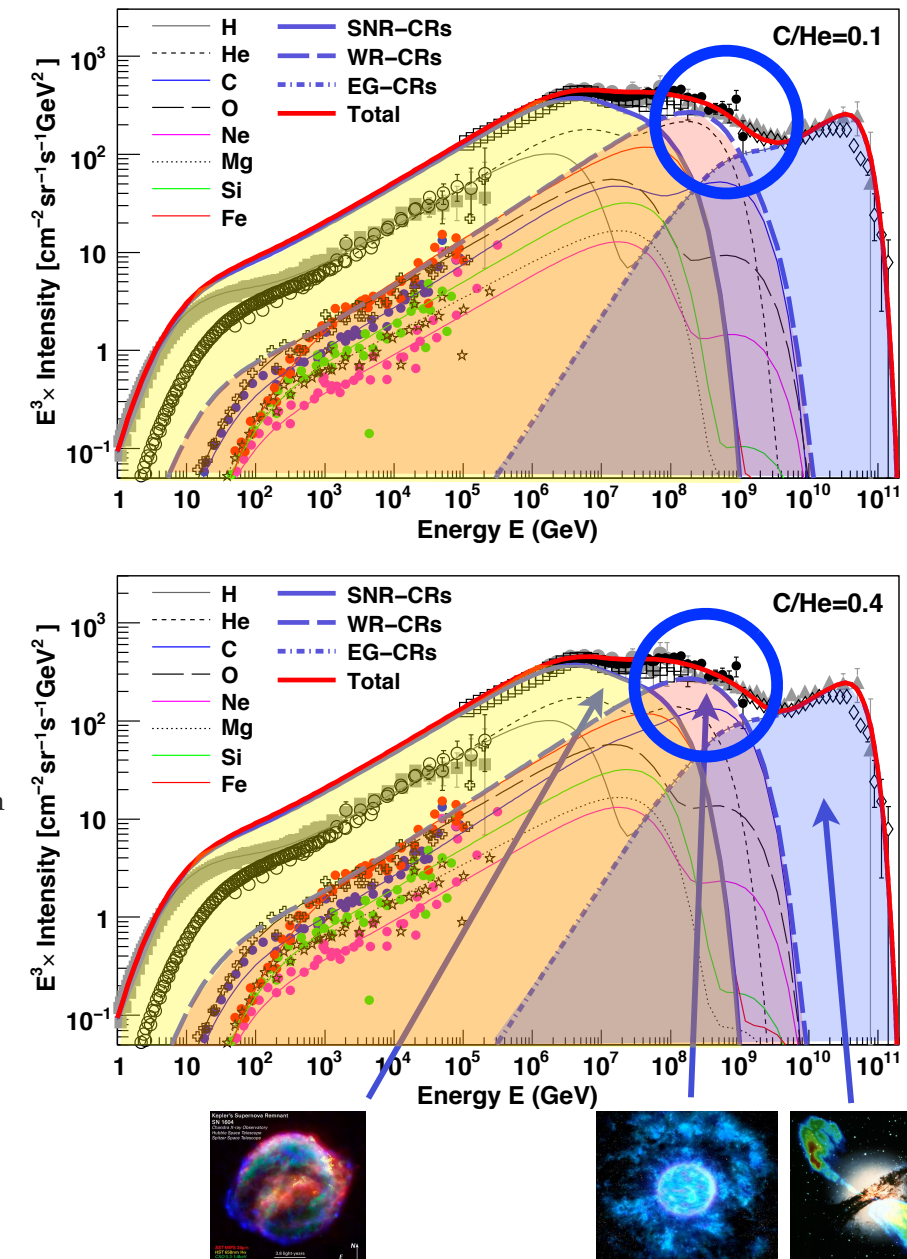


Table 3. Injection energy of SNR-CRs used in the calculation of all-particle spectrum in the WR-CR model (Figure 6).

Particle type	C/He = 0.1 $f \times 10^{49}$ ergs)	C/He = 0.4 $f \times 10^{49}$ ergs)
Proton	8.11	8.11
Helium	0.67	0.78
Carbon	2.11×10^{-2}	0.73×10^{-2}
Oxygen	2.94×10^{-2}	2.94×10^{-2}
Neon	4.41×10^{-3}	4.41×10^{-3}
Magnesium	6.03×10^{-3}	6.03×10^{-3}
Silicon	5.84×10^{-3}	5.84×10^{-3}
Iron	5.77×10^{-3}	5.77×10^{-3}



Mean logarithmic mass ($\ln A$)

WR-CR (C/He=0.4) + EG scenarios

$$\langle \ln A \rangle \equiv \sum_i r_i \ln A_i, \quad \langle \ln A \rangle = \frac{X_{\max}^{\text{meas}} - X_{\max}^p}{X_{\max}^{\text{Fe}} - X_{\max}^p} \cdot \ln A_{\text{Fe}}.$$

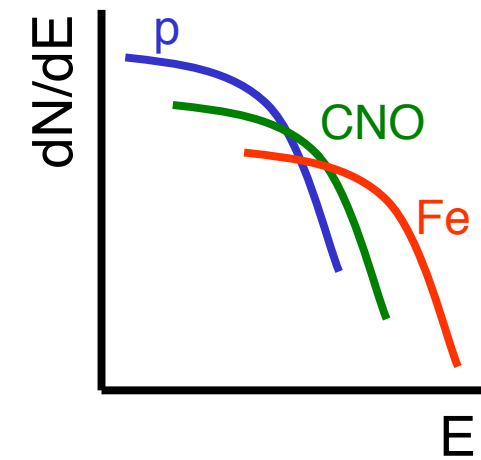
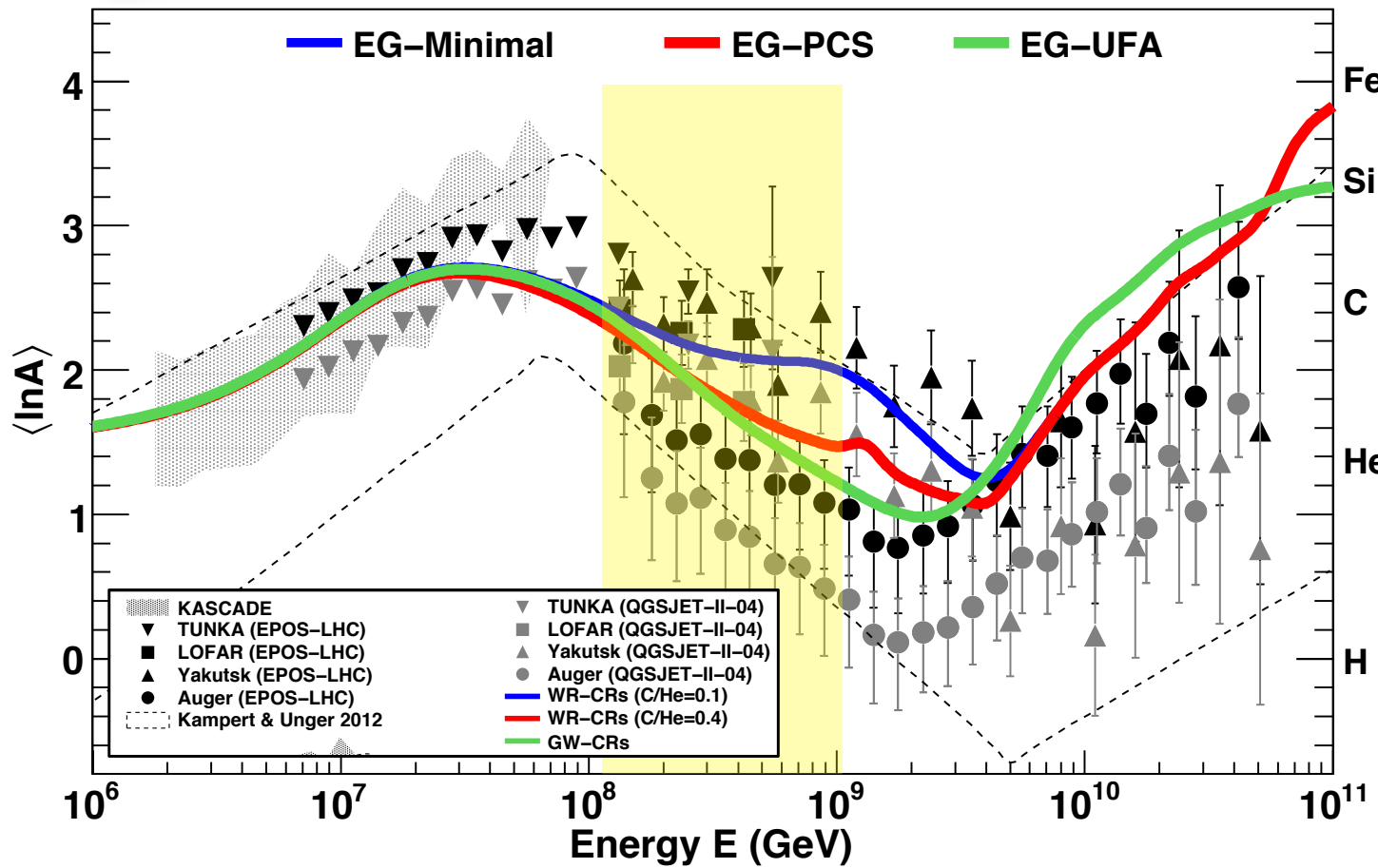


Fig. 11. Mean logarithmic mass for the three different EG-CR models combined with the WR-CR ($C/He = 0.4$) model. Data are the same as in Figure 8. Results obtained using WR-CR ($C/He = 0.1$) model are shown in Appendix B.

Cosmic rays at the knee

Results and implications

- knee in all-particle spectrum at ~ 4.5 PeV caused by fall-off of light elements (p, He)
- experimental (world) data indicate rigidity-dependent fall-off of individual elements
(in particular unfolding by KASCADE[-Grande] and IceCube/Top)
- spectrum above knee is superposition of individual spectra (elemental knees)
 - > fine structure in all-particle spectrum
 - > end of galactic CR component
- astrophysical origin of knee:
combination of maximum energy attained in sources (Supernovae)
(Hillas criterion)
and leakage from Galaxy
- 2nd galactic component at $\sim 10^{17}$ eV?
- extra-galactic origin $> 10^{18}$ eV